

DISCLAIMER

This report was prepared as an account of work sponsored by an agency of the United States Government. Neither the United States Government nor any agency thereof, nor any of their employees, makes any warranty, express or implied, or assumes any legal liability or responsibility for the accuracy, completeness, or usefulness of any information, apparatus, product, or process disclosed, or represents that its use would not infringe privately owned rights. Reference herein to any specific commercial product, process, or service by trade name, trademark, manufacturer, or otherwise does not necessarily constitute or imply its endorsement, recommendation, or favoring by the United States Government or any agency thereof. The views and opinions of authors expressed herein do not necessarily state or reflect those of the United States Government or any agency thereof.

EGG-2441
Distribution Category: UC-80

EXTENDED LIFE ALUMINIDE FUEL FINAL REPORT

L. G. Miller
J. M. Beeston

EGG--2441
DE86 012602

Published June 1986

EG&G Idaho, Inc.
Idaho Falls, Idaho 83415

Prepared for the
U.S. Department of Energy
Idaho Operations Office
Under DOE Contract No. DE-AC07-ID01570

MASTER

DISTRIBUTION OF THIS DOCUMENT IS UNLIMITED
eb

DISCLAIMER

This report was prepared as an account of work sponsored by an agency of the United States Government. Neither the United States Government nor any agency Thereof, nor any of their employees, makes any warranty, express or implied, or assumes any legal liability or responsibility for the accuracy, completeness, or usefulness of any information, apparatus, product, or process disclosed, or represents that its use would not infringe privately owned rights. Reference herein to any specific commercial product, process, or service by trade name, trademark, manufacturer, or otherwise does not necessarily constitute or imply its endorsement, recommendation, or favoring by the United States Government or any agency thereof. The views and opinions of authors expressed herein do not necessarily state or reflect those of the United States Government or any agency thereof.

DISCLAIMER

Portions of this document may be illegible in electronic image products. Images are produced from the best available original document.

ABSTRACT

As the price of fuel fabrication, shipment of both new and spent fuel, and fuel reprocessing continue to rise at a rapid rate, researchers look for alternate methods to keep reactor fuel costs within their limited funding. Extended fuel element lifetimes, without jeopardizing reactor safety, can reduce fuel costs by up to a factor of two. The Extended Life Aluminide Fuel (ELAF) program was started at the Idaho National Engineering Laboratory (INEL) as a joint project of the United States Department of Energy (DOE), the University of Missouri, and the Massachusetts Institute of Technology research reactors. Fuel plates of Advanced Test Reactor (ATR) type construction were fabricated at Atomics International and irradiated in the ATR at the INEL. Four fuel matrix compositions were tested (i.e., 50 vol% UAl_x cores for reference, and 40, 45 and 50 vol% UAl_2 cores). The 50 vol% UAl_2 cores contained up to 3 grams U-235 per cm^3 of core. Three plates of each composition were irradiated to peak burnup levels of 3×10^{21} fission/ cm^3 of core. The only observed damage was due to external corrosion at similar rates experienced by UAl_x fuel elements in test reactors.

SUMMARY

The Extended Life Aluminide Fuel (ELAF) program was started at the Idaho National Engineering Laboratory (INEL) as a joint project of the United States Department of Energy (DOE), the University of Missouri, and the Massachusetts Institute of Technology. For the program, 30 fuel plates were constructed to a maximum fuel loading that could be produced on a commercial basis. These contained UAl_2 and UAl_3 fuel (UAl_x) cores, with maximum boron content as used in the Advanced Test Reactor (ATR) at the Idaho National Engineering Laboratory. The maximum boron content was incorporated to reduce initial reactor reactivity. The UAl_2 fuel core was used to gain higher uranium content. The test program was planned so that the fuel plates would be irradiated to a maximum fission density of $3\text{--}4 \times 10^{21} \text{ f/cm}^3$ (about 50% burnup for the 50 vol% fuel plate cores). This burnup is about twice that presently allowed in university reactors.

An ELAF fuel core with 73 wt% of the brittle phase (UAl_x) gave excellent performance to a burnup of $1.84 \times 10^{21} \text{ f/cm}^3$ with a peaking factor of 1.63 (peak burnup of $3.0 \times 10^{21} \text{ f/cm}^3$).

The ELAF fuel plates operated at surface temperatures of about 395 K (120°C) with the only evidence of failure due to pitting corrosion.

Blister temperatures from post irradiation tests of 763 K (for the UAl_3 composition) and 776 K (for the UAl_2 composition) indicated large margins of safety from overheating for short periods of time.

The 50 vol% UAl_2 composition plates performed as good, or better, than the 50 vol% UAl_3 composition plates and will provide higher fuel loading. Although pitting corrosion caused the failure of three plates of the UAl_2 composition, a large pit that would have produced failure was found in the UAl_3 composition.

Neither the pitting corrosion rate, or the probability of pitting, seemed any greater in the ELAF plates than fuel elements in other reactors when consideration is taken of the plate surface temperature and the time in the water.

Reaction of the UAl_2 to produce UAl_3 and the $\text{U}_{1-x}\text{Al}_4$ defect phase causes an increase in core volume of 6 to 12%. The core volume percent thus approaches 60 vol% of the brittle constituent.

It is recommended that the specification for oxygen in the powder blends be examined with the view of reducing the allowed oxygen.

It is recommended that management of the fuel element irradiation sequence be considered as a way to reduce the depth of pitting corrosion and extending fuel element life.

ACKNOWLEDGEMENTS

The authors would like to thank L. D. Koeppen and J. W. Rogers for contributing the section on Fission Product Radionuclide Distributions in ELAF Fuel Plates that is included in Appendix A.

CONTENTS

ABSTRACT	ii
SUMMARY	iii
ACKNOWLEDGEMENTS	iv
ACRONYMS AND ABBREVIATIONS	viii
1. INTRODUCTION	1
2. PLATE DESIGN AND IRRADIATION HISTORY	2
2.1 Irradiation	2
3. TEST EXAMINATIONS	4
3.1 Visual Examination and Photography	4
3.2 Oxide Removal	4
3.3 Dimensional Measurements	4
3.4 Immersion Density and Swelling	4
3.4.1 Swelling Determined from Thickness Measurements	10
3.4.2 Core Thickness Change by Metallography	10
3.5 Metallography	12
3.6 Scanning Electron Microscopy	15
3.7 Blister Tests	23
3.8 Pit Replication	32
3.9 Pitting Corrosion Rate	38
3.10 Gamma Ray Spectroscopy	38
3.11 Radiochemical Analyses for Burnup	41
4. DISCUSSION	43
4.1 Swelling and Fuel Phase Instability	43
4.2 Fuel Core Integrity and Bubble Formation	43
4.3 Blister Behavior and Potential Swelling	44
4.4 Pitting Corrosion and Plate Life	44
4.5 Maximum Fission Density	45

5. CONCLUSIONS AND RECOMMENDATIONS	46
REFERENCES	47
APPENDIX A—IRRADIATION DATA	A-1
APPENDIX B—CORE AND PLATE DATA	B-1

FIGURES

1. Irradiation history	3
2. Typical surface appearance of the irradiated plates before and after oxide removal	5
3. ELAF plate shearing and punching schematic	6
4. Core swelling versus burnup from immersion density	9
5. Core swelling versus burnup from thickness measurements	12
6. Plate and core thickness before and after irradiation	14
7. Microstructure of core and cladding of 50 vol% UAl_x	16
8. Microstructure of 45 vol% and of 40 vol% UAl_2	17
9. Fuel grains of UAl_x in aluminum matrix. UAl_2 , UAl_3 and UAl_4 just discernable with Magomet etch	18
10. SEM photograph of fractured surface by secondary emission, plate 013	19
11. SEM photograph of fractured surface by secondary emission, plate 032	20
12. SEM photograph of fractured surface by back scatter emission (plate 032) identifies region A of Kevex-ray examination	21
13. Examination of fuel grain A for UAl_2 , UAl_3 , UAl_4 and U	22
14. SEM photographs of plate 007, composition 50 vol% UAl_x	24
15. SEM photographs of plate 019, composition 50 vol% UAl_2	25
16. SEM photographs of plate 006, composition 50 vol% UAl_x	26
17. SEM photographs of plate 013, composition 50 vol% UAl_2	27
18. SEM photographs of plate 028, composition 45 vol% UAl_2	28
19. SEM photographs of plate 030, composition 40 vol% UAl_2	29
20. SEM photographs of plate 013, acid etch, 50 vol% UAl_2	30
21. Blister temperature as a function of the burnup	32

22.	Photographs of blister samples from 50 vol% UAl_2 and UAl_3	33
23.	Photographs of blister samples from 45 vol% and 40 vol% UAl_2	34
24.	Typical photographs of replica areas on oxide stripped plates	35
25.	SEM photographs of two of the replicated pits	39

TABLES

1.	Immersion density of sheared sections of irradiated plates	7
2.	Calculation of preirradiated density of sheared sections	8
3.	Instability of UAl_2 phase during plate processing	9
4.	Thickness measurements of irradiated plates	11
5.	Comparison of metallurgical core thickness change with immersion density change and plate thickness change	13
6.	Image analysis of voidage	15
7.	Comparison of core thickness change during fabrication and irradiation	15
8.	Blister temperatures	31
9.	Measured pit depths and calculated maximum total pitting corrosion	36
10.	Relative radionuclide activity of the twelve plates in counts per second for the maximum, average, and punching positions	40
11.	Ratios of isotopic maximum gamma counts per second to those of the burnup punching position	41
12.	Mass spectral isotopic ratios for ELAF burnup samples	42
13.	Burnup of ELAF fuel plates from isotopic ratios, peaking factor, and PDQ calculations	42

ACRONYMS AND ABBREVIATIONS

AI	Atomics International
ATR	Advanced Test Reactor
DOE	United States Department of Energy
ELAF	Extended Life Aluminide Fuel
INEL	Idaho National Engineering Laboratory
MITR	Massachusetts Institute of Technology Reactor
MURR	Missouri University Research Reactor
NDT	Nondestructive testing
SEM	Scanning Electron Microscopy

EXTENDED LIFE ALUMINIDE FUEL FINAL REPORT

1. INTRODUCTION

The Extended Life Aluminide Fuel (ELAF) Program^{1,2} conducted by EG&G Idaho for the Department of Energy, University of Missouri, and Massachusetts Institute of Technology had an objective of determining whether fuel loading and burnup limits for fuel elements in university research reactors could safely be increased beyond the limits presently allowed by reactor licensing restrictions. For the program, 30 fuel plates were constructed to a maximum fuel loading that could be produced on a commercial basis. These contained UAl_2 and UAl_3 fuel (UAl_x) cores, with maximum boron content as used in the Advanced Test Reactor (ATR) at the Idaho National Engineering Laboratory. The maximum boron content was incorporated to reduce initial reactor reactivity. The UAl_2 fuel core was used to gain higher uranium content. The test program was planned so that the fuel plates would be irradiated to a maximum fission density of $3-4 \times 10^{21}$ f/cm³ (about 50% burnup for the 50 vol% fuel plate cores). This burnup is more than twice that presently allowed in university reactors.

The UAl_x dispersion fuel system was developed^{3,4} to meet a need in the high flux, high power Advanced Test Reactor (ATR). Several features of the UAl_x dispersion fuel system are reported^{5,6,7,8} to extend its performance capability in high flux reactors. The powder dispersion causes voidage to

be fabricated into the fuel matrix, which may accommodate fission products. The UAl_x structure has exceptional tolerance for fission gas retention, and burnable poisons can be readily dispersed in the fuel matrix.

Uranium aluminide fuel plates with lower fuel loading than the ELAF plates have been successfully irradiated to fission densities almost as high.^{9,10} The ATR fuel plates containing principally UAl_3 , range from 40 to 60 wt% UAl_x , while plates described in the literature¹⁰ contain 45.5 or 54.5 wt% UAl_2 , or 50 wt% UAl_3 . These ELAF experimental plates contain 64 to 73.3 wt% UAl_x —principally UAl_2 , or 67.4 wt% UAl_x —principally UAl_3 . This fuel loading corresponds to the presence of the brittle constituent of 40 to 50 vol%. This introduces the question of whether the fuel core will retain a sufficiently ductile behavior during irradiation to resist blister formation. The recent rolling test program at Atomic International (AI)¹¹ indicates current technology can be used to produce quality fuel plates on a production line basis, and the eminently good irradiation performance of the UAl_x fuel in test reactors⁹ and experimental plates^{3,4,5,6,7,8,10} indicates that failure should not occur in the fuel.

Preliminary reports^{2,12} indicated that the principal problem would be pitting due to corrosion.

2. PLATE DESIGN AND IRRADIATION HISTORY

Fuel plate dimensions were selected to fit the ATR I-hole configuration and to provide the plate area required for testing. The 12 plate configuration for a test insertion is shown in Appendix A, Figure A-1. Thickness of plates and cores, and plate construction methods were selected to match the Missouri University Research Reactor (MURR) and ATR fuel. Extrapolation of the test data to a 1.524-mm (0.060-in.) plate will provide MIT with the required supporting data for extended fuel burnup in the Massachusetts Institute of Technology Reactor (MITR).

The finished plates measure $25.4 \pm 0.127 \times 317.5 \pm 0.762 \times 1.27 \pm 0.025$ mm ($1.000 \pm 0.005 \times 12.50 \pm 0.030 \times 0.050 \pm 0.001$ in.). The fuel core dimensions are $\sim 20.32 \times 266.7 \times 0.508$ mm ($0.8 \times 10.5 \times 0.02$ in.). A 9.535-mm (3/8-in.) hole centered in the top end of each plate provided a means for individual plate removal in the canal or hot cell.

The UAl_x powder was prepared, and 30 fuel plates were fabricated by AI. The U-235 enrichment was $93.0 \pm 1.0\%$ for all batches. Chemical analysis of the JF and JJ blends is given in Appendix B. The metal impurities were less than 0.3%, with no individual impurity exceeding 600 ppm. No free metallic uranium was present in any powder samples as determined by x-ray analysis. Other core and plate data are given in Appendix B.

Nondestructive testing (NDT) inspections for nonbond and minimum cladding thickness met the accepted criteria of the ATR Fuel Element Specification.¹³ Fabrication was made according to specification ES-50607A.¹⁴

2.1 Irradiation

Irradiation was begun in the ATR I-9 facility in July 1981, and continued in I-13 until June 1986 (Figure 1). The thermal flux in the facility varies between 3 and 7×10^{13} n/cm²s. The peak gamma heat in the facility of 1.55 W/g was used with corrosion film estimates in the MACABRE computer code to calculate maximum fuel plate temperatures versus operating time. The maximum nominal and

2σ plate temperatures were 395 and 407 K, respectively; these decreased with operating time.

During the irradiation period, the 30 plates were inserted in the reactor in groups of 12. Until the end of the period, each plate was removed, as required, in order to inspect for corrosion pit depth (Figure 1). If the corrosion pit depth of any plate was estimated to be approaching 6 mil, that plate was removed and a new plate inserted for the next reactor cycles. Eleven inspection intervals were recorded. At the start of the test program, three plates failed by pitting corrosion after 172 full power days.¹²

Neutron flux and burnup calculations were made with the PDQ neutron diffusion-depletion program through the irradiation history of the fuel plates. Two-dimensional XY and RZ-4 energy group PDQ problems were developed to model the tests. In the burnup calculation for each test cycle, a correction factor was applied so that the calculated thermal neutron flux matched the measured value obtained from the flux monitors, which were placed in the test and removed after each test cycle.

The extent of burnup from these calculations was used, along with the inspection for pitting, to guide the test termination for each plate and for the end of irradiation. The goal of the program was to reach a maximum burnup of 3.3×10^{21} f/cm³. Because of peaking, expected at the sides and top or bottom of the plates, the calculated peak burnup before the end of irradiation was allowed to reach 4.2×10^{21} f/cm³.

Gamma ray spectroscopy was done on 12 plates selected according to the maximum burnup for that composition group. The gamma ray spectroscopy showed some peaking. The extent of the peaking on the gamma scans was limited by the size of the collimator and scanner characteristics. The results of the gamma ray scanning will be presented in Section 3.10.

Radiochemical analysis for burnup was made on the twelve plates selected for highest burnup from the four composition groups (50 vol% UAl_2 , 45 vol% UAl_2 , 40 vol% UAl_2 , and 50 vol% UAl_3). The analysis is given in Section 3.11.

		I-9 SE Lobe MWd				I-13 SW Lobe							
		7237	5068	1094	1516	1512	1510	1098	672	860	637	744	1770
Dates		7/19/81 to 5/6/82	10/1/82 to 3/16/83	1/27/84 to 3/7/84	3/7/84 to 4/24/84	4/24/84 to 6/17/84	6/17/84 to 9/9/84	9/9/84 to 10/21/84	10/21/84 to 11/23/84	11/23/84 to 1/20/85	1/20/85 to 2/24/85	2/24/85 to 3/31/85	3/31/85 to 6/23/85
Plate No.	Composition principal constituent												
001	50 vol% UAl_3												
003													
004													
005													
006													
007													
008													
009													
010													
013	50 vol% UAl_2												
015													
016				Failed									
017													
018			Failed										
019													
020													
022	45 vol% UAl_2												
023			Failed										
024													
025													
026													
027													
028													
029	40 vol% UAl_2												
030													
031													
032													
033													
034													
035													
036													
		172	136	37	39.7	43.0	58.4	31.5	30.7	35.8	26.4	31	72.3
		Reactor days at power											

End of Irradiation

8 0998

End of Irradiation

0 0998

Figure 1. Irradiation history.

3. TEST EXAMINATIONS

Twelve plates were removed from the reactor on June 23, 1985, and allowed a decay time to cool before the 27 plates were shipped to the hot cell for measurements. After each inspection period, those plates not reinserted in the reactor were stored in the ATR canal. The test examinations for this report included: visual examination and photography; dimensional measurements before and after oxide removal; oxide removal; immersion density; metallography; scanning electron microscopy; pit replication on fifteen plates not selected for destruct tests; gamma ray spectroscopy; and radiochemical analysis for burnup.

3.1 Visual Examination and Photography

Visual examination of the plates revealed small pits and corrosion spots with some scratches due to handling. Typical surface appearance of the irradiated plates, before and after oxide removal, are shown in Figure 2. A deep pit in the side of plate No. 004 is shown in Figure 2(c). The depth of this pit will be presented in Section 3.9. No blistering or oxide spalling was seen. The oxide thickness will be discussed in Section 3.3.

Corrosion and pitting behavior is discussed in Section 3.9.

3.2 Oxide Removal

Oxide thickness was measured by eddy current technique on 12 plates in July 1982. Additional plates were measured on December 20, 1984, and at the end of the irradiation on June 26, 1985. The oxide thickness increased with time in the reactor, as expected. Only normal oxide thickness occurred. The values are given in Section 3.4.1. In the hot cell, after the thickness of the plates was measured with a micrometer, the oxide was removed and the plate thickness remeasured.

Oxide removal from the plates in the hot cell was accomplished in a solution of 20 g of chromic acid (CrO_3) and 35 ml of 85% phosphoric acid in one liter of distilled water. The plates were held in a holding rack and stripped in the boiling solution until the oxide was gone (about 10 minutes).

3.3 Dimensional Measurements

Thickness measurements were made in the canal, using a dial indicator, and in the hot cell, using a micrometer. The thickness measurements in the hot cell were made before and after removal of the oxide. The results are presented in Section 3.4.1.

3.4 Immersion Density and Swelling

The immersion density of the samples (2 x 3/4 in. sections) sheared from the core region from each of the twelve plates (Figure 3) was done by the method described in ASTM B 311 (1979). The density (D) was calculated from the formula:

$$D = \frac{AE}{A-B}$$

where

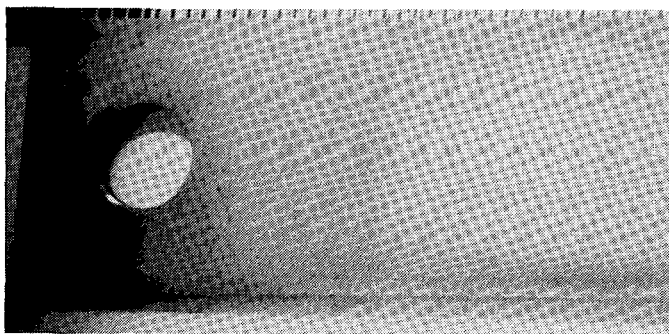
A = weight of specimen in air (g)

B = weight of specimen in water (g)

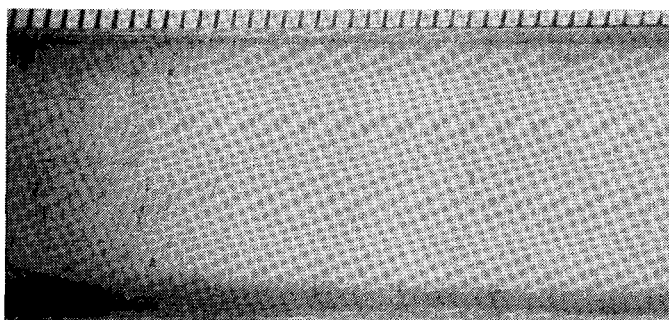
E = density of water in g/cm^3 (20°C for all samples).

The dry and wet weights, and the immersion density calculated by the formula, are given in Table 1. The preirradiated density for the sheared sections was calculated from the core and plate specifications for all fabricated plates from Table B-1.^a The calculated, preirradiated, sheared plate density of the sections was obtained by using the deburred core compact weight, the core volume from the void volume measurements, and other data as given in Table 2. The plate core thickness can then be calculated from these values, and the core surface area obtained from radiographic fuel core measurements of the plate.¹⁵ The calculated, preirradiated, sheared plate density and the plate core thickness are given in Table 2. It is noted that the plate core thickness obtained is less than the average metallographic core thickness for the sample from each composition group. Since the production plates have been hot rolled and blister annealed, relative

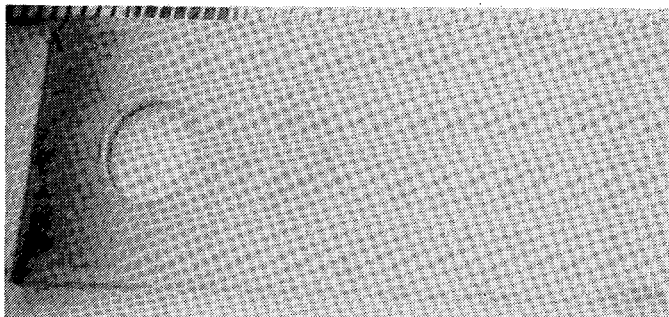
a. Appendix B.



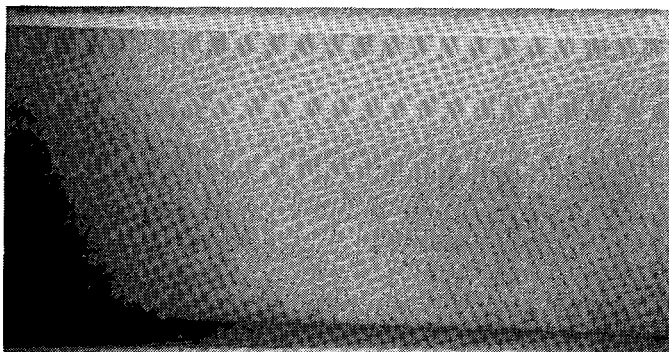
(a) Plate 016 before oxide removal



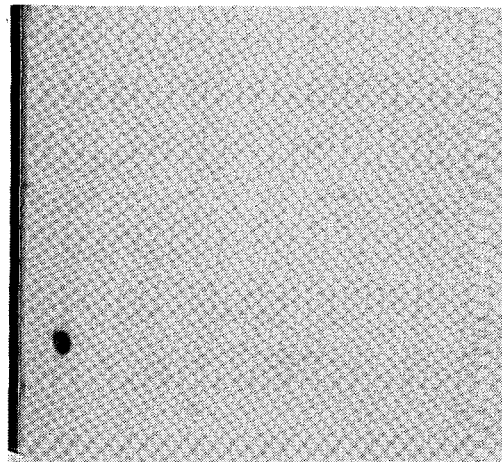
(b) Plate 016 before oxide removal



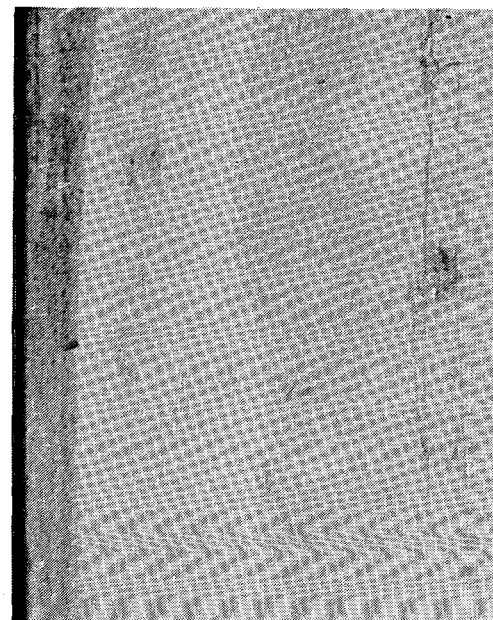
(d) Plate 018 after oxide removal



(e) Plate 016 after oxide removal

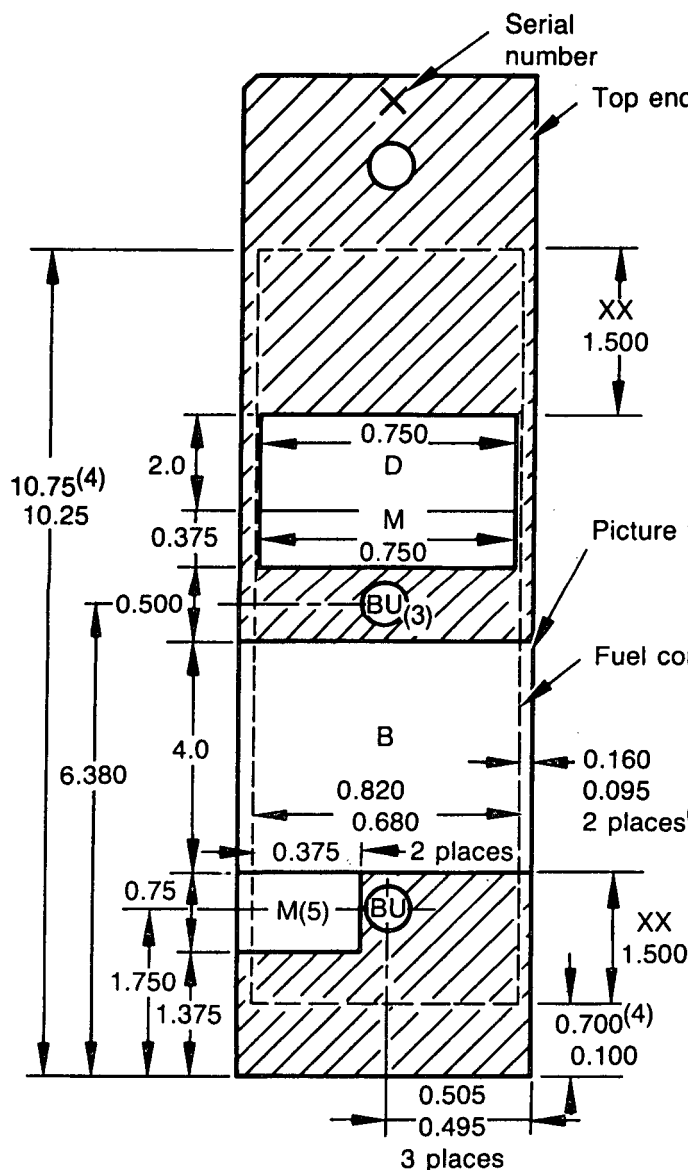


(c) Plate 004 before oxide removal
with deep pit on side of plate



(f) Plate 013 after oxide removal

Figure 2. Typical surface appearance of the irradiated plates before and after oxide removal.



Legend

M = Met Sample⁽⁵⁾

BU = Burnup Sample⁽³⁾

D = Density Sample

B = Blister Sample

XX = Dogbone Area⁽²⁾

/// = Scrap

Met samples to be mounted
so polished surface is
closest to density samples

(1) Region of the fuel core within
one and one-half inches from its ends,
where thickening can occur during the
rolling process.

(2) The window-shaped aluminum
frame which hold the fuel core.

(3) Burnup samples to be punched
on axial and transverse center
lines as shown.

(4) Reference demension only.

(5) Bottom met sample to be
punched as close to BU samples as
possible.

Scale: None

Dimensions in inches

6 6689

Figure 3. ELAF plate shearing and punching schematic.

Table 1. Immersion density of sheared sections of irradiated plates

Plate Number	Dry Weight (g)	Wet Weight (g)	Measured ^a Density (g/cm ³)	Preirradiated Calculated Section Density (g/cm ³)	Density Decrease (%)	CSAP PDQ Average Burnup (x 10 ⁻²¹ f/cm ³)	Punch ^b Fission Density
005	3.7845	2.6299	3.2718	3.3320	1.81	1.80	1.28
006	3.1313	2.1680	3.2447	3.3462	3.03	2.30	1.73
007	4.1006	2.8521	3.2785	3.3297	1.54	1.48	1.06
013	4.2433	3.0061	3.4236	3.5992	4.88	2.98	2.02
019	4.2186	3.0141	3.4961	3.6100	3.16	2.13	1.49
020	4.1226	2.9312	3.4541	3.5768	3.43	2.24	1.72
022	4.0864	2.8989	3.4350	3.5251	2.56	1.82	1.22
027	4.2564	3.0223	3.4428	3.5081	1.86	1.94	1.36
028	3.9421	2.7715	3.3615	3.5120	4.29	2.61	1.96
030	3.8557	2.6951	3.3162	3.4097	2.74	2.25	1.52
032	4.2891	2.9967	3.3127	3.4365	3.60	2.14	1.49
033	3.7788	2.6481	3.3360	3.4224	2.52	2.00	1.42

a. Calculated from the formula $D = AE/(A - B)$ where E (the density of water at a temperature of 20°C) was taken as 0.9982 g/cm³.

b. Table 13 plus 10%. The low punch fission density plus 10% gives an average fission density equivalent to the CSAP PDQ average (see Section 3.11).

amounts of the aluminide phases UAl_2 , UAl_3 and UAl_4 have changed (there is less UAl_2 and more UAl_4 than in the fuel powder charge), Table 3. The stability of the UAl_2 phase in compact 1JF038YD was investigated by taking pieces of the compact and giving each piece the heat treatment indicated (Table 3). The analyses of the pieces were done by x-ray, similar to the powder blend JF. The as compacted values for UAl_2 , UAl_3 , and UAl_4 (Table 3) of 71, 28, and 1, are to be compared with those of the powder blend JF values for UAl_2 , UAl_3 , UAl_4 , respectively, of 67, 33, and < 1, with U alloy not detected. The calculated core thickness from the core compact weight and volume is lower than the metallurgical sample for each group by 4 to 10% (Table 2). This difference in the core thickness is attributed to the lack of stability of the UAl_2 phase during plate processing and the consequent growth of the core thickness. The calculated preirradiated sheared plate density is dependent upon the relative core and clad thickness. This density is given in Table 2 for the metallurgical core thickness of the metallurgical sample plates, as well as for the calculated core thickness. The calculated density from

the computed core thickness is lower than that calculated from the metallurgical samples by 1 to 3%. Since the calculated preirradiated density from the metallurgical sample core thickness gives a higher swelling value, these are the values used in computing the swelling in Table 1.

The swelling (density decrease) from the immersion density measurements is plotted in Figure 4 for the burnup^a of each plate. It is noted that the immersion density of the sheared section also gives an average measurement (peaking is seen in the thickness measurements). A linear least squares analysis for the PDQ^b fission density (Table 1) gives an equation

a. The burnup was taken from the nuclear calculations. It is approximately the same as that measured for the burnup punching times the peaking factor, and is the burnup value used for all the figures and text except as otherwise noted (especially Sections 3.11 and 4).

b. A two dimensional neutronics diffusion code.

Table 2. Calculation of preirradiated density of sheared sections

Plate Number	Deburred Core Compact Weight (g)	Core ^a Volume V _c (cm ³)	Core Compact Density g/cm ³	Radiographic Surface Area (cm ²)	Core ^b Thickness (cm)	Core U Weight (cm)	U Density g/cm Core	U Atom Density a/cm ³ Core x10 ⁻²¹	Preirradiated Plate Thickness (cm)	Clad Thickness (cm)	Core ^c Weight per cm ²	Clad ^d Weight per cm ²	Section Weight per cm ²	Preirradiated ^e Calculated Density (g/cm ³)	Metallurgical ^f Core Thickness For Group (cm)	Preirradiated ^g Calculated Density (g/cm ³)
005	11.94	2.908	4.106	53.828	0.0540	5.73	1.97	5.04	0.1295	0.0755	0.222	0.205	0.427	3.295	0.0574	3.3320
006	11.95	2.883	4.145	53.618	0.0538	5.73	1.99	5.09	0.1300	0.0762	0.223	0.207	0.430	3.307	0.0574	3.3462
007	11.95	2.912	4.104	53.465	0.0545	5.73	1.97	5.04	0.1298	0.0753	0.224	0.204	0.428	3.298	0.0574	3.3297
	Ave	2.901		Ave 53.637	Ave 0.0541		Ave 1.98									
013	13.70	2.998	4.570	54.230	0.0553	7.93	2.65	6.78	0.1295	0.0742	0.253	0.202	0.455	3.507	0.0617	3.5992
019	13.68	2.956	4.628	53.996	0.0547	7.92	2.68	6.86	0.1318	0.0771	0.253	0.209	0.462	3.508	0.0617	3.6100
020	13.69	3.002	4.560	53.946	0.0556	7.92	2.64	6.77	0.1321	0.0765	0.254	0.208	0.462	3.492	0.0617	3.5768
	Ave	2.985		Ave 54.057	Ave 0.0552		Ave 2.66									
022	13.01	2.860	4.550	53.159	0.0538	7.12	2.49	6.37	0.1295	0.0757	0.245	0.206	0.451	3.476	0.0572	3.5251
027	13.03	2.891	4.507	53.593	0.0539	7.13	2.47	6.32	0.1293	0.0754	0.243	0.205	0.448	3.462	0.0572	3.5081
028	13.00	2.877	4.519	53.543	0.0537	7.12	2.47	6.32	0.1295	0.0758	0.243	0.206	0.449	3.476	0.0572	3.5120
	Ave	2.876		Ave 53.432	Ave 0.0538		Ave 2.48									
030	12.51	2.877	4.348	53.090	0.0542	6.32	2.20	5.63	0.1318	0.0776	0.236	0.211	0.447	3.387	0.0561	3.4097
032	12.51	2.845	4.397	53.055	0.0536	6.32	2.22	5.68	0.1308	0.0772	0.236	0.210	0.446	3.404	0.0561	3.4365
033	12.50	2.875	4.348	53.593	0.0536	6.32	2.20	5.63	0.1295	0.0759	0.233	0.206	0.439	3.391	0.0561	3.4224
	Ave	2.866		Ave 53.246	Ave 0.0538		Ave 2.21									

a. Core volume is calculated from core and plate data, Appendix B.

b. Core thickness equals core volume divided by radiographic surface area.

c. Core weight per cm² equals core thickness times core compact density.

d. Clad weight per cm² equals clad thickness times Al 6061 density (2.715 g/cm³).

e. Preirradiated calculated density equals section weight per cm² divided by plate thickness (cm).

f. Metallurgical core thickness for group is given in Reference 5, Table 32.

g. Preirradiated calculated density from metallurgical core thickness.

Table 3. Instability of UAl_2 phase during plate processing

Sample Number	Heat Treatment	Relative Amounts of Aluminide Phase		
		UAl_2	UAl_3	UAl_4
038I	As compacted	71	28	1
038II	Outgassing cycle (500°F, 5 hr)	74	25	1
038III	Outgassing plus hot rolling (910°F, 2 hr)	35	60	5
038III-1	Outgassing plus hot rolling plus blister anneal (925°F, 1 hr)	20	75	5
Typical ATR Powder Blend	Before compacting or heat treatment	8	68	24

$$\frac{\Delta V}{V}\% = -2.13 + 2.37(B)$$

with correlation coefficient, r , of 0.93, where B is the burnup in units of 10^{21} f/cm³. The regression analysis for the punch fission density plus 10% (Table 1) is

$$\frac{\Delta V}{V}\% = -1.82 + 3.14(B)$$

where $r = 0.91$.

The correlation coefficients, r , of 0.93 or 0.91 indicate that the data from all the plates fit the equations very well. The relationship indicates an induction period for swelling equivalent to a fission density of about 1×10^{21} f/cm³. After this induction period, the slope of the equation of 2.37, or 3.14, corresponds to a value of 2.6 noted by other investigators^{9,10} for low temperature-low burnup fuel plates. The slope corresponds to a low

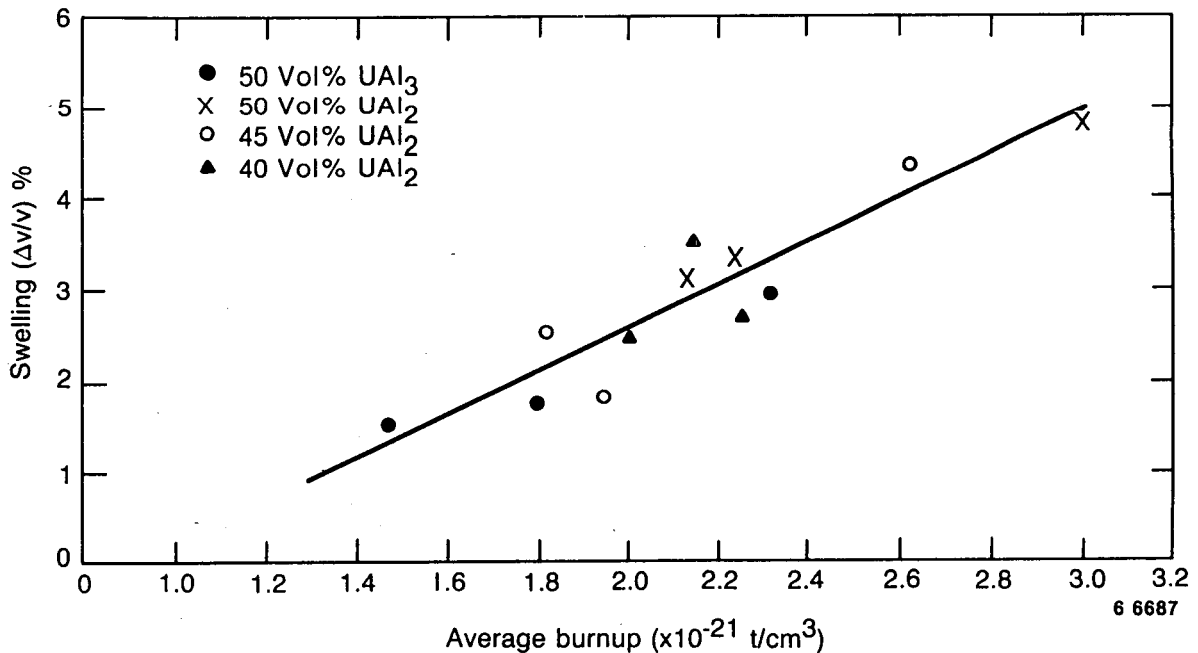


Figure 4. Core swelling versus burnup from immersion density.

relative atomic volume increase for the fission fragments (transmutation products).

3.4.1 Swelling Determined from Thickness Measurements.

The measurement of plate thickness was made in both the hot cell and in the canal (in the hot cell before and after oxide stripping, and in the canal before oxide stripping). In the canal, the oxide thickness was measured by eddy current technique. In the hot cell, the thickness measurements were made with a micrometer. In the canal, the thickness measurements were made with a dial gage mounted on a fixture. Because of variability in the measurements, the thickness measurements were taken to be less accurate than the hot cell measurements. The width of the plates after irradiation was measured in the hot cell and in the canal. Within the accuracy of the measuring technique, no increase in width was detected. Most of the plates had a width less than the original width of 1.005 to 1.008 in. This decrease in width was attributed to corrosion and to sliding the plates in and out of the irradiation fixture for inspection (which was conducted 11 times during the irradiation). From the lack of a width increase, it is postulated that practically all the swelling increase occurs in the thickness direction. The thickness was measured for all plates (except plate 013) in 15 places (5 along the length and 3 on the width) and in one reference position (at the top of the plate) before and after oxide stripping. For plate 013, the thickness was measured in 10 places and averaged. However, on the high side of the plate, the results are averaged separately and a high spot is also given (Table 4). In other plates, peaking in thickness was less than 4%.

The hot cell plate thickness measurements, as well as some canal plate oxide thickness measurements by eddy current, are given in Table 4. The eddy current thickness measurements and the canal plate thickness measurements tended to be slightly larger than the hot cell measurements. The plate thickness measurements in the canal were assumed to be not as accurate because of the variance of the measurements. Hence, only the hot cell plate thickness measurements are given in Table 4. The lower oxide thickness in the hot cell is presumably due to loss of water of hydration. The plate thickness measurements in the hot cell were only accurate to 0.001 cm, as indicated in the column for the reference (position above the fuel) plate thickness. However, the fourth place accuracy indicated in the original plate thickness measurements is doubtful

for some of the plates, so that the reference plate thickness instead of the original plate thickness was used for the core swelling ($\Delta t/t$) calculation for these plates, as indicated in Table 4. The core swelling is calculated from the difference in plate thickness (Δt) divided by the core thickness (t) taken for the composition group.

The micrometer measurements showed a peaking in swelling along one side of plate 013, which was related to the burnup. This peaking also can be seen in the gamma scan results of this plate (Section 3.10). This peaking was looked for in the measurements of other plates. Micrometer measurements were taken along each side and down the middle of each plate; however, because of the position of the micrometer on the plate, measurements were less than 0.002 cm and not tabulated. For plate 013, peaking amounted to a 0.003 cm difference from the average of 10 measurements (as indicated for the high side and high spot, Table 4). Since 0.001 cm is the limit of sensitivity of the micrometer, the fourth place given in Table 4 for the measurements is a mathematical convenience.

The core swelling (except for the high side of plate 013) was plotted in Figure 5 versus the PDQ average burnup, and examined by linear least squares fitting curves. When two points that appear to have too high a swelling in comparison with burnup (due to inaccuracy in the measurement) are eliminated (plates 001 and 010), the swelling for the remaining 25 plates can be represented by the equation

$$\frac{\Delta t}{t}\% = 0.25 + 2.38(B)$$

where B is the average burnup in units of 10^{21} f/cm³. The correlation coefficient, r , of 0.92 indicates a good fit of all the data, so that the swelling of plates in the four groups appear to be similar. Examination by regression analysis of the punch fission density gives

$$\frac{\Delta t}{t}\% = 0.33 + 3.35(B)$$

with $r = 0.86$, a correlation coefficient that is not as good.

3.4.2 Core Thickness Change by Metallography.

The core thickness of the metallography samples at 50X was measured in at least 10 places, at fixed intervals, and averaged. The core thickness change was then calculated using the core thickness calculated in Table 2. The average thickness

Table 4. Thickness measurements of irradiated plates

Plate Number	Original Plate Thickness (cm)	Reference Plate Thickness (cm)	Before Oxide Stripping (cm)	After Oxide Stripping (cm)	Sum Oxide Thickness Both Sides (mm)	Core ^a Thickness Change $\Delta t/t$ (%)	CSAP PDQ Average Burnup (f/cm ³ x 10 ⁻²¹)	Ratio Swelling to Burnup	Canal Oxide Thickness Measurements Both Sides (mm)	Punch ^b Fission Density	Ratio Swelling to Fission Density
001	0.1295	0.130	0.1332	0.1322	0.010	4.1	1.03	4.0	—	—	—
003	0.1295	0.131	0.1325	0.1321	0.004	2.0	0.69	2.9	—	—	—
004	0.1300	0.131	0.1327	0.1325	0.002	2.8	0.88	3.2	0.005	—	—
005	0.1295	—	0.1346	0.1321	0.005	4.8	1.80	2.7	0.016	1.28	3.8
006	0.1300	—	0.1340	0.1329	0.011	5.4	2.30	2.3	0.008	1.73	3.1
007	0.1298	—	0.1324	0.1321	0.003	4.3	1.48	2.9	0.008	1.06	4.1
008	0.1298	0.130	0.1323	0.1319	0.004	3.5	1.23	2.8	0.007	—	—
009	0.1306	—	0.1330	0.1321	0.009	2.8	0.75	3.7	0.006	—	—
010	0.1300	—	0.1338	0.1320	0.018	3.7	0.77	4.8	0.007	—	—
013	0.1295	—	0.1348	0.1341	0.007	8.4	2.98	2.8	0.030	2.02	4.2
015	0.1300	—	0.1317	0.1308	0.009	1.5	1.00	1.5	—	—	—
017	0.1298	—	0.1318	0.1313	0.005	2.7	1.53	1.8	0.007	—	—
019	0.1318	0.130	0.1343	0.1331	0.012	5.6	2.13	2.6	0.010	1.49	3.8
020	0.1321	0.130	0.1337	0.1332	0.005	5.8	2.24	2.6	0.011	1.72	3.4
022	0.1295	—	0.1342	0.1321	0.021	4.8	1.82	2.6	0.010	1.22	3.9
024	0.1303	—	0.1323	0.1318	0.004	2.8	1.15	2.4	0.006	—	—
025	0.1298	—	0.1319	0.1313	0.006	2.8	1.15	2.4	—	—	—
026	0.1300	—	0.1328	0.1317	0.011	3.1	1.08	2.9	—	—	—
027	0.1293	—	0.1329	0.1316	0.013	4.3	1.94	2.2	0.023	1.36	3.2
028	0.1295	—	0.1340	0.1330	0.010	6.5	2.61	2.5	0.015	1.96	3.3
029	0.1303	—	0.1325	0.1321	0.004	3.3	1.04	3.2	0.005	—	—
030	0.1318	0.131	0.1335	0.1337	0.002	5.0	2.25	2.2	0.011	1.52	3.3
031	0.1308	—	0.1339	0.1331	0.008	4.3	1.36	3.2	0.019	—	—
032	0.1308	—	0.1337	0.1335	0.002	5.0	2.14	2.3	0.016	1.49	3.4
033	0.1295	—	0.1329	0.1323	0.006	5.2	2.00	2.6	0.003	1.42	3.7
034	0.1318	—	0.1339	0.1332	0.007	2.6	1.61	1.6	0.006	—	—
036	0.1321	—	0.1342	0.1329	0.013	1.5	0.54	2.8	0.012	—	—
013	high side	—	0.1378	0.1376	0.002	14.7	3.0	4.9	—	3.0 ^c	—
013	high spot (bottom)	—	0.1400	0.1400	0.000	19.1	4.2	4.5	—	3.0 ^c	—

a. The core thickness change (swelling calculation) is based on a core thickness of 0.054 cm for all except the 50 vol% UAl₂ for which 0.055 cm was used (see Table 2). The original plate thickness was used for all plates except those for which the reference plate thickness is shown.

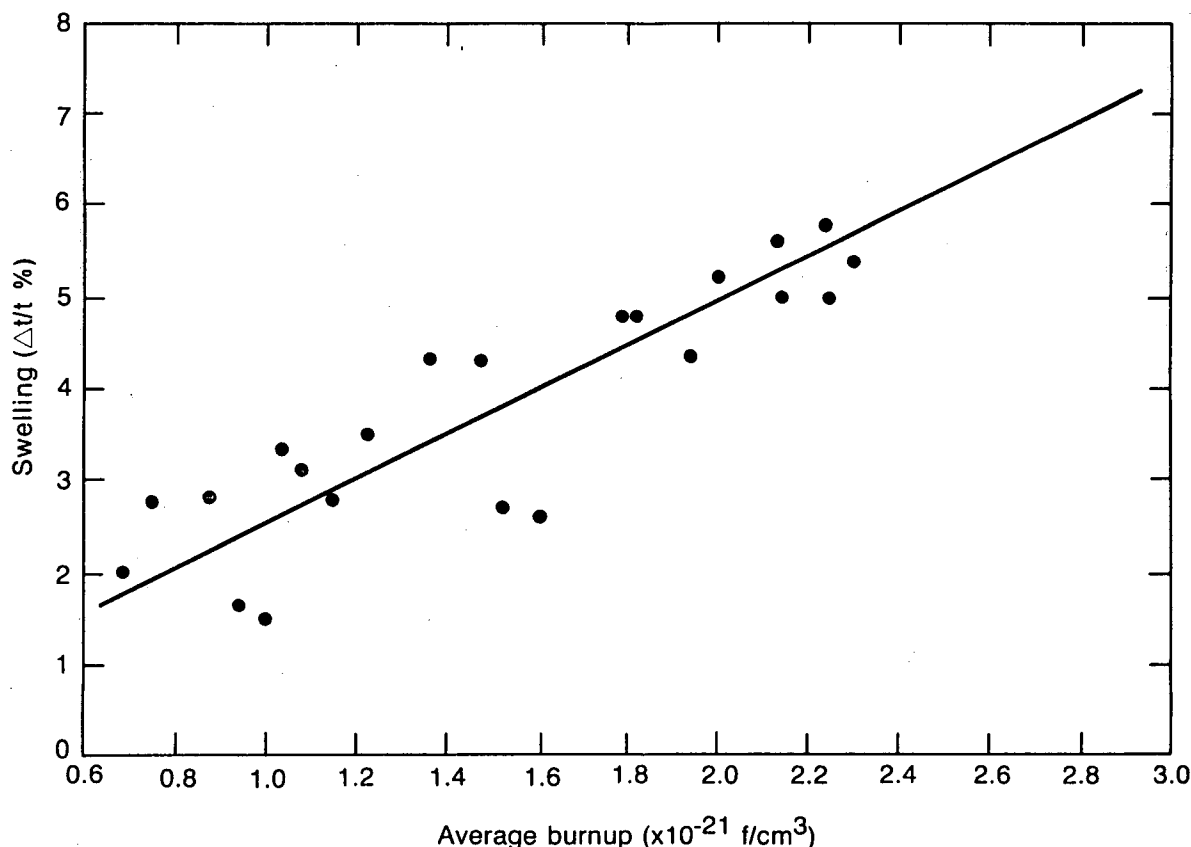
b. Table 13 plus 10%. The low punch fission density plus 10% gives an average fission density equivalent to the CSAP PDQ average. See Section 3.11.

c. Table 13.

values^a and the calculated core thickness change is given in Table 5; a comparison with immersion density and plate thickness measurements is also given. It is noted that core thickness change, as measured by metallography, is larger than the

immersion density change or the plate core thickness change. Since the metallurgical core thickness change includes changes due to reaction of the fuel with the cladding, as well as that due to swelling, the larger values seem reasonable. Photographs of plates No. 002 and 014, used for metallography and not irradiated, are shown at 50X in Figure 6(a) and (b). Photographs of plates No. 007 and 013 after irradiation are shown in Figure 6(c) and (d). The voidage or brittle phase pullout during polishing appears similar in photographs taken before and after irradiation of plates from the same

a. If an attempt is made to correct the average thickness values by multiplying by the ratio of the oxide stripped plate thickness (Table 4) to the metallography measured plate thickness, the percent thickness change becomes more random with respect to burnup. Rounding of the plate during polishing apparently produces this effect; hence, the average measured core thickness from the metallography was used.



6 6686

Figure 5. Core swelling versus burnup from thickness measurements.

composition group (50 vol% UAl_3 , for plates No. 002 and 007; and 50 vol% UAl_2 for plates No. 014 and 013). An image analysis of the voidage was made as seen in Table 6.

From the comparison in Table 6 for plates 007 and 013 which were irradiated, and plates 002 and 014 which were not, it is seen that the void volume has not changed much with the core thickness increase due to irradiation.

A comparison of average core thickness of the four groups (50 vol% UAl_3 , 50 vol% UAl_2 , 45 vol% UAl_2 , and 40 vol% UAl_2) as determined from the core volume and radiographic surface area,^a with that of the metallurgical core thickness measured before irradiation^a and after irradiation^b gives an indication of the relative stability of the three aluminide phases (UAl_2 , UAl_3 and UAl_4). As

a. Table 2.

b. Table 5.

is seen in Table 7, the 50 vol% UAl_2 changes most during plate fabrication with an 11.8% change in core thickness. It is noted, however, that the total change from fabrication and irradiation is about the same as for the other groups at 13% total change.

3.5 Metallography

The metallography was done on $3/8 \times 3/4$ in. punchings from the middle of the fuel plate (Figure 3). A metallography sample was taken from each of the 12 plates. The aim of the metallography was to show the microstructure of the core and cladding, the clad-core interface, the thickness of the core and cladding, and the integrity of the fuel. The sections were examined on the metallograph and on the scanning electron microscope. For the examination, the sections (punchings) were mounted and polished with 6 and then 3 micron diamond paste. The samples were then polished and etched with Magomet No. 40-6440AB (MgO , 1-5 micron, pH 8-9.5 in water). A repolish was

Table 5. Comparison of metallurgical core thickness change with immersion density change and plate thickness change

Plate Number	Average Core Thickness (cm)	Metallurgical Core Thickness Change (%)	Immersion Density Change (%)	Plate-Core Thickness Change (%)
005	0.0615	13.9	1.81	4.8
006	0.0601	11.7	3.03	5.4
007	0.0625	14.7	1.54	4.3
Avg	0.0613			
013	0.0634	14.6	4.88	8.4
019	0.0628	14.8	3.16	5.6
020	0.0605	8.8	3.43	5.8
Avg	0.0622			
022	0.0607	12.8	2.56	4.8
027	0.0605	12.2	1.86	4.3
028	0.0628	16.9	4.29	6.5
Avg	0.0613			
030	0.0601	10.9	2.74	5.0
032	0.0593	10.6	3.60	5.0
033	0.0597	11.4	2.52	5.2
Avg	0.0597			

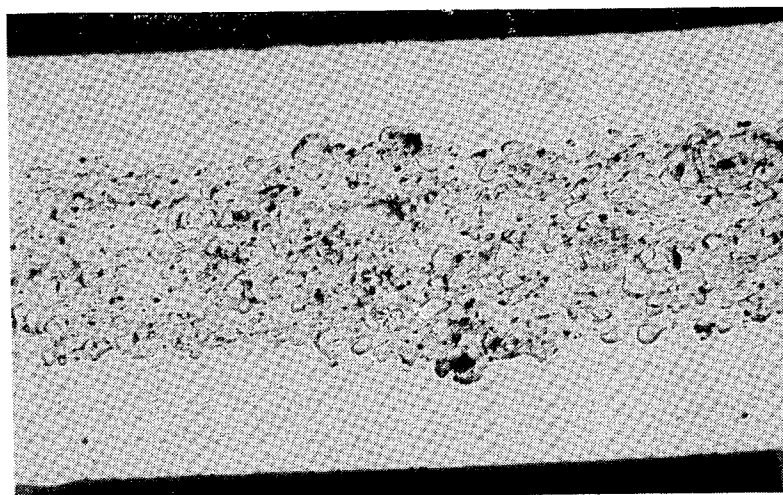
done by hand on one sample, and etched with 15% sulfuric acid/85% hydrogen peroxide. The results of the acid etch will be described in the scanning electron microscopy section.

The thickness of the core and cladding of the 50 vol% UAl_3 and 50 vol% UAl_2 is shown in Figure 6. The thickness has been discussed in the section on thickness changes. The voidage before and after irradiation appears to be about the same at 50X and was measured by image analysis as about the same. Thus, although the voidage has not filled with the swelling, the integrity of the fuel looks sound (free from blisters and cracks).

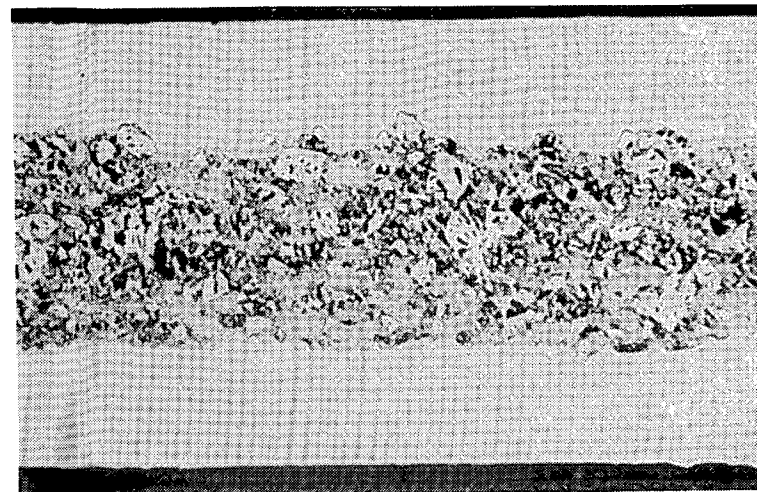
Although the metallography samples were punched to include all of the core (Figure 3), so that the effect of the burnup peaking might be examined, it was not evident in the metallography samples. The fuel structure looked sound at the ends of the plate width. Scanning electron microscopy was more limited in the extent of scanning that could be achieved, but no effect was detected by SEM. The structure looked sound except for some small bubbles which will be described in Section 3.6.

The microstructure of the core and cladding is shown in Figure 7(a) through (d) for the 50 vol%

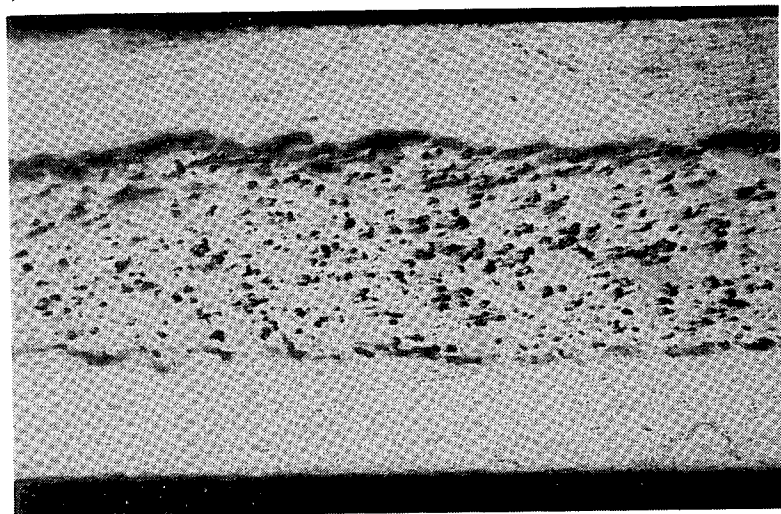
UAl_3 and 50 vol% UAl_2 at 200X and 500X. Although the cladding microstructure shows a tangled structure due to irradiation damage, the integrity of the fuel looks good. A fission fragment stopping zone (at the fuel-clad interface) can be seen, which is about 10-20 microns in width. This zone etches lighter than the 6061 Al cladding. The polished and etched (Magomet) fuel surface looks sound, so that few bubbles can be seen in the surface at 500X. In Figure 8 (a) through (d), the microstructure of the polished surface of the 45 vol% and 40 vol% fuel core composition can also be seen at 200X and 500X. Again, the microstructure looks sound. No bubbles or cracks can be seen in fuel grains. An effort was not made to distinguish metallographically the relative amounts of the three phases UAl_2 , UAl_3 and UAl_4 in the fuel grains, since the plates were irradiated at a temperature (120°C) making this distinction difficult. The Magomet etch just makes the phases discernible (Figure 9). It was expected that reductions in the relative amounts of UAl_2 and UAl_3 , because of reaction with the aluminum matrix, would occur as shown in Table 3, and as shown for plates irradiated at low temperature (70°C) in the literature.¹⁰ As long as an excess of the aluminum matrix is present and bubbles and cracks are not seen, the



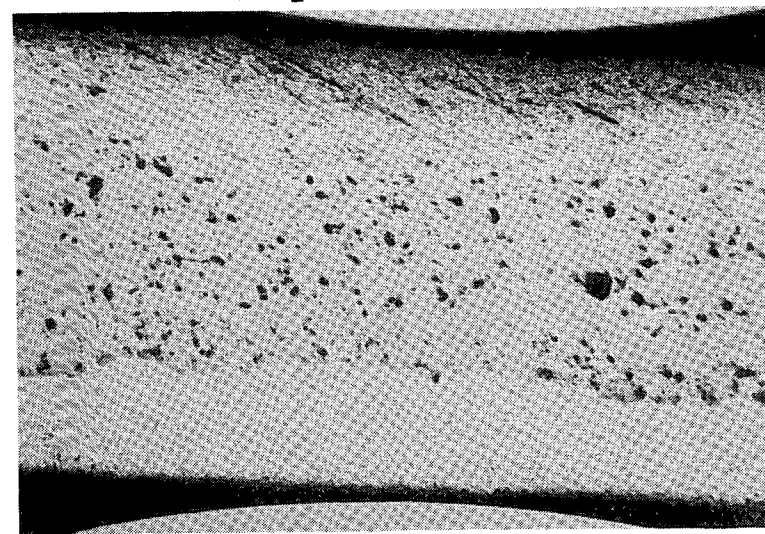
(a) Plate No. 002 before irradiation; composition 50 vol%, UAl_3 , void vol. 6.2%, 50x



(b) Plate No. 014, before irradiation; composition 50 vol%, UAl_2 , void vol. 8.3%, 50x



(c) Plate No. 007, burnup $1.48 \times 10^{21} \text{ f/cm}^3$; composition 50 vol% UAl_3 , void vol. 9.1% 50x



(d) Plate No. 013, burnup $2.98 \times 10^{21} \text{ f/cm}^3$; composition 50 vol% UAl_2 , void vol. 10.1% 50x

Figure 6. Plate and core thickness before and after irradiation.

Table 6. Image analysis of voidage

	Plate No. 002	Plate No. 007	Plate No. 013	Plate No. 014
Void vol%	6.2	9.1	10.1	8.3
Void vol% by Reference 15	7.5 \pm 0.4 ^a	8.04	11.04	11.01 \pm 0.8 ^b

a. Average of group (9 plates) for 50 vol% UAl₃.

b. Average of group (7 plates) for 50 vol% UAl₂.

fuel core behavior is judged to be sound. An examination of the effect of the reactions was made by Scanning Electron Microscopy (SEM).

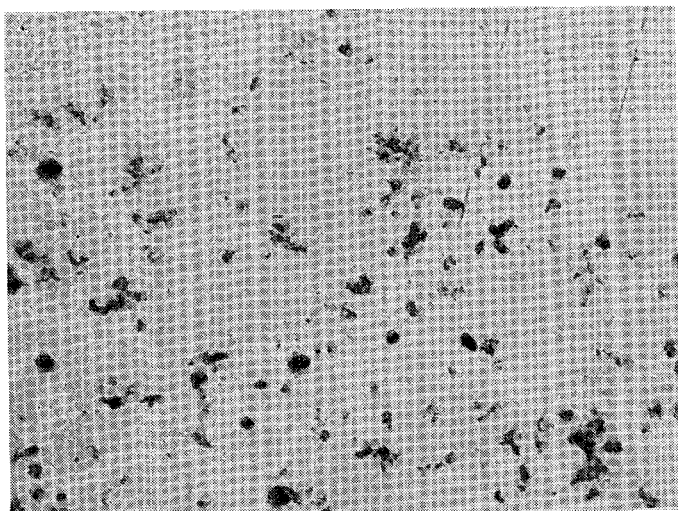
3.6 Scanning Electron Microscopy

Scanning electron microscopy was performed on fractured surfaces of the fuel as well as on the polished and etched surfaces. The examination of the fractured surfaces¹⁶ will be discussed first. Small punchings (~2 mm) of plates 013 and 032 containing UAl₂, and plate 006 containing UAl₃, were obtained.¹⁶ The punchings were fractured through the fuel, and the fractured surface examined on the SEM by secondary and back scatter emission, and by Kevex-ray emission (Figures 10, 11, 12 and 13). The secondary emission photographs of plates 013 and 032 (Figures 10 and 11) show patches of voids, or small bubbles, and patches of ductile tearing of the aluminum matrix. The centers of the fuel grains

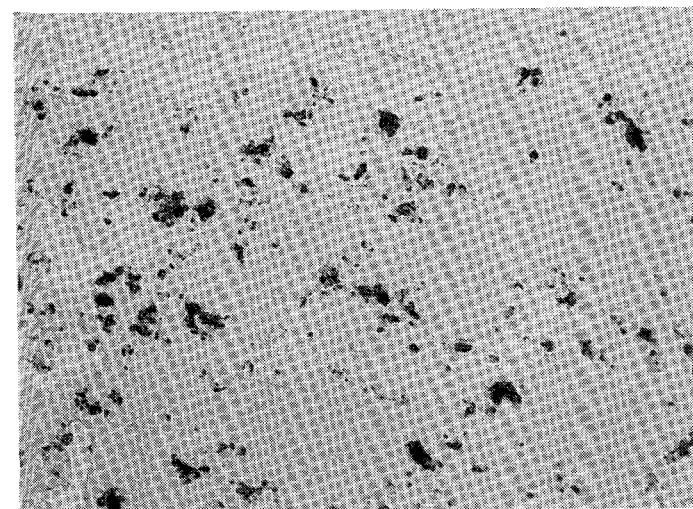
are relatively free of any defects (voids or bubbles) at 600X, and at higher magnification (2000X), Figure 13(a). Back scatter emission (Figure 12) shows a difference in contrast due to the three phases (UAl₂, UAl₃, and UAl₄) as was seen in Figure 9 by metallography. The identification of these three phases was made by Kevex-ray (Figure 13). A grain in Figure 12 (magnified to about 2000X and the regions identified as 2, 3, 4) and a phase of U-O was examined by Kevex-ray and indicated in Figure 13(c), (d), (e) and (f). The regions were identified respectively, as UAl₂, UAl₃, UAl₄, and a phase of U, probably an oxide. The presence of the U phase is surprising, although present in small amounts (<1%). Small bubbles were associated with this U phase. It was not detectable in the powder blend, nor in the compact examined by x-ray analysis (Table 3). The U phase is found in void regions, where accessibility of aluminum is limited, or trapped oxygen would be present. It was also

Table 7. Comparison of core thickness change during fabrication and irradiation

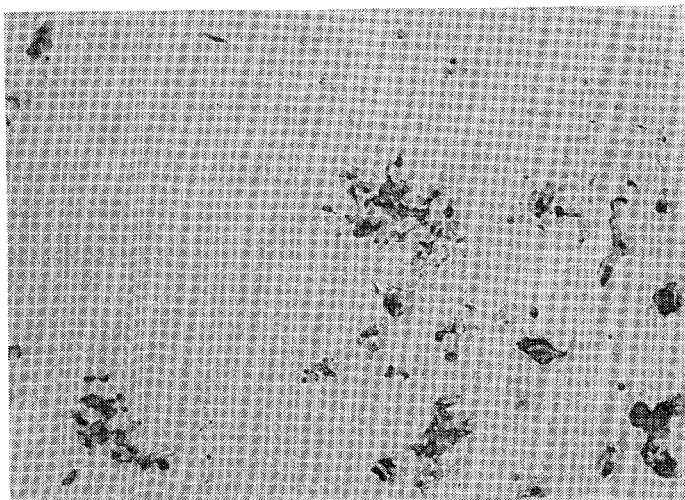
Plate Number	Principal Composition of Group	Calculated Average Core Thickness (Table 2)	Metallurgical		Change After Fabrication (%)	Change After Irradiation (%)	Total Change (%)
			Before Irradiation (Table 2)	After Irradiation (Table 5)			
006-007	50 vol% UAl ₃	0.0541	0.0574	0.0613	6.1	6.8	12.9
013-020	50 vol% UAl ₂	0.0552	0.0617	0.0622	11.8	0.8	12.6
022-028	45 vol% UAl ₂	0.0538	0.0572	0.0613	6.3	7.4	13.7
030-033	40 vol% UAl ₂	0.0538	0.0561	0.0597	4.3	6.4	10.7



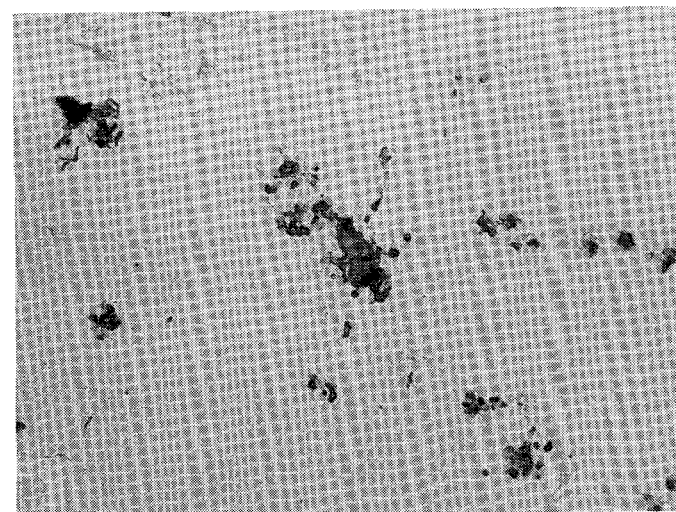
(a) Plate No. 005, composition 50 vol% UAl_3 , burnup $1.8 \times 10^{21} \text{ f/cm}^3$ 200x



(b) Plate No. 013, composition 50 vol% UAl_2 , burnup $2.98 \times 10^{21} \text{ f/cm}^3$ 200x

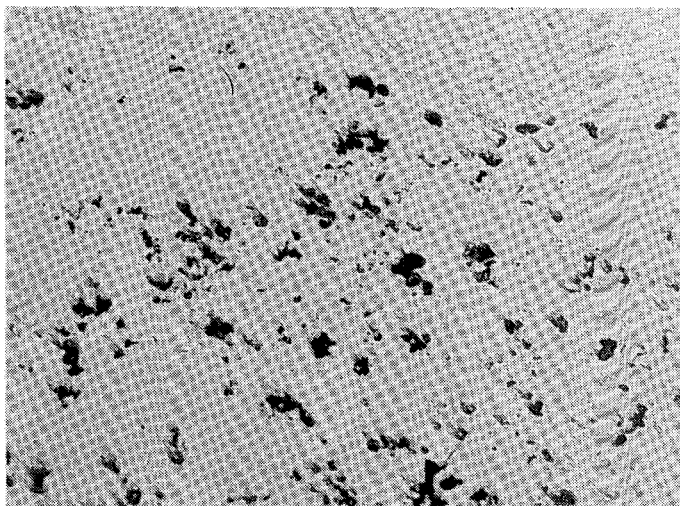


(c) Plate No. 005, composition 50 vol% UAl_3 , burnup $1.8 \times 10^{21} \text{ f/cm}^3$ 500x

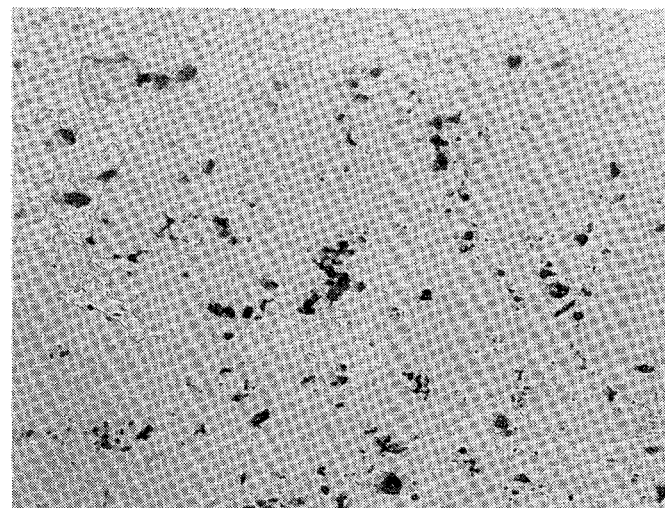


(d) Plate No. 013, composition 50 vol% UAl_2 , burnup $2.98 \times 10^{21} \text{ f/cm}^3$ 500x

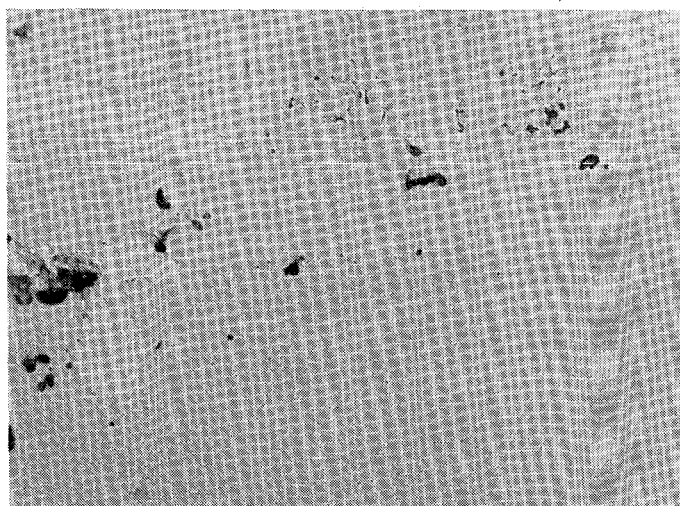
Figure 7. Microstructure of core and cladding of 50 vol% UAl_x .



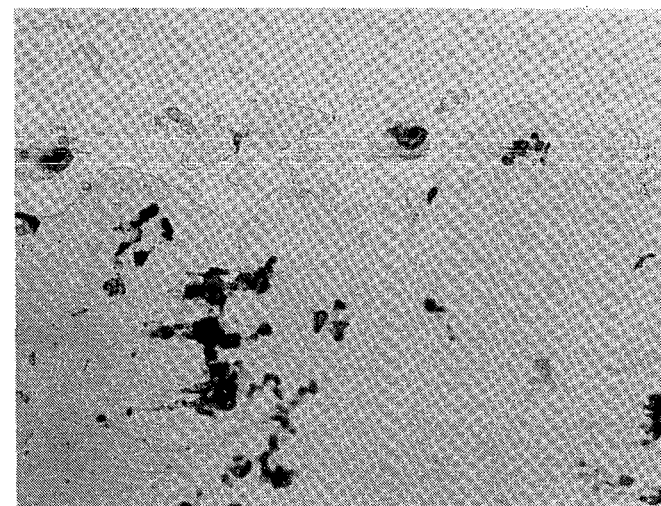
(a) Plate No. 027, composition 45 vol% UAl_2 , burnup $1.94 \times 10^{21} \text{ f/cm}^3$ 200x



(b) Plate No. 033, composition 40 vol% UAl_2 , burnup $2.0 \times 10^{21} \text{ f/cm}^3$ 200x

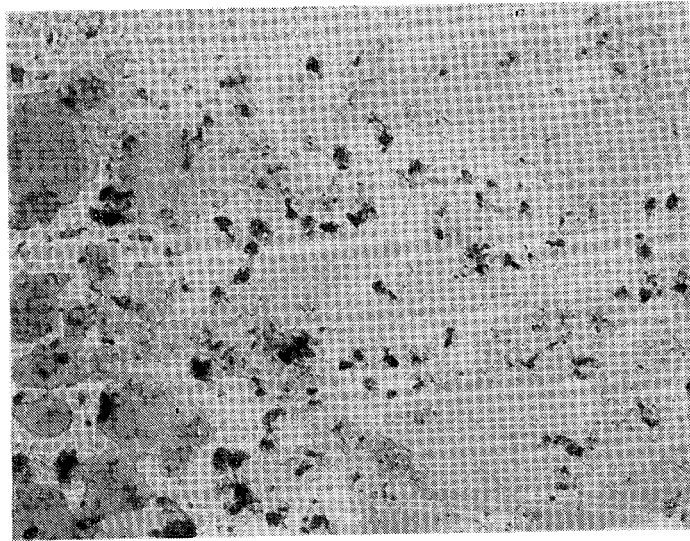


(c) Plate No. 027, composition 45 vol% UAl_2 , burnup $1.94 \times 10^{21} \text{ f/cm}^3$ 500x

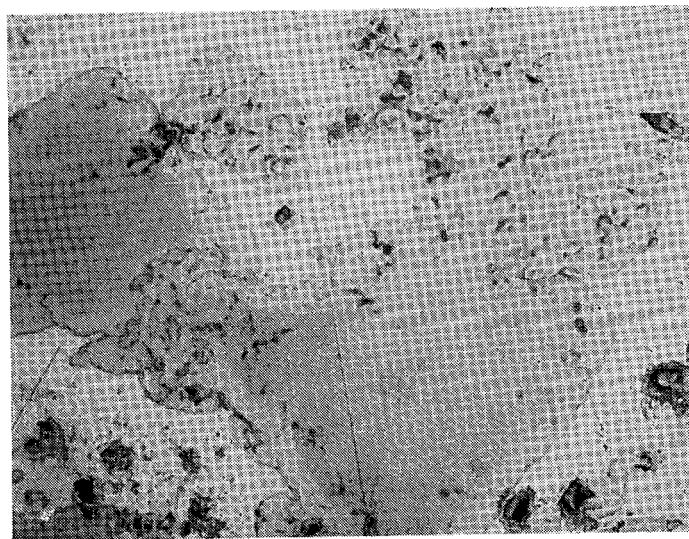


(d) Plate No. 033, composition 40 vol% UAl_2 , burnup $2.0 \times 10^{21} \text{ f/cm}^3$ 500x

Figure 8. Microstructure of 45 vol% and of 40 vol% UAl_2 .



(a) Plate 032 metallography 200x



(b) Plate 032 metallography 500x

Figure 9. Fuel grains of UAl_x in aluminum matrix. UAl_2 , UAl_3 and UAl_4 just discernable with Magomet etch.



Figure 10. SEM photograph of fractured surface by secondary emission, plate 013.

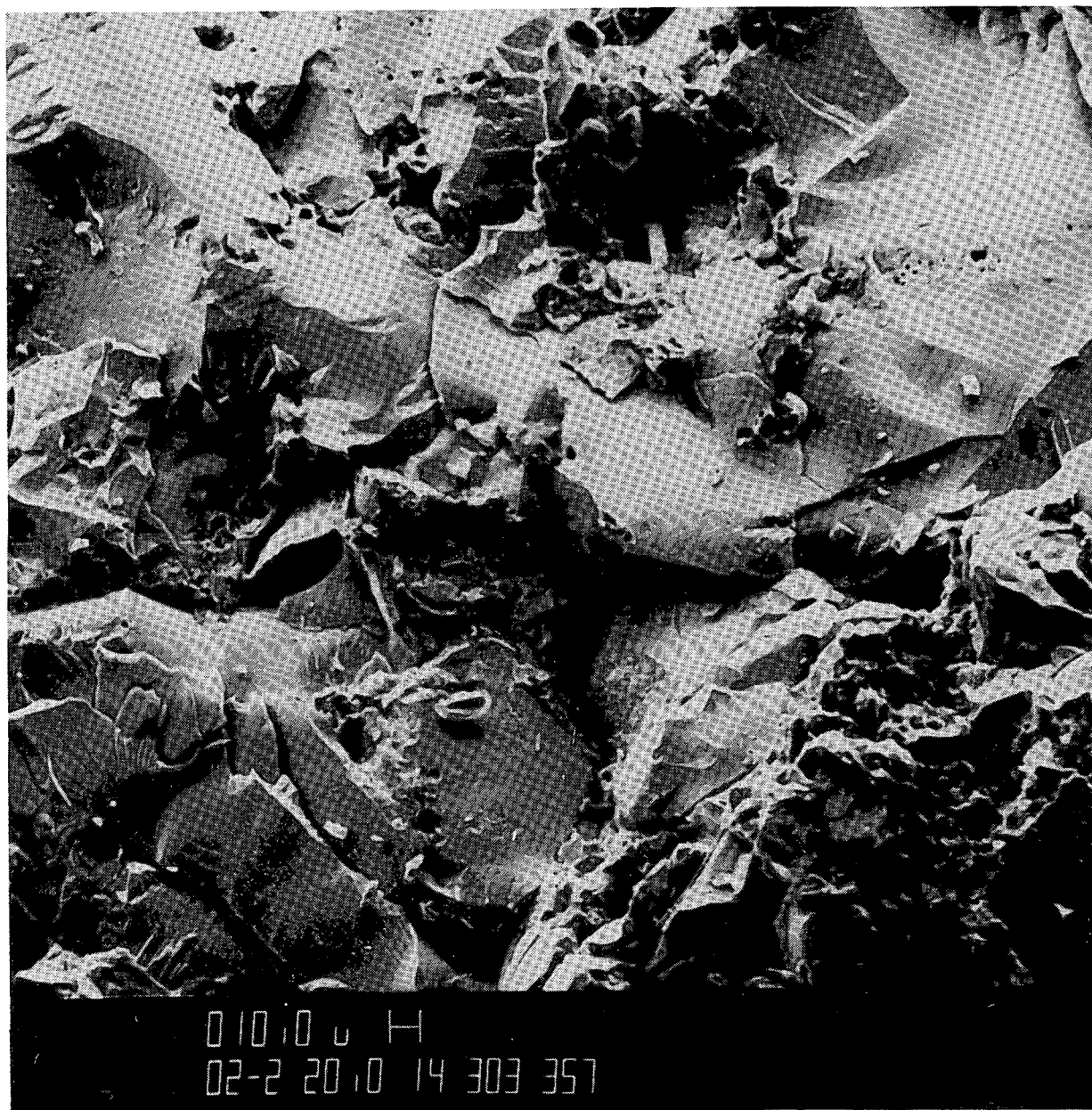


Figure 11. SEM photograph of fractured surface by secondary emission, plate 032.

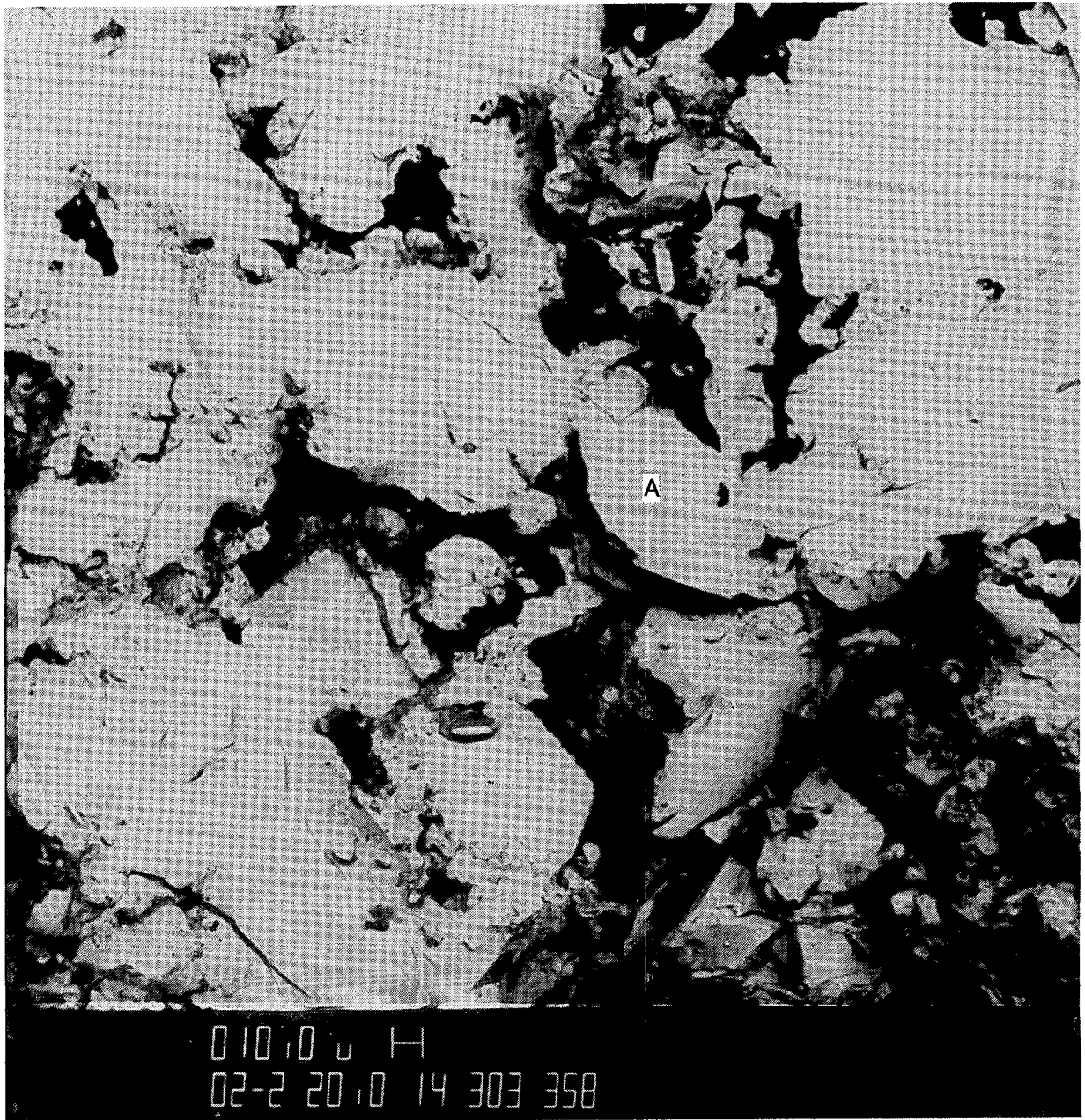
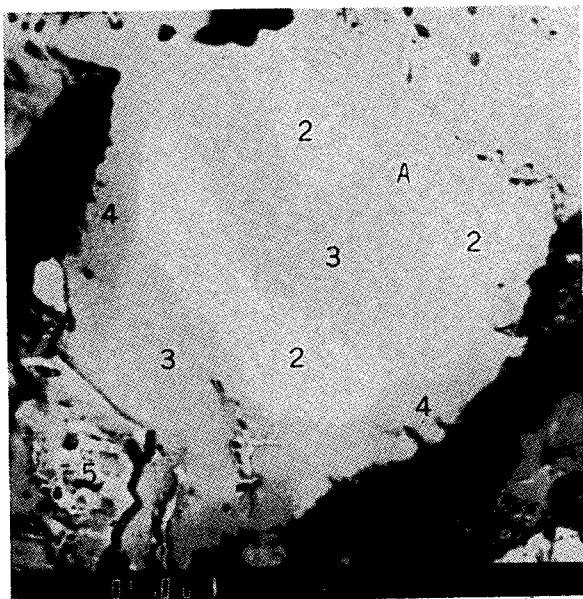
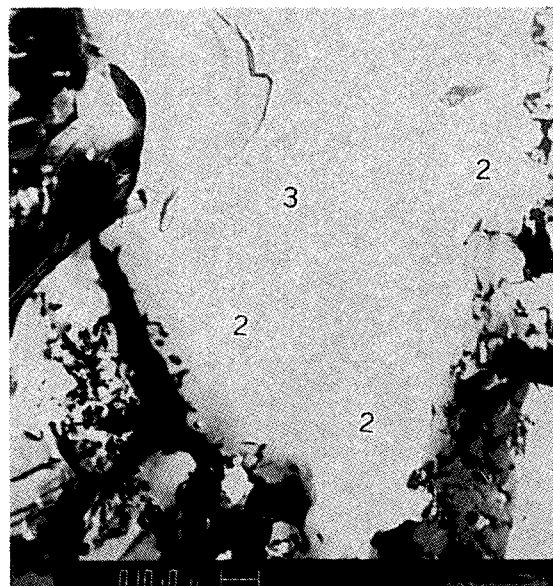


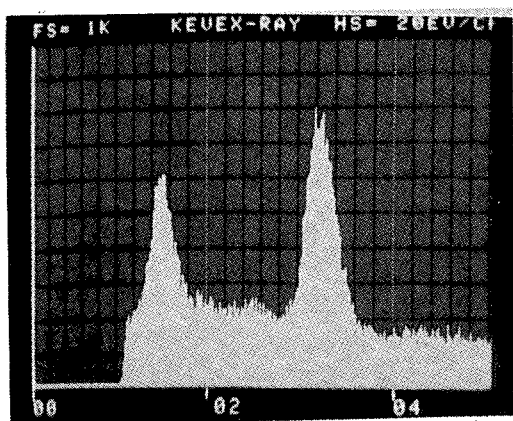
Figure 12. SEM photograph of fractured surface by back scatter emission (plate 032) identifies region A of Kevex-ray examination.



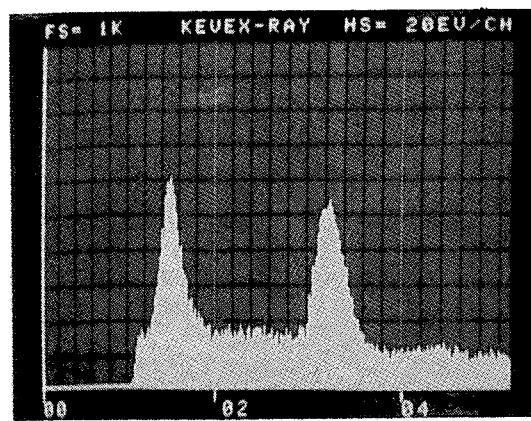
(a) Grain A for Kevex-ray examination



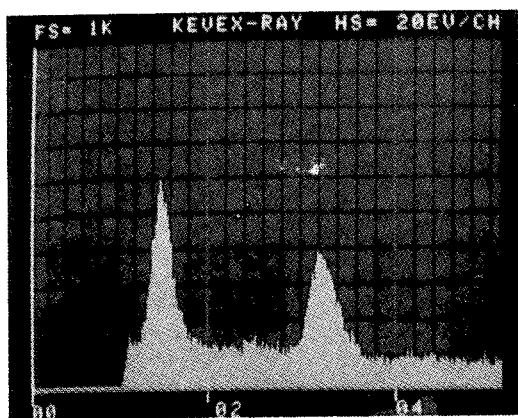
(b) Another fuel grain



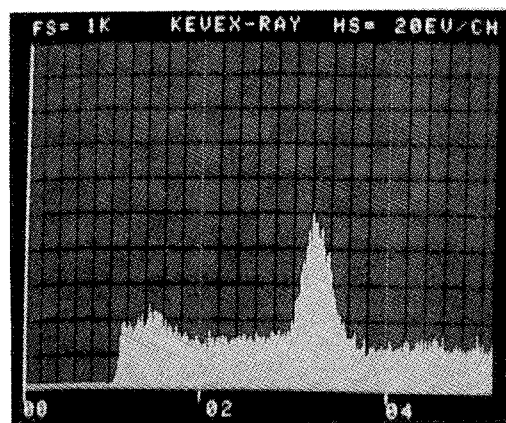
(c) Region 2, UA_{12}



(d) Region 3, UA_{13}



(e) Region 4, UA_{12}



(f) Region 5, U

Figure 13. Examination of fuel grain A for UA_{12} , UA_{13} , UA_{14} and U.

found at the outskirts of the fuel grains, where reaction with the aluminum matrix occurred; pickup of surface oxygen on aluminum powder would have taken place. The outskirts of the fuel grains are also the regions where UAl_4 predominates. The photograph of Figure 13(a) was examined on the image analyzer to determine the percent of UAl_2 , UAl_3 , and UAl_4 in that fuel grain. The percentages obtained were UAl_2 , 17%; UAl_3 , 50%; and UAl_4 , 33%. These percentages are to be compared with those of sample 038III-I that had received the heat treatment outgassing, hot rolling, and blister anneal (925°F, 1 hr). The percentages of sample 038III-I are UAl_2 , 20%; UAl_3 , 75%; and UAl_4 , 5% (Table 3). Thus, irradiation has reduced the percent of UAl_2 and increased the percentage of UAl_4 present in the fuel grains.

Samples of the powder from UAl_3 and UAl_2 composition blends were examined by SEM for any evidence of uranium separate from aluminum. The Kevex-ray examination showed no uranium separate from aluminum in over 70 particles taken from each of the samples of the JJ and JF composition blends. Variances in the atomic percent of uranium and aluminum occurred. This was especially true in the weight percent; however, aluminum was always present with the uranium.

SEM examination was performed on the polished and etched surfaces of the metallography samples for any evidences of bubbles, cracking, or irradiation damage. The SEM surface examination was performed on an Amray SEM 1200B, which had been modified to accept irradiated samples. The top 1/4 in. of the metallurgical mounts were sliced on a Leeco Varicut saw and mounted on a SEM stem for insertion into the SEM. The surface was coated with gold (on an Ernest F. Fullam Sputter Coater at 100 microns vacuum) to provide surface conductivity and enhance contrast. The surface was examined at 200X, 500X, 1000X, and 3000X on all 12 samples. Any difference in irradiation damage was slight. A polishing and etching effect between the Magomet and the 15% sulfuric acid - hydrogen peroxide was noticed, wherein some of the Magomet particles were trapped in the voids or etch pits. These were small, less than 5 microns, and randomly distributed in the cladding as well as the fuel. These white Magomet particles were eliminated after the repolish and etch with 15% sulfuric acid - hydrogen peroxide.

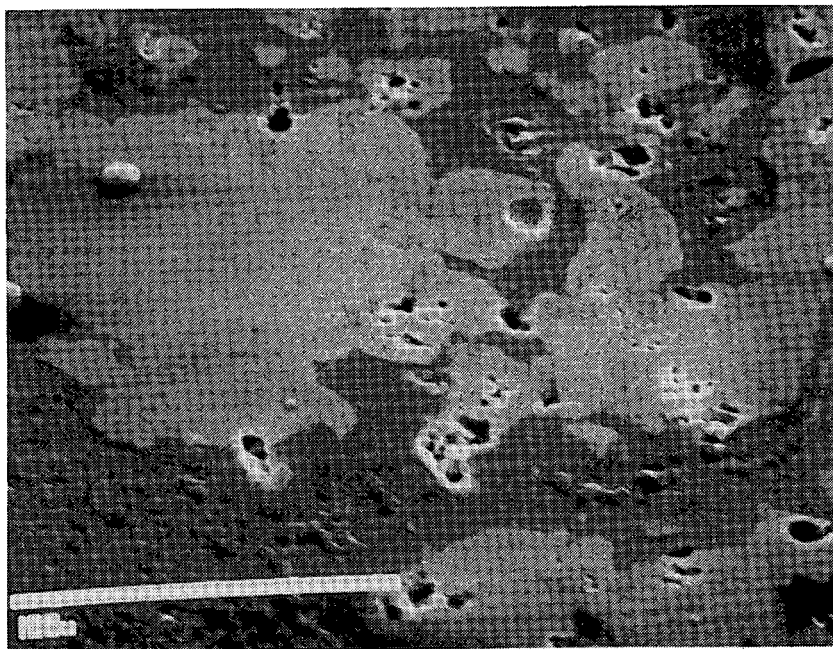
Representative photographs of low burnup plates (No. 007 and No. 019) from 50 vol%

groups, as well as representative photographs of plates of high burnup from each composition group are presented (e.g., plate No. 006 from 50 vol% UAl_3 ; plate No. 013 from 50 vol% UAl_2 ; plate No. 028 from 45 vol% UAl_2 ; and plate No. 030 from 40 vol% UAl_2), Figures 14 through 19. Photographs of plate No. 013, after the repolish and acid etch, are also shown, Figure 20. The SEM photographs, with their larger depth of field at focus, show the fabrication voids more clearly than the metallography photographs. For example, compare Figure 7(c) of plate No. 005 with Figure 14(a) of plate No. 007 (both at 500X). The low burnup of the 50 vol% UAl_3 (plate No. 007) and the 50 vol% UAl_2 (plate No. 019) show little difference in fuel damage (Figures 14 and 15). The four compositions (50 vol% UAl_3 , 50 vol% UAl_2 , 45 vol% UAl_2 , and 40 vol% UAl_2) also show little difference in damage to the fuel (Figures 16, 17, 18, and 19). The white bubbles appearing in Figures 14 through 19 (where the plates were finished with a Magomet polish-etch) are eliminated in Figure 20(a) through 20(f) (where they were repolished with 6 and then 3 micron diamond paste and acid etched). The cladding in Figure 20(f) shows some etch pits. These pits were present in the cladding of all the plates.

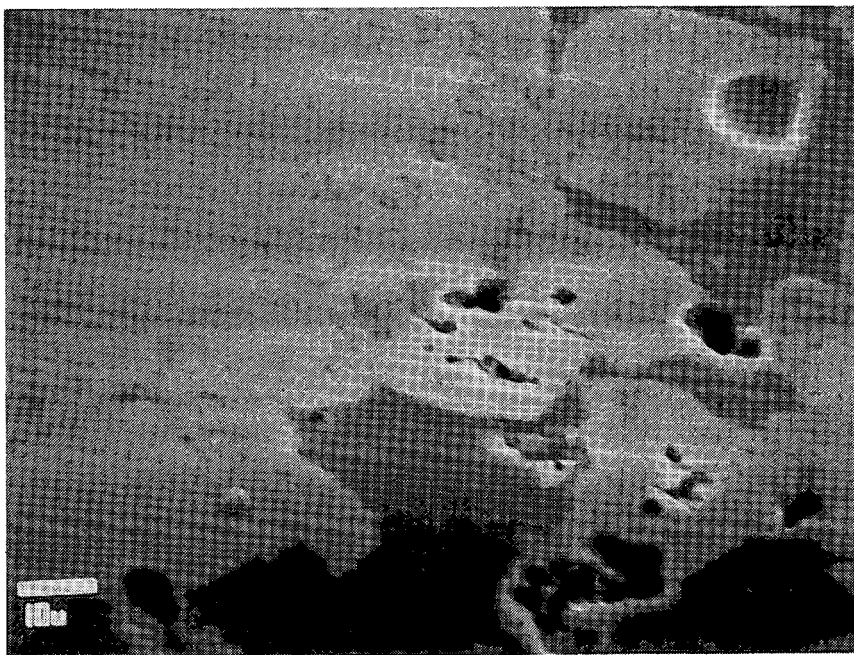
3.7 Blister Tests

Blister testing is used as a means of evaluating the behavior of the fuel core with respect to fission gas agglomeration. As the fission gas agglomerates, visible blistering of the fuel plate surface occurs. The blister test is conducted by starting at a furnace temperature slightly above the peak plate operating temperature, and heating in successive increased temperature steps for periods of one-half hour. Thus, at a temperature above the third from the last step, the plate section would have been heated for one and one-half hours, plus longer times at lower temperatures. When a blister is first discerned, the test is terminated for that sample.

The maximum nominal and two sigma plate operating temperatures were 395 K and 407 K, respectively, which decreased with operating time. The initial heating temperature step was at 563 K for one-half hour. Since the blister test heating is terminated after the blisters are visually detected, the blister temperature for a one hour anneal is taken as the step temperature before the test is terminated and blisters are visually detected. The



(a) Fuel at 500x, dark area is matrix aluminum

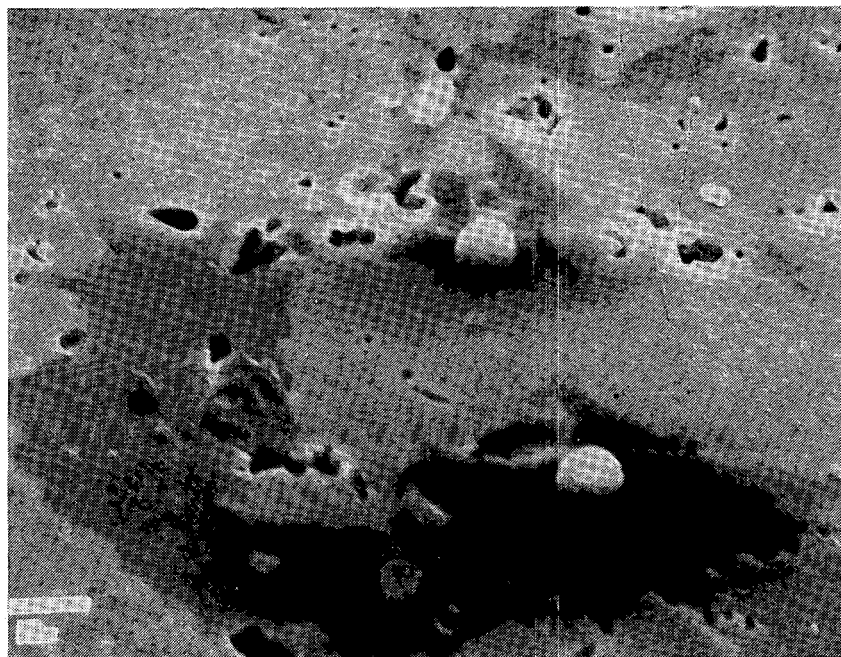


(b) Fuel at 1000x, dark area is matrix aluminum

Figure 14. SEM photographs of plate 007, composition 50 vol% UAl_x .

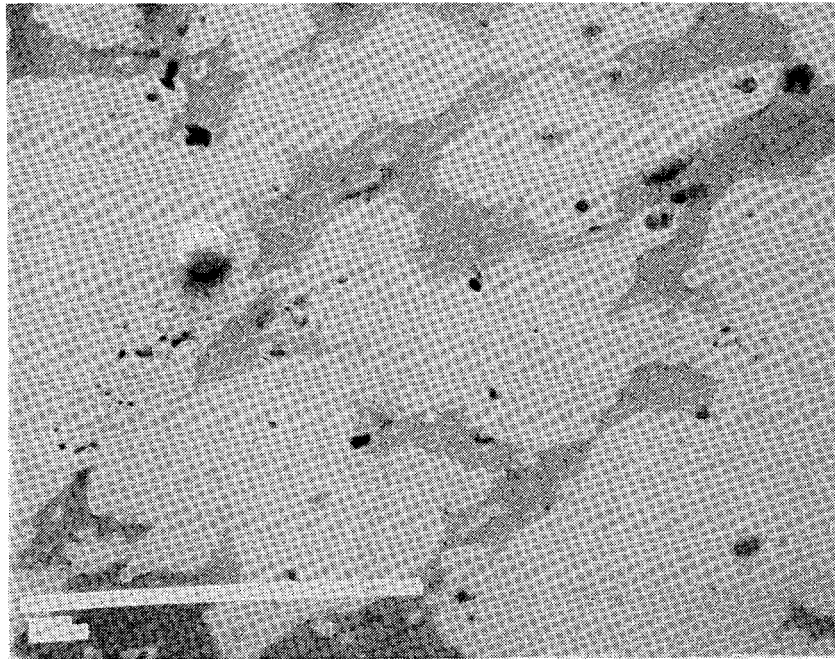


(a) Fuel at 500x

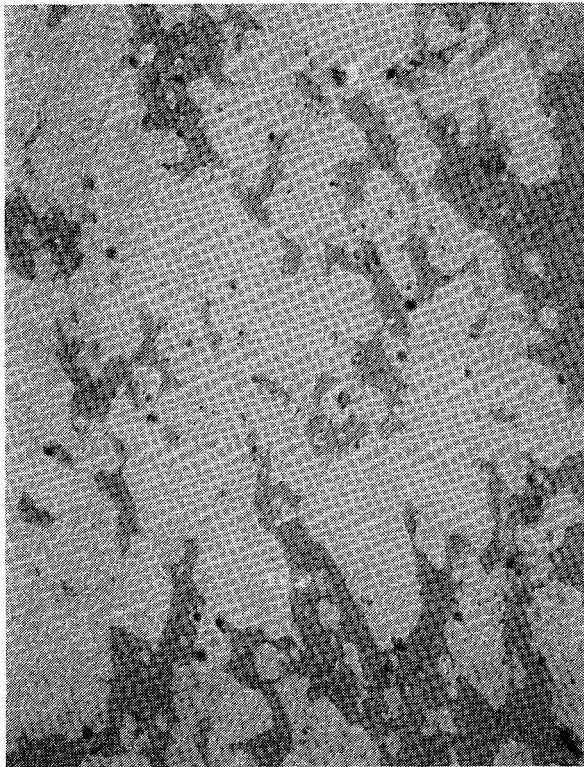


(b) Fuel at 1000x

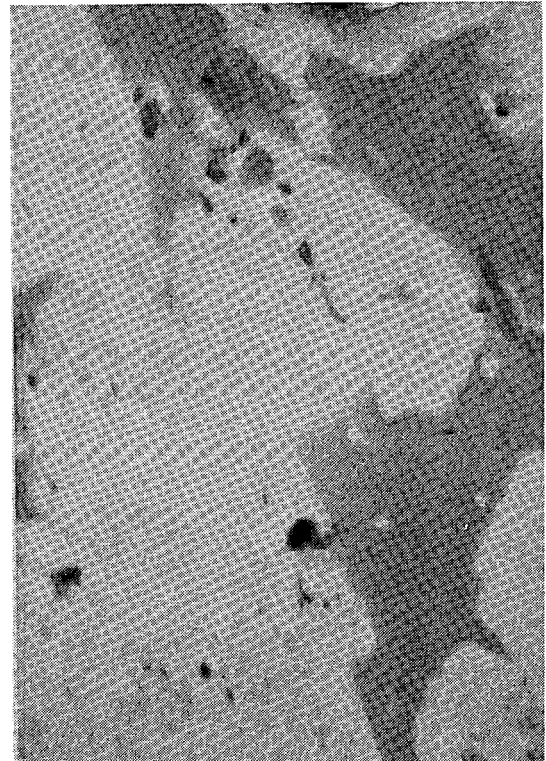
Figure 15. SEM photographs of plate 019, composition 50 vol% UAl_2 .



(a) Fuel at 500x

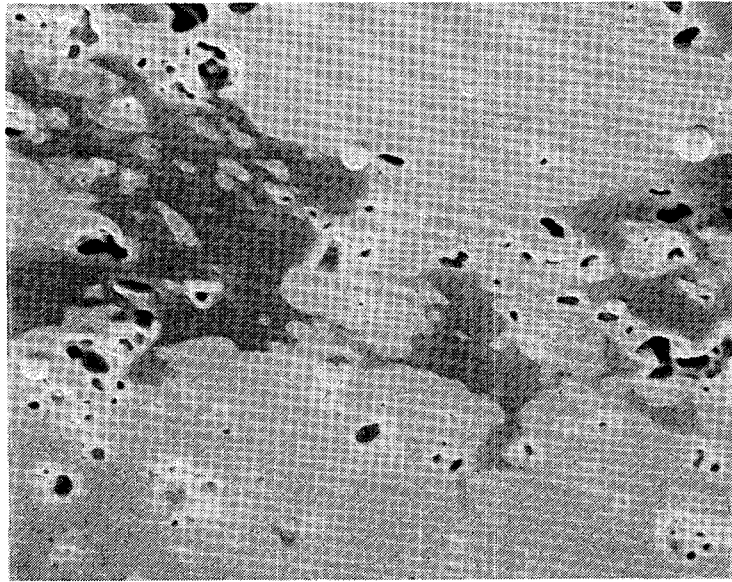


(b) Fuel at 200x

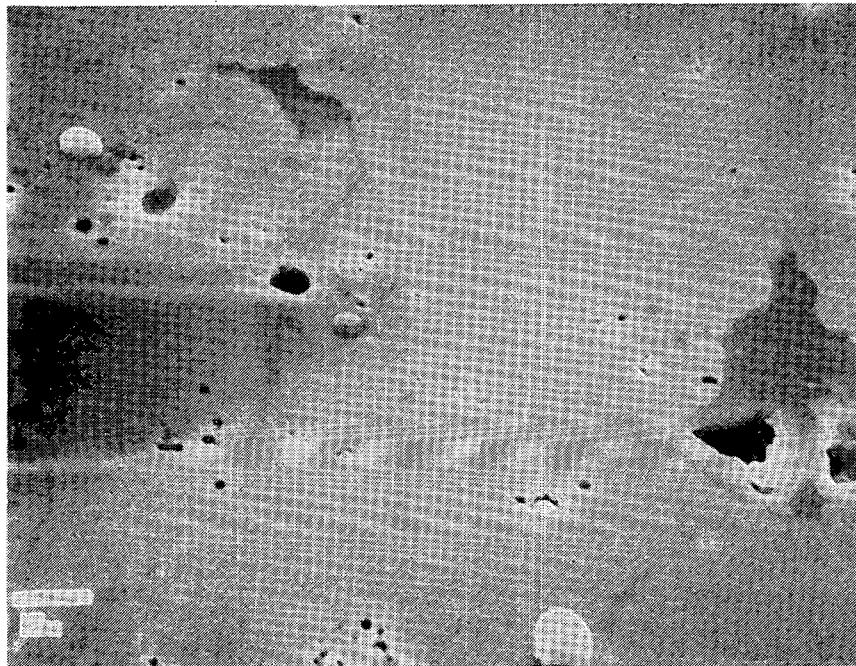


(c) Fuel at 1000x

Figure 16. SEM photographs of plate 006, composition 50 vol% UAl_x .

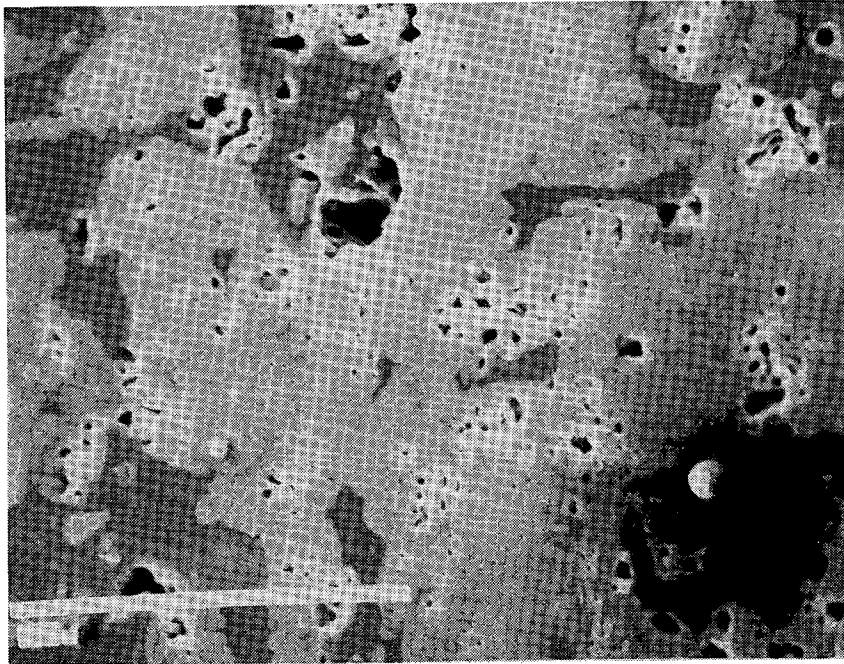


(a) Fuel at 500x

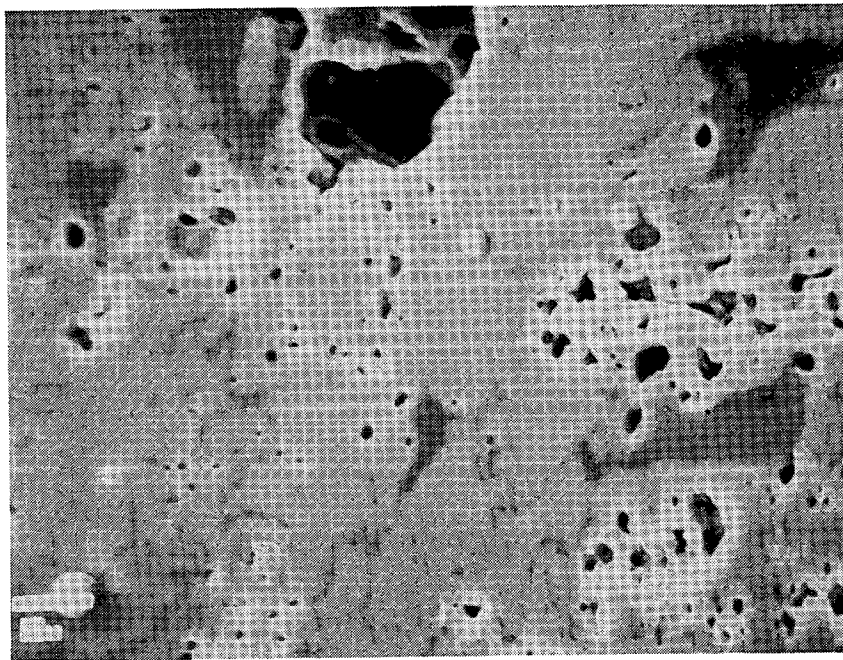


(b) Fuel at 1000x

Figure 17. SEM photographs of plate 013, composition 50 vol% UAl_2 .

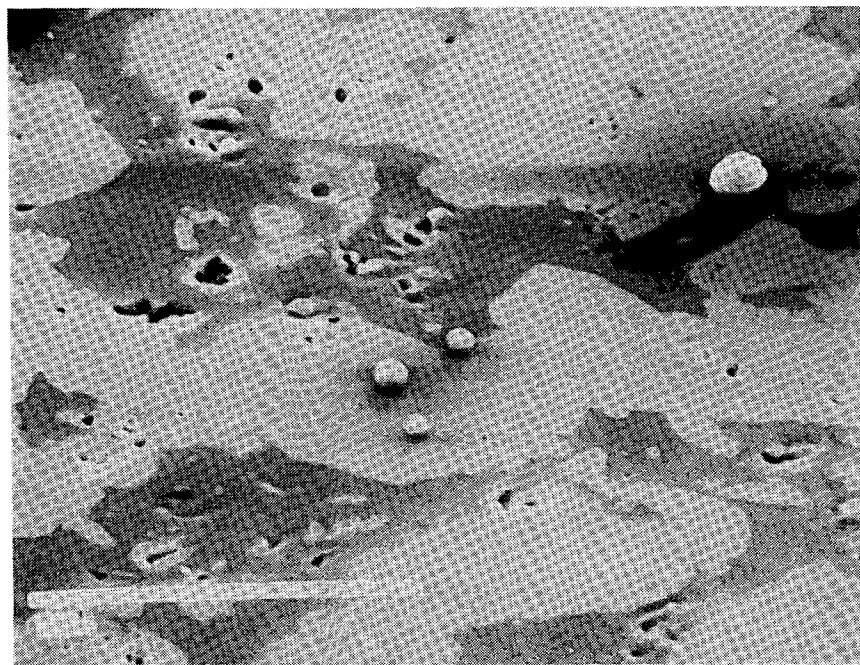


(a) Fuel at 500x

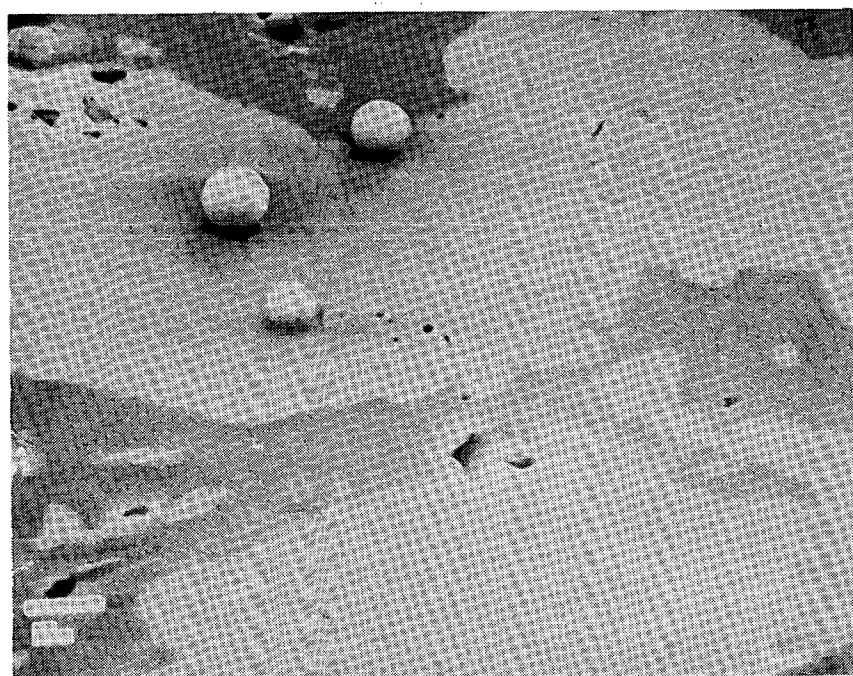


(b) Fuel at 1000x

Figure 18. SEM photographs of plate 028, composition 45 vol% UAl_2 .

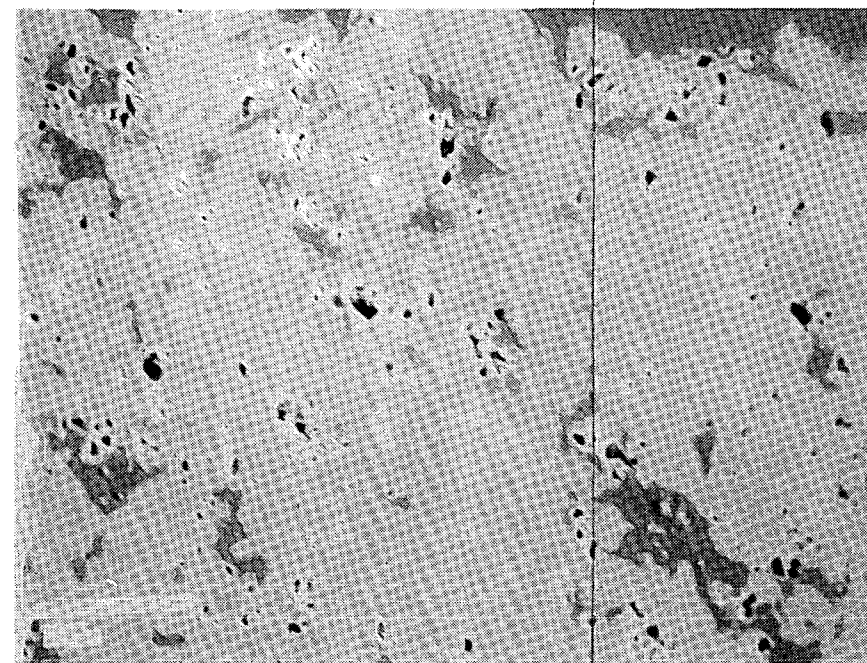


(a) Fuel at 500x

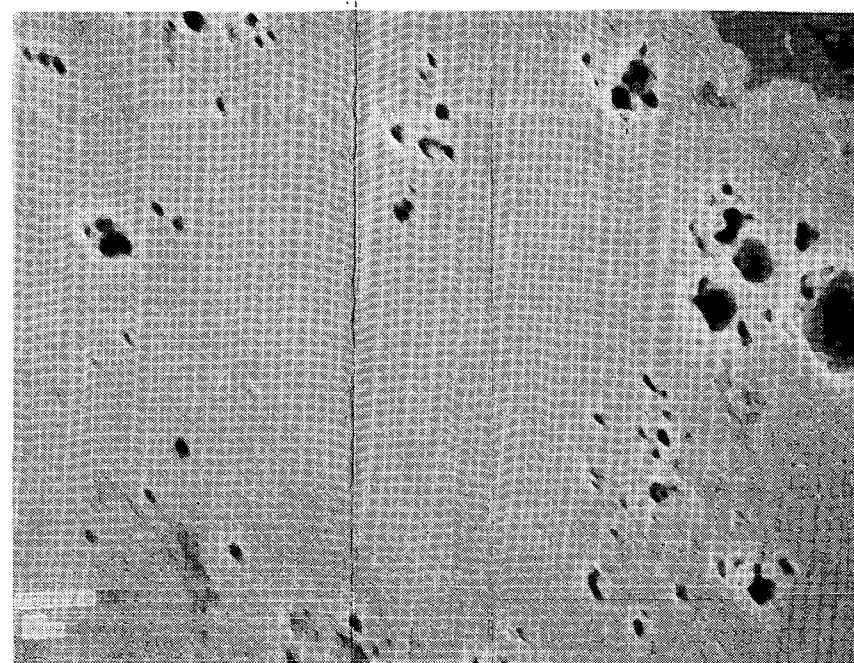


(b) Fuel at 1000x

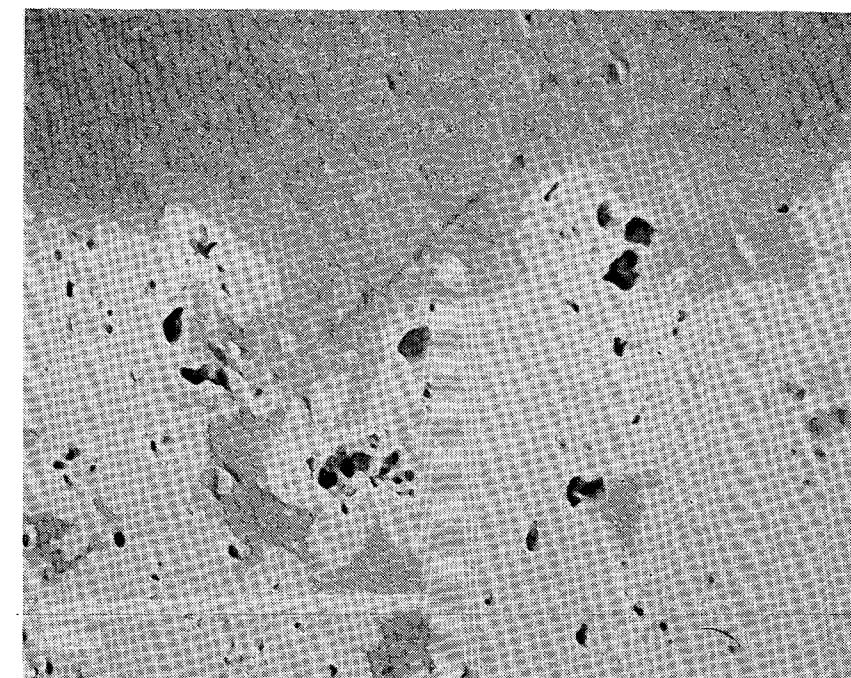
Figure 19. SEM photographs of plate 030, composition 40 vol% UAl_2 .



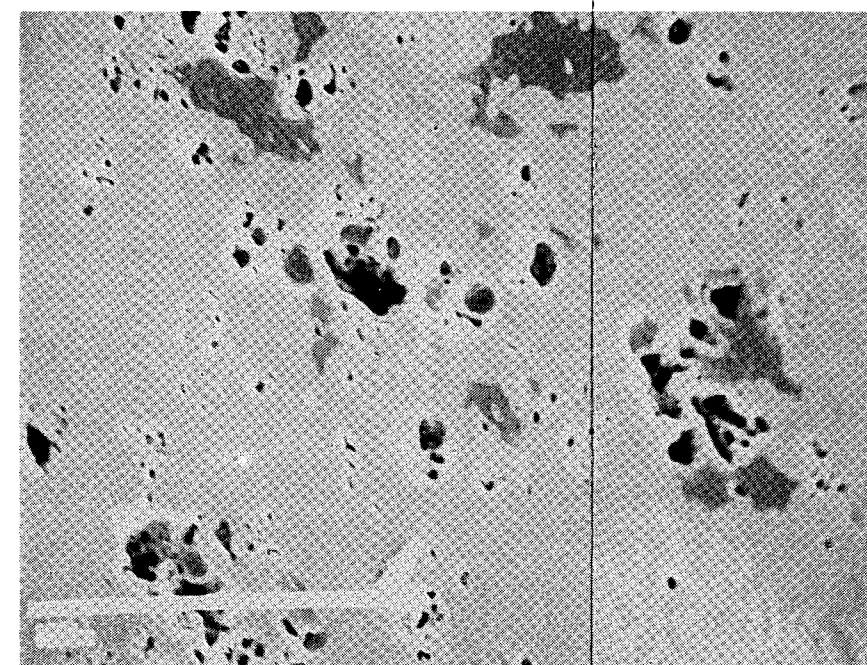
(a) Fuel at 200x



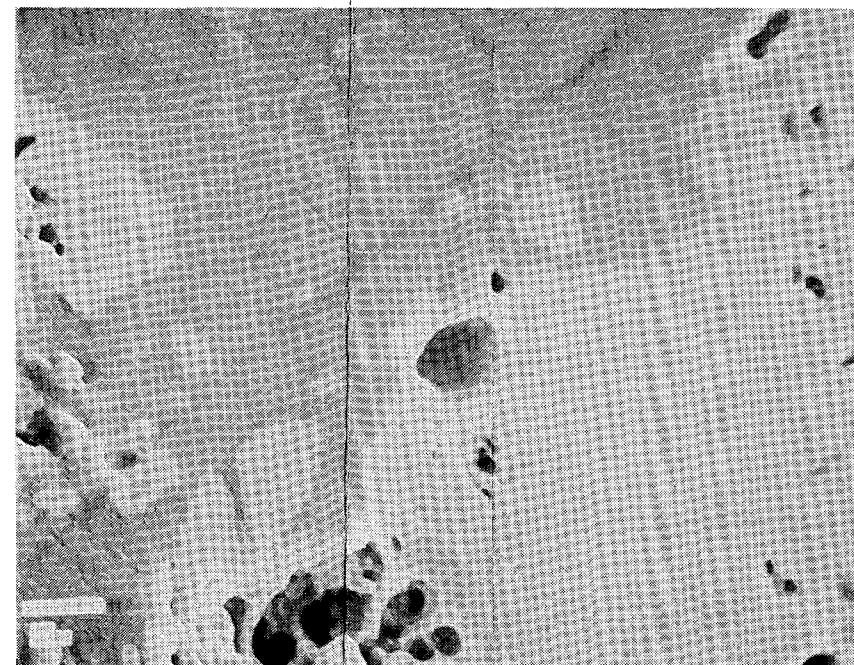
(c) Fuel at 1000x



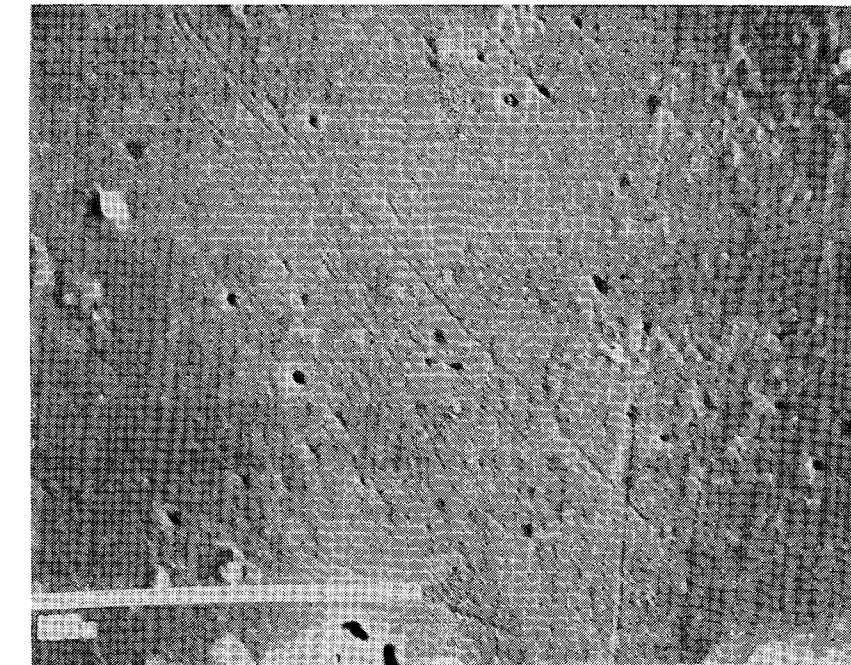
(e) Fuel-clad interface at 500x



(b) Fuel at 500x



(d) Fuel-clad interface at 1000x



(f) Cladding at 500x

Figure 20. SEM photographs of plate 013, acid etch, 50 vol% UAl_2 .

Table 8. Blister temperatures

Plate Number	CSAP PDQ Average Burnup (f/cm ³ x 10 ⁻²¹)	Peak Fission ^a Density cf/cm ³ x 10 ⁻²¹)	Punch Fission Density Plus 10%	Blister Temperature	
				K	°C
005	1.80	1.64	1.28	743	470
006	2.30	2.17	1.73	743	470
007	1.48	1.33	1.06	803	530
013	2.98	3.00	2.02	743	470
019 ^b	2.13	1.94	1.49	833	560
020	2.24	2.07	1.72	713	440
022	1.82	1.95	1.22	773	500
027	1.94	2.21	1.36	773	500
028	2.61	2.71	1.96	773	500
030	2.25	2.08	1.52	773	500
032 ^b	2.14	1.98	1.49	833	560
033	2.00	1.66	1.42	773	500

a. Table 13.

b. Did not blister.

blister temperatures are given in Table 8. For a burnup of about 2×10^{21} f/cm³, the blister temperature is greater than 743 K (470°C) for all the plates except No. 020, which was determined as 713 K (440°C). For the twelve plates, the blister temperature is not strongly dependent upon the burnup as seen in Table 8 and Figure 21. The linear least squares analysis of the blister temperatures, in terms of the CSAP PDQ average burnup, gives the line indicated in Figure 21. Photographs of the blister samples are shown in Figures 22(a) through (f) for the 50 vol% composition, and Figure 23(a) through (f) for the 45 and 40 vol% UAl₂. The average of blister temperatures for the three plates of UAl₃ composition was lower (763 K) than for the nine plates of UAl₂ composition (776 K).

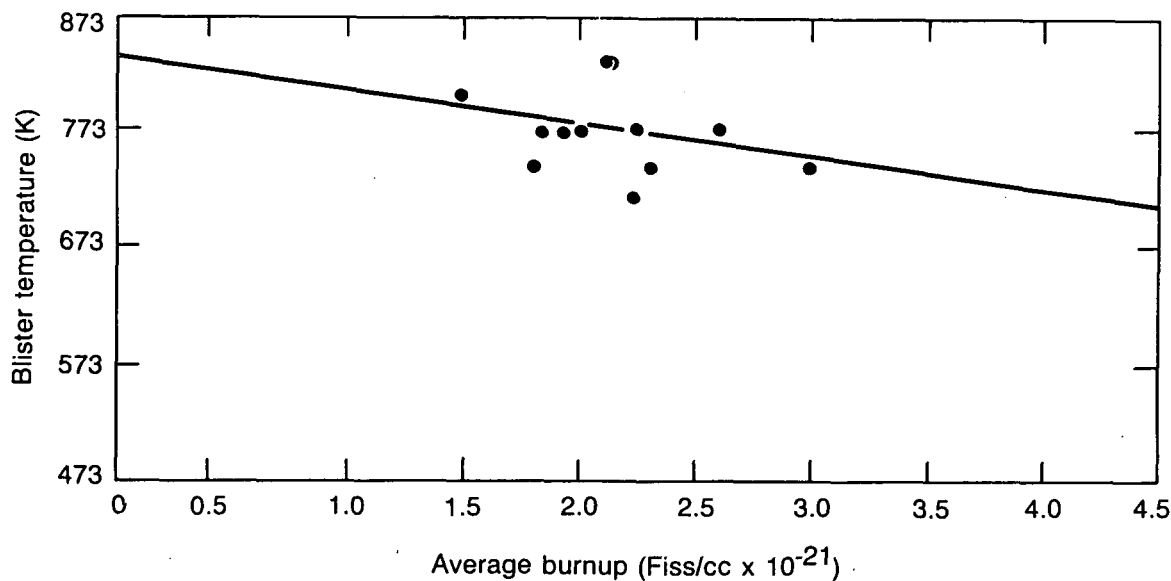
The linear least squares regression analysis of the blister temperatures (T) in degrees K, as a function of burnup (B), in units of 10^{21} f/cm³, (Table 8) gives the equation,

$$T = 832 - 27.4 B$$

where the correlation coefficient (r) is 0.3. Examination by regression analysis of the punch fission

density plus 10% was slightly better where $r = 0.38$ and $T = 845 - 47.1(B)$. This value of 0.3 (or 0.38) indicates a poor correlation, so that the dependency of the blister temperature (T) on the burnup is not very strong. The linear least squares regression analysis was also evaluated for the peak burnup, since bubbles might be expected in the region of peak burnup. This correlation was not any better with $r = 0.3$.

Two of the plates of UAl₂ composition did not blister at the end point test temperature, which is selected to prevent melting of the aluminum. One of the plates [No. 019-Figure 22(e)] is from the composition 50 vol% UAl₂, and the other [plate No. 032-Figure 23(e)] is from the composition 40 vol% UAl₂. These two plates did not have the lowest burnup. Plate No. 019 had an average burnup of 2.13×10^{21} f/cm³, and plate No. 032 had an average burnup of 2.14×10^{21} f/cm³. The plate with the lowest average burnup (No. 007) of 1.48×10^{21} f/cm³ blistered at a temperature 30 K less than No. 019 and 032. One expects the peak burnup, which would give the maximum fission products, to drive the blister temperature. However,



6 6688

Figure 21. Blister temperature as a function of the burnup.

it is noticed that the plates blister in the center, a region of lower burnup but lower strain constraint.

It is significant that the high fuel loading 50 vol% UAl_2 , even at the highest burnup, does not blister at a lower temperature than the 50 vol% UAl_3 . It is also significant that the high fuel loading UAl_2 or UAl_3 (50 vol%) plates blister at temperatures comparable with normally loaded plates presently in use.⁹

3.8 Pit Replication

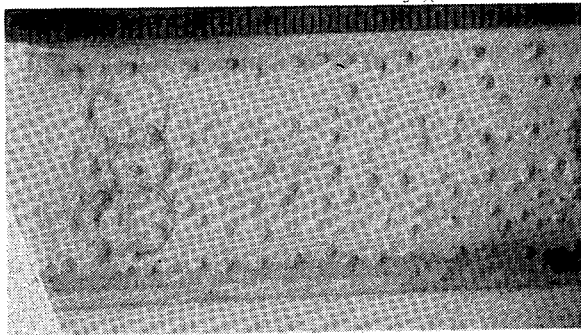
Replication was done on the 15 plates that were not to be included in the destruct tests. All 27 plates were examined after oxide removal on the hot cell periscope and pictures were taken of pit regions. On 15 plates, as each pit region was identified, a ring (1 in. diameter by 1/2 in. high) was laid in place and filled with silicone rubber (either Dow Corning 3110 or G.E. RTV 60). The 12 plates used for destruct tests were not replicated to eliminate the need for cleanup on these plates. On the 30 sides of the 15 plates, 45 pit regions were identified and replicated. Pit regions were identified on all but 6 of the 30 sides. The pit regions on the 12 destruct plates looked similar to those replicated, except that the largest pits appeared to be on those plates to be replicated (specifically plates 004, 015, and 031), Figure 24 (a) through (d).

After the replicas had set up (about 16 hr), they were removed from the plate surface, ultrasonically cleaned, and coated with gold in a bell jar to

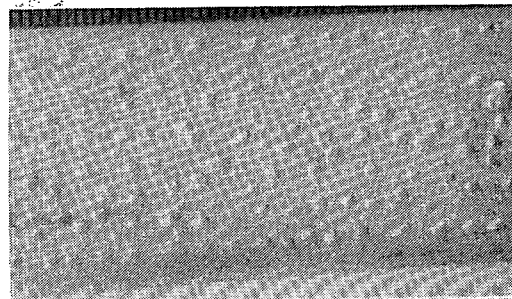
increase the contrast. The replica on plate No. 025 tore off, so no pits were measured on this plate. Pit height on the replica (pits on the surface became peaks on the negative replica) was measured on a Unitron TMD-3721 microscope at 400X. The microscope featured a dial gauge with readout to 0.0001 in. on the fine focus and indication as to height or depth. This was very convenient for these measurements. The microscope stage also contained micrometer screws with readout to 0.0001 in. A turret objective provided lower magnification for survey and locating the pits.

Eighty-two pits were measured ranging in depths from 16.0 mil (0.4 mm) to 0.4 mil (0.01 mm), Table 9. The 16.0 mil deep pit was on the cladding edge, hence no fission product leakage occurred. It was also one of the plates (004) taken out during the fuel plate failure and stored in canal water for a long time (Table 9).¹² The measurement of the pit diameter was about six times greater than the depth, a measurement useful in estimating the pit depth during inspection. The pit depths (height on the negative replica) are given in Table 9 for the 14 plates on which pits were measured (arranged in decreasing size). The next deepest pit (7 mil) was also in the side plate cladding [Figure 24(d)]. Most of the pits were about 1 mil deep (average 1.4 ± 1.9 for 82 pits measured), Table 9.

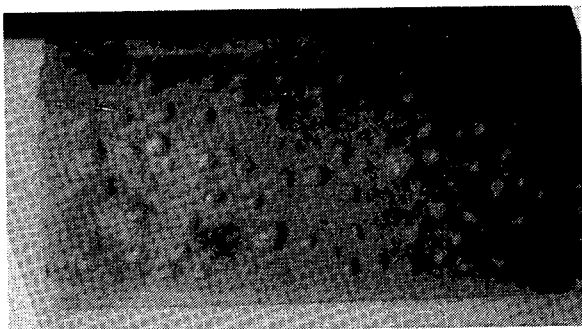
Scanning electron microscope photographs from the replicas of the largest pit (plates No. 004, 16 mil deep and 40 mil diameter) and



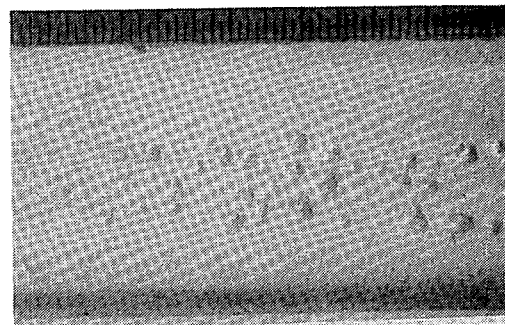
(a) Plate No. 005, blister T, 743 K



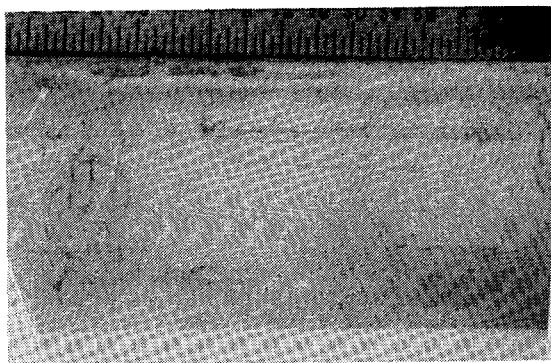
(b) Plate No. 006, blister T, 743 K



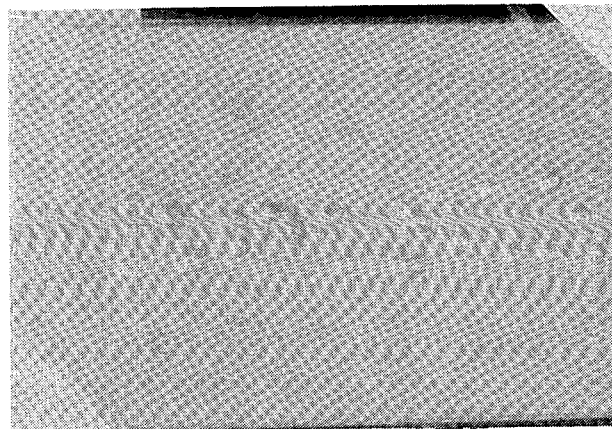
(c) Plate No. 007, blister T, 803 K



(d) Plate No. 013, blister T, 743 K

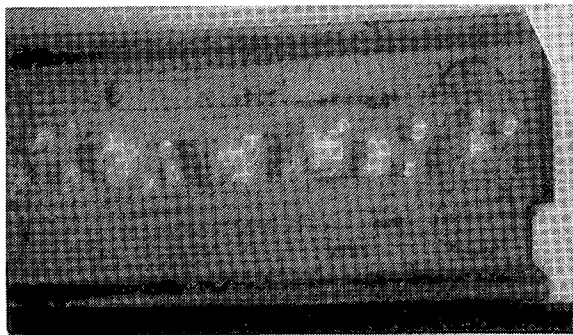


(e) Plate No. 019, blister T, 833 K



(f) Plate No. 020, blister T, 713 K

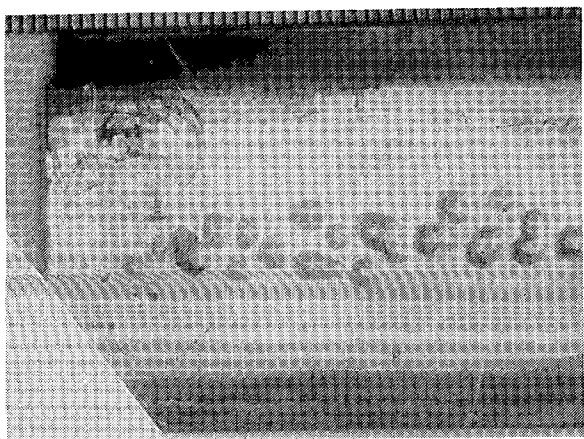
Figure 22. Photographs of blister samples from 50 vol% UAl_2 and UAl_3 .



(a) Plate No. 022, blister T, 773 K



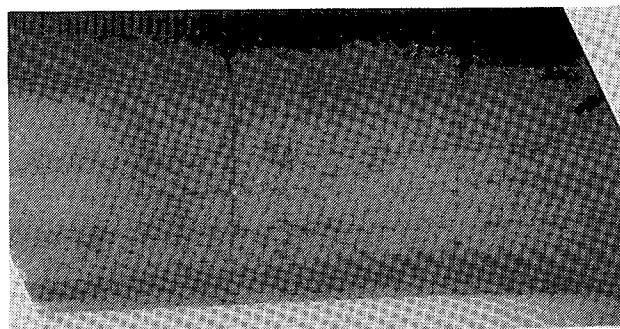
(b) Plate No. 027, blister T, 773 K



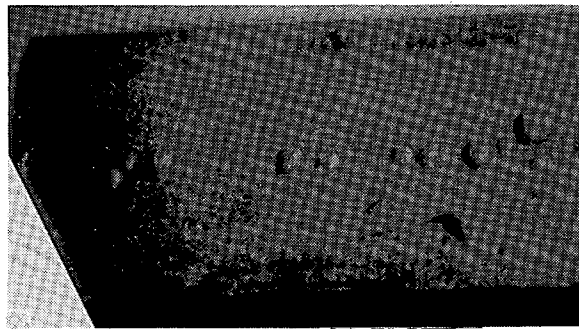
(c) Plate No. 028, blister T, 773 K



(d) Plate No. 030, blister T, 773 K

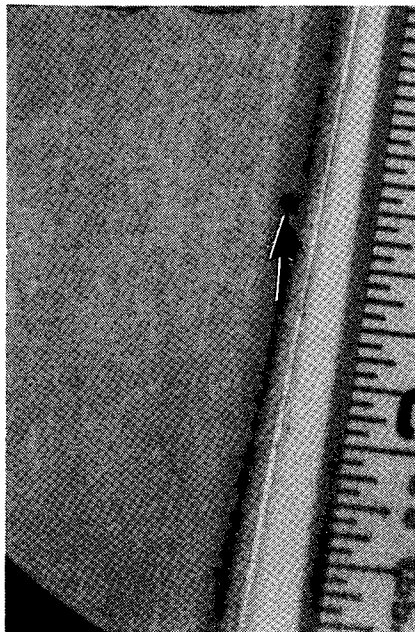


(e) Plate No. 032, blister T, 833 K

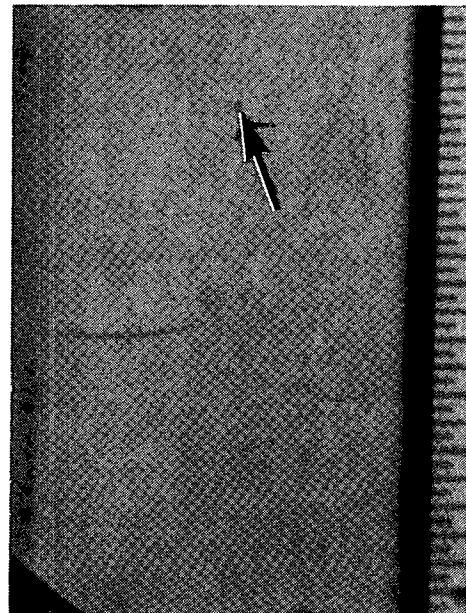


(f) Plate No. 033, blister T, 773 K

Figure 23. Photographs of blister samples from 45 vol% and 40 vol% UAl_2 .



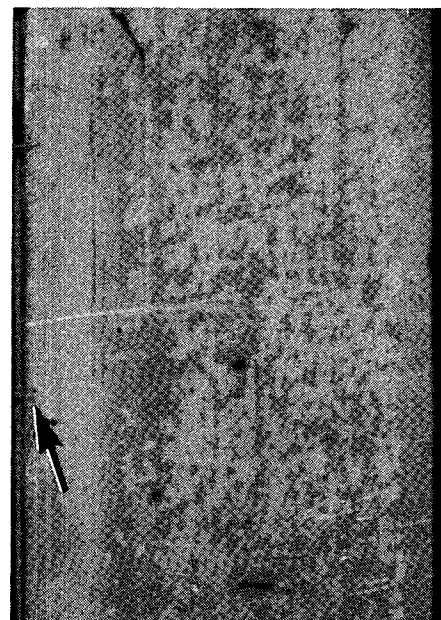
(a) Plate No. 004, 16 mil deep pit



(b) Plate No. 004, 2 mil deep pit



(c) Plate No. 015, 1.5 mil deep pit



(d) Plate No. 031, 7.0 mil deep pit

Figure 24. Typical photographs of replica areas on oxide stripped plates.

Table 9. Measured pit depth and calculated maximum total pitting corrosion

Plate No.	Pit		Time at Power (days)	Time in Canal (days)	Calculated Maximum Corrosion at Pit		
	No.	Depth (mils)			At Power (mils)	In Canal (mils)	Total (mils)
001	1	3.0	261.6	132	5.2	0.8	6.0
	2	2.5					
	3	0.9					
	4	0.7					
	5	0.6					
	6	0.6					
	7	0.5					
003	1	1.8	136	87	2.7	0.5	3.2
	2	1.8					
	3	1.2					
	4	0.9					
004	1	16.0	172	1192	3.4	7.1	10.5
	2	2.0					
	3	1.6					
	4	1.6					
	5	1.5					
	6	1.2					
	7	1.1					
	8	1.1					
	9	1.1					
	10	0.7					
	11	0.7					
	12	0.5					
	13	0.4					
008	1	1.0	261.5	50	5.2	0.3	5.5
	2	0.9					
	3	0.4					
009	1	1.1	196.1	50	3.9	0.3	4.2
	2	0.8					
	3	0.8					
	4	0.8					
	5	0.6					
	6	0.5					
010	1	1.6	196.1	50	3.9	0.3	4.2
	2	1.2					
	3	1.1					
	4	1.1					
	5	1.1					
	6	1.0					
	7	0.7					
	8	0.7					

Table 9. (continued)

Plate No.	Pit		Time at Power (days)	Time in Canal (days)	Calculated Maximum Corrosion at Pit		
	No.	Depth (mils)			At Power (mils)	In Canal (mils)	Total (mils)
015	1	1.5	136	877	2.7	5.2	7.9
	2	1.5					
	3	1.1					
	4	1.1					
017	1	0.8	172	1192	3.4	7.1	10.5
	2	0.8					
	3	0.8					
	4	0.7					
024	1	1.0	172	1192	3.4	7.1	10.5
	2	1.0					
	3	0.9					
026	1	1.5	173	521	3.4	7.1	6.5
	2	1.5					
	3	1.1					
	4	0.9					
	5	0.9					
029	1	1.4	172	1192	3.4	7.1	10.5
	2	1.3					
	3	0.6					
	4	0.5					
	5	0.4					
031	1	7.0	212.7	474	4.2	2.8	7.0
	2	4.5					
	3	1.6					
	4	1.1					
	5	0.6					
	6	0.5					
	7	0.5					
034	1	1.0	333.9	50	6.6	0.3	6.9
036	1	2.0	72.4	379	1.4	2.3	3.7
	2	1.9					
	3	1.4					
	4	1.4					
	5	1.2					
	6	1.2					
	7	1.2					
	8	1.1					
	9	1.1					
	10	0.8					
	11	0.8					
	12	0.5					

representative pits (plate No. 010 about 1 mil deep and 4 mil diameter) are shown in Figure 25 (a) and (b).

3.9 Pitting Corrosion Rate

Metal penetration can be expressed in terms of the maximum pit depth and the average of the 10 deepest pits. For the 14 plates, the 10 deepest pits include one that would have penetrated the cladding had it not been in the side plate area. The average of the ten deepest pits (Table 9) is 0.11 mm (4.3 mil). The pitting factor is determined from weight loss, defined as the ratio of the deepest metal penetration to the average metal penetration. The ratio of the maximum pit depth to the average pit depth gives an approximation of the pitting factor. The ratio is 3.8. A pitting factor of one represents uniform corrosion. The larger the pitting factor, the greater the probability of failure by pitting.

The maximum total pitting corrosion was calculated for the 27 plates (including the 14 plates given in Table 9) for the total time each plate was in the water (i.e., the time at power and the time in the canal). The calculation for the maximum pitting corrosion is based on the equation given¹² as

$$CR_{\max} = 7.6 \times 10^{-24} T^{7.25} \text{ in./day} \quad (1)$$

where T = fuel plate surface temperature, K.

The fuel plate surface temperature at reactor power was taken as an average value for the calculation of 347 K, and in the canal of 294 K. The fuel plate surface temperature was determined from the oxide thickness at the end of the irradiation and the ATR startup equation¹⁷ given as

$$X = 10,344 \theta^{1.1} \exp \frac{-12,602}{\theta R} \quad (2)$$

where

X = oxide thickness (mils)

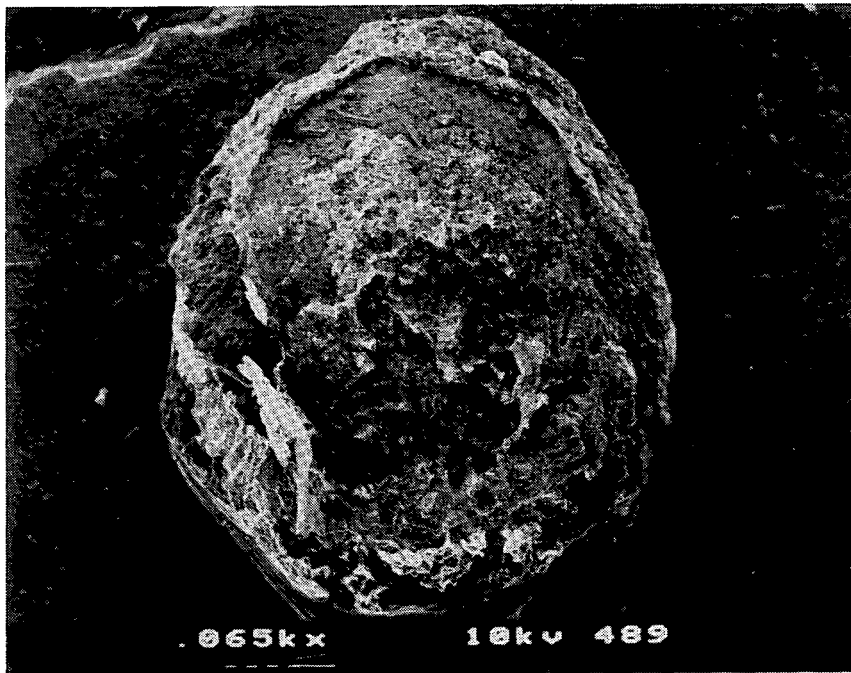
θ = hours in reactor.

The measured pitting corrosion of 14 plates is compared with that calculated for these plates at power and in the canal (Table 9). The calculated values for the maximum pitting corrosion of the other 13 plates, for which measured values were not obtained, were of similar magnitude. The highest maximum value was 14.6 mils for plate No. 006;

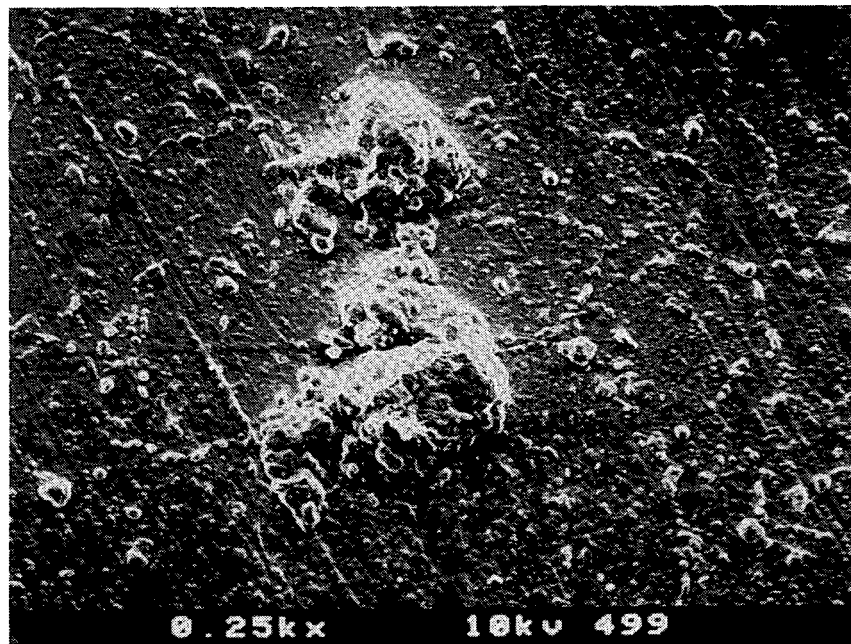
the lowest maximum value was 6.6 mils for plate No. 033. Thus, the calculated value for the maximum total pitting corrosion by Equation 1 does approximate the measured value. Comparison of the calculated maximum pitting corrosion of 10.5 mils, with the measured value of 16 mils for plate No. 004, indicates that the equation for the maximum pitting corrosion rate is about right, since the plate in the canal would have been at a slightly higher temperature for part of the time. Considering the other measured values of the pit depths (Table 9) in light of the calculated maximum pit depth, indicates that the pit incubation time is not negligible or that most of the pits do not propagate at the maximum rate. Discussion of the pitting corrosion is given in Section 4.4.

3.10 Gamma-Ray Spectroscopy

The 12 fuel plates removed from the ATR reactor on June 23, 1985, were examined by gamma-ray spectrometry measurements at the TRA Hot Cell Facility.¹⁸ The purpose of the measurements was to determine the distribution of gamma-ray emitting fission product radionuclides in the fuel. These results will be combined with radiochemical analyses of samples taken from the fuel plates to determine the peak fuel burnup (fission density) in each plate. The measurement results for the positions from which the burnup punchings were taken are given in relative counts per second for each individual radionuclide in Table 10. The radionuclides identified are ⁹⁵Zr, ¹⁰³Ru, ¹³⁴Cs, ¹³⁷Cs, and ¹⁴⁴Ce for each of the 12 plates. The counts per second for each radionuclide at the maximum, and the punching positions, are tabulated in Table 10. Also given in Table 10 is the average of 19 measurements of each radionuclide on each plate. Since no efficiency calibrations exist, quantitative activities and gamma-intensities are undetermined; therefore, the counts per second of one radionuclide are not related to another radionuclide. All the data were decay corrected to 6-23-85 at 2000 hr. The punching position point counts were taken at the 6.4 in. distance from the bottom of the fuel plate and at the axial centerline. The actual area viewed was 0.055 in. by 0.688 in. or 0.038 in.². Appendix A contains a copy of the gamma-ray spectroscopy report.¹⁸ Table 11 contains ratios of the maximum gamma counts per second in any position measured to that at which the burnup punching was taken. These ratios (maximum gamma counts per second of one area to that of the burnup punching)



(a) Plate No. 004 largest pit, 16 mil deep in side cladding



(b) Plate No. 010, 2 pits, depth about 1 mil

Figure 25. SEM photographs of two of the replicated pits.

Table 10. Relative radionuclide activity of the twelve plates in counts per second for the maximum, average, and punching positions

Plate Number	⁹⁵ Zr			¹⁰³ Ru			¹³⁴ Cs			¹³⁷ Cs			¹⁴⁴ Ce		
	Punch	Avg	Max	Punch	Avg	Max	Punch	Avg	Max	Punch	Avg	Max	Punch	Avg	Max
5	225	231	248	400	412	446	8.58	9.22	11.0	31.6	33.5	37.9	116	121	131
6	325	337	365	458	473	512	21.6	23.5	27.0	44.0	46.9	52.7	230	242	268
7	389	400	442	553	561	617	7.16	7.69	9.04	25.4	26.4	30.1	155	163	193
13	33.1	35.0	39.7	9.1	10.2	12.3	18.6	20.2	27.6	48.9	51.6	62.8	155	163	193
19	619	660	745	906	961	1072	11.4	12.4	14.9	35.0	38.8	43.3	346	378	427
20	789	802	849	1153	1172	1234	15.4	16.3	18.6	44.4	46.2	50.8	443	460	497
22	476	508	629	692	734	915	8.2	9.0	13.1	28.6	30.8	39.7	279	303	381
27	32.7	35.3	43.5	10.3	10.3	12.8	8.13	9.0	13.2	29.7	32.3	41.9	143	155	199
28	452	454	497	641	645	711	22.2	23.3	30.7	47.9	49.3	56.5	337	345	386
30	389	455	533	542	624	737	13.0	14.7	17.6	33.1	39.0	44.5	305	352	408
32	4.1	4.6	5.5	—	—	—	8.41	9.1	10.5	32.8	35.7	39.2	75.8	82.3	92.9
33	—	—	—	—	—	—	5.56	6.0	6.49	31.9	34.0	36.8	48.7	51.3	56.1

represent the measured burnup peaking that occurred in each plate. The plates in each composition group (50 vol% UAl₂, etc.) were placed in the I-hole fixture for the irradiation history as indicated in Appendix A, Table A-1 and Figure A-1. Positions B and D, where the plate edge was toward the reactor core, generally produced higher

peaking in one edge of these plates. The plates were moved about as seen in Table A-1, which tended to reduce this edge effect. The selection of the peaking factor from the gamma-scan data (to represent the maximum burnup for each plate) is complicated by the limited number of isotope counts on each plate, the relative size of the gamma-scan area, and a

Table 11. Ratios of isotopic maximum gamma counts per second to those of the burnup punching position

Plate Number	Ratios For Isotopes					Maximum ^a Peaking Factor
	⁹⁵ Zr	¹⁰³ Ru	¹³⁴ Cs	¹³⁷ Cs	¹⁴⁴ Ce	
005	1.10	1.12	1.28	1.20	1.13	1.41
006	1.12	1.12	1.25	1.20	1.17	1.38
007	1.14	1.12	1.26	1.19	1.25	1.39
013	1.20	1.35	1.48	1.28	1.25	1.63
019	1.20	1.18	1.31	1.24	1.23	1.44
020	1.08	1.07	1.21	1.14	1.12	1.33
022	1.32	1.32	1.60	1.39	1.37	1.76
027	1.33	1.24	1.62	1.41	1.39	1.78
028	1.10	1.11	1.38	1.18	1.15	1.52
030	1.37	1.36	1.35	1.34	1.34	1.51
032	1.34	—	1.25	1.20	1.23	1.47
033	—	—	1.17	1.15	1.15	1.29

a. Maximum peaking factor is the maximum isotopic ratio for each plate plus 10%.

possible blister area. The limited number (19) of isotope counts on each plate may mean that the peak count was missed. The relative size of the gamma-scan collimator area (0.038 in.²) to a possible peaking (blister) area (0.003 in.²) may tend to level out (miss) the maximum counts. To accommodate these effects, the calculated PDQ average to minimum peaking factor was evaluated. The average to the minimum peaking was about 10%, which was added to the maximum isotopic ratio for each plate to obtain an overall maximum peaking factor (Table 11).

3.11 Radiochemical Analyses for Burnup

The punchings for burnup analyses were taken 6.380 in. from the bottom of the plate and at the axial centerline. The punchings were 0.25 in. in diameter with an area of 0.049 in.². The punchings taken at the axial and horizontal centerline are in a region of uniform burnup, although it is a region of expected lowest burnup in each plate. Because of the uniformity of burnup expected in this centerline punching, and in order to limit program costs, this centerline punching was the one on which radiochemical analyses were done for burnup. Therefore, it is pointed out that (generally) any other region referred to, or examined, would have a higher burnup than that of the punching analyses. For this reason, in referring to a burnup of a region, the PDQ average or peak burnup is used. This peak burnup is the lowest burnup multiplied by the peaking factor from Table 11. This peak burnup is about the same as that of the PDQ average burnup calculated, which was used to guide the irradiation

and determine plate removal at the end of irradiation (Section 2.1). The ratio of the average PDQ fission density to the minimum fission density is 1.1; hence, in Tables 1, 4, and 8, 10% is added to the low fission density to obtain an average.

The burnup of each punching was obtained from the isotopic ratios (Table 12) by means of a computer program used for high enrichment test reactor fuels.¹⁹ The irradiation history (Figure 1) was divided into sequential power factor intervals. Considering results from previous analyses¹⁹, and the 4 group ATR PDQ calculated flux in the homogenized fuel plate region inside the ELAF assembly, the capture to fission cross section, α , was taken to be $\alpha = 0.196 \pm 0.01$. The program iterates the data until it converges on an apparent fluence and the measured isotopic ratios, and prints out a final ²³⁶U/²³⁵U ratio. A number of checks were made on the calculational procedure and data, including: a change in α to the ATR core region;¹⁹ the gamma spectroscopy cesium 134, 137 results; and total uranium concentration in the punchings. These checks did not change the calculated burnup for the punching position (Table 13) significantly. For example, an α of 0.215 for the ATR core region¹⁹ reduced the burnup by about 6%, which is to be expected because of the harder spectrum in the ATR core region. Therefore, the punching burnup given in Table 13 is considered to be representative of the measured isotopic ratios and is generally the lowest burnup of the fuel plate. Multiplication of this low punching position burnup by the peaking factor (Table 10) for each plate then produced the peak fission density given in Table 13. The average PDQ calculated fission density is given (Table 13) for comparison. It is found to be approximately the same as the peak fission density.

Table 12. Mass spectral isotopic ratios for ELAF burnup samples

Sample	Atom Ratios			
	$\%^{235}\text{U}$	$\%^{238}\text{U}$	$\%^{236}\text{U}$	$\%^{234}\text{U}$
5	85.40	7.07	6.30	1.23
6	81.98	7.54	9.16	1.32
7	87.32	6.37	5.09	1.22
13	83.78 (83.73) ^a	7.19	7.79	1.25
19	86.92	6.58	5.29	1.20
20	84.95 (85.06) ^a	7.48	6.33	1.23
22	87.63	6.59	4.62	1.16
27	86.95	6.60	5.29	1.16
28	83.19	7.42	8.14	1.24
30	85.15 (84.64) ^a	6.97	6.75	1.12
32	85.25	6.95	6.58	1.22
33	85.56	6.86	6.33	1.22

a. Analyzed twice.

Table 13. Burnup of ELAF fuel plates from isotopic ratios, peaking factor, and PDQ calculations

Plate Number	Uranium Atom Density ($\times 10^{-21}/\text{cc}$)	Punching Burnup (% Heavy Element)	Pending Fission Density ($\text{f}/\text{cm}^3 \times 10^{-21}$)	Peak Fission Density ($\text{f}/\text{cm}^3 \times 10^{-21}$)	Average PDQ Calculation Fission Density ($\text{f}/\text{cm}^3 \times 10^{-21}$)
5	5.04	22.9	1.16	1.64	1.80
6	5.09	30.8	1.57	2.17	2.30
7	5.04	19.0	0.96	1.33	1.48
13	6.78	27.2	1.84	3.00	2.98
19	6.86	19.7	1.35	1.94	2.13
20	6.77	23.1	1.56	2.07	2.24
22	6.37	17.4	1.11	1.95	1.82
27	6.32	19.7	1.24	2.21	1.94
28	6.32	28.2	1.78	2.71	2.61
30	5.63	24.4	1.38	2.08	2.25
32	5.68	23.7	1.35	1.98	2.14
33	5.63	23.0	1.29	1.66	2.00

4. DISCUSSION

4.1 Swelling and Fuel Phase Instability

The ELAF plates were irradiated at a nominal calculated temperature of 395 K (122°C) to simulate university fuel plate conditions. This temperature is about 55 K lower than the nominal temperature for ATR fuel plates^{8,9} and intermediate to some other UAl_x experimental plates^{6,10}. The swelling behavior of these plates was similar to other UAl_x fuel plates when compared at equivalent irradiation temperature and burnup. For example, at a burnup of 2.5×10^{21} f/cm³, the swelling obtained in the ATR plates^a was 6.5%, while the swelling of the ELAF plates^a was 6.2%. The peaking in the swelling of plate 013 (Table 4) of 14.7% for the high side, and 19.1% for the high spot, occurs at the higher irradiation temperatures of 150-165°C (in Reference 10) at about this fission density. From other UAl_x fuel plates¹⁰, at 70°C, the value is about 9% for thickness and for immersion in carbon tetrachloride. From these ELAF tests (immersion density in water with photoflo as a wetting agent), the swelling value was somewhat lower at 3.8% for this average burnup of 2.5×10^{21} f/cm³. All of these swelling tests indicate that the UAl_x fuel-aluminum matrix plates are resistant to the agglomeration of fission gas. The fission product gas is apparently accommodated (for the most part) in solution in the UAl_x microstructure, most probably in the UAl_4 microstructure. The UAl_4 body-centered-orthorhombic structure contains a variable number of aluminum atoms (from 4.5 to 4.9).^{8,20,21} Thus, the structure contains some empty uranium sites, or sites with smaller aluminum atoms, which may accommodate fission gas products. Therefore, the defect structure of UAl_x may provide the explanation for the low swelling of these fuels to fairly high burnup (3.0×10^{21} f/cm³ peak for plate 013 in local areas).

As shown in Tables 5 and 7, swelling based on the metallurgical core thickness change includes core changes due to reaction of the UAl_2 and aluminum to produce UAl_3 and UAl_4 . Therefore, this method gives swelling values that are too high for irradiation alone. The swelling determined by water immersion density is low because of the low average

fission density. The measurement was repeated with the same results. It is noted that since differences are taken in numbers of about the same magnitude, slight inaccuracies cause large changes in the values. It is recommended that the plate-core thickness change ($\Delta t/t$) from Table 4 or Table 5 be taken as the swelling value for these tests. These are approximately the same as determined for the three failed plates.¹²

As noted in these tests and by others,^{8,10,20,21,22,23} UAl_3 is a more stable phase than UAl_2 . UAl_2 reacts with aluminum to give UAl_3 and the nonstoichiometric $U_{1-x}Al_4$ phase. The reaction causes a measurable change in the fuel core thickness and volume, but not in the swelling due to irradiation. The swelling as measured by immersion density and plate thickness was determined by the presence of the fission products which mainly stay in solution. As seen in Table 7, approximately one-half the change in core thickness was due to the reaction of UAl_2 and Al to produce UAl_3 and UAl_4 . This change principally occurred during the fabrication process.

The amount of oxygen in the powder blend (0.37% oxygen by weight in JJ blend and 0.11% oxygen by weight^b in the JF blend) is evidently present as UO_2 ^{16,21} or U_3O_8 ²⁴. There may be additional oxygen pickup during grinding and compaction of the powder, as occurs in just a half-hour at temperatures less than 350°C, especially in UAl_2 .^{23,24} This U-O phase is evidently the source of the small bubble formation as seen in Figures 10 and 11.¹⁶ The topography of the U-O phase resembles the appearance of the film of U_3O_8 on the surface of UAl_4/Al .²⁴

4.2 Fuel Core Integrity and Bubble Formation

The fuel core integrity was very good. No cracks or blisters were found and the fission products were principally retained within the fuel structure. A fission fragment stopping zone about 10-20 microns in width was seen at the fuel-clad interface. No bubbles could be seen in this zone, or the fuel surface at 500X by metallography, or by SEM on the

a. From thickness measurements.⁹

b. Appendix B.

polished surfaces at higher magnification. With the SEM on the fracture surfaces, Hoffman¹⁶ did see small bubbles wherever he saw the U-O phase. The amount of this phase and associated bubbles was not sufficient to affect the integrity of the fuel core as determined by inspection or by blister testing. In over 70 powder particles examined by Kevex-ray on the SEM, this phase was not found in the JJ and JF blend powders before fabrication.

The presence and relative amounts of voids after irradiation indicate that the swelling due to the solid fission products has not filled the void spaces as seen in Figure 6 and Table 6. Difficulties in polishing (scratches from the brittle phase) have been attributed to pull out of these brittle intermetallic particles, however the voids are seen after irradiation,³⁻⁹ as well as before. The low swelling behavior of the UAl_x fuels has been thought to be partly due to the filling of these voids with the solid fission products.³⁻⁹ The magnitude of this effect (even at high burnup) is unresolved, although the presence of the voids with the ductile aluminum matrix does not appear detrimental. This seems to be true even at these high burnups where some small bubbles have been detected around the U-O phase.

4.3 Blister Behavior and Potential Swelling

The blister temperatures of the plates with UAl₂ as the principal constituent were generally as high as those with UAl₃ as the principal constituent. For example, the average blister temperature of the three UAl₃ plates was 763 K, while that of the nine UAl₂ plates was 776 K. However, one plate of the UAl₂ composition blistered at 713 K, while two plates of the UAl₂ composition did not blister at 833 K (at burnups of $> 2 \times 10^{21}$ f/cm³). Thus, the variability of the blister temperature of the plates of the UAl₂ composition was greater than might be expected. This variability might be explained by pockets of gas bubbles associated with the U-O phase, formed during fabrication of the plates. The U-O phase was also found¹⁶ in the plates of UAl₃ composition. When the blister temperatures of these ELAF plates were compared with blister temperatures of the ATR composition plates,⁹ all the blister temperatures fell within the three sigma scatter band except the 713 K temperature of plate 020.

The potential swelling of plates of the UAl₃ or UAl₂ composition, as determined from this work,

would seem to depend most strongly on these U-O phase pockets and associated gas bubbles. The U-O phase probably is formed during the powder grinding and plate rolling fabrication processes and could be diminished by reducing the specification allowed for oxygen (Appendix B).

4.4 Pitting Corrosion and Plate Life

Oxide formation and pitting corrosion in aluminum surfaces has received considerable study.²⁵⁻³² It is our aim to show that the pitting corrosion of these ELAF plates was not excessive (as compared to other reactor elements,⁹ or other conditions¹⁰) when consideration is made of the temperature and time in the reactor or in the canal (Table 9). As indicated in Section 3.9, when Equation (1) is used to calculate the maximum pitting corrosion of the ELAF plates (Table 9) an estimate results which is reasonable (e.g., as for plate 004) or which overestimates the measured maximum pit depth for most of the plates. But, on one plate (007) the estimate is the same as the measured maximum value. Equation (1) was derived from data from the failed ELAF plates,¹² ATR fuel element corrosion data,³³ and Engineering Test Reactor (ETR) fuel element corrosion data³⁴ and allows calculation of the pitting corrosion of the other 14 plates with reasonable values. Therefore, it is evidence that the pitting corrosion in the ELAF plates is not excessive.

Evaluation of pitting corrosion and the application of statistics to the analysis^{35,36} indicates, as with the ELAF failed plates,¹² that the measured pit depths can be represented by two straight lines. One line, for pit depths (X) below 2.0 mils, can be represented by the equation

$$Y = -0.114 + 0.43 x$$

with a correlation coefficient of $r = 0.998$. The other line, for pit depths (X) above 2.0 mils, can be represented by the equation

$$Y = 0.69 + 0.034 x,$$

with correlation coefficient of $r = 0.94$. These high correlation coefficients indicate that extreme probability statistics³⁵ can represent the data. The value of Y is the reduced variate; i.e., a function of

$$\frac{M}{n + 1},$$

where M is the rank of the pit depth, arranged in increasing order of pit depth (X), from one to the total number and n is the total number. The values of Y and X were examined by linear least squares regression analysis, and plotted on extreme probability paper. The return period (i.e., the number of pits at which to expect a pit of a given depth) is different for the small and large pits. For the small pits (< 2 mils) one would expect to have over 10,000 pits before getting one with a depth of 7 mils, while for the large pits (> 2 mils) the return period is 50. This representation indicates that the pit incubation time is large or that most of the pits do not propagate at the maximum rate. It has been postulated^{30,31,37} that a critical pitting potential and a protection potential exists for aluminum. Below the critical pitting potential the pit may not initiate or may not grow. The pitting potential decreases with increasing temperature. Other factors also affect the probability that pits will initiate on the fuel plate surface such as: corrosivity of the solution, the solution velocity, the specimen area, and the time of exposure. Because of the occluded cell associated with pitting, the maximum corrosion rate will be less affected by the solution velocity than will pitting initiation. Thus, most of the pits as measured for the ELAF plates are much less than the maximum. During the early stages of pit initiation or growth, the pitting potential is rather unstable. The high concentration of corrosion promoting ions may be swept away by convection currents or the solution velocity. Gravity may have an effect on vertical surfaces, since a difference in solution concentration within a pit is necessary for its continuing activity. Thus, in this irradiation, conditions allow the formation of many pits that do not grow, and a few that do, as protection of the pit is established.

The plate life can thus be affected by the management of the fuel element irradiation sequence and time. Interruption and storage of the fuel elements change the conditions for pit initiation and growth; namely, pitting potential, solution corrosivity, and solution velocity. Interruption and storage of the fuel elements may affect gravity conditions with deposit of solids.

4.5 Maximum Fission Density

Although the fission density given for the punching positions in Table 13, (and as stated in Section 3.11) is considered to be representative of the measured isotopic ratios for the ELAF fuel plate punchings, there are two factors which could have affected the maximum values of burnup. The first is the variance on alpha (α), the capture to fission cross section in the I-9 facility. The variance was estimated to be ± 0.01 for the spectrum in the I-9 and I-13 facility, in which the plates were irradiated. The effect of this variance (of α on the fission density) was examined. It was found to produce less than a 10% change in the burnup. The second factor was a constant difference between the PDQ calculated fission density and the fission density obtained from the punchings with α equal to 0.196. This constant difference amounted to a factor of 1.42 ± 0.055 for the 12 plates. It was not possible at this time to assess which was more accurate: the PDQ calculated fission densities, or the fission densities calculated from the mass spectroscopic isotopic ratios with α equal to 0.196. Therefore, conservative values of the maximum fission density are considered to be those from the measured isotopic ratios times the peaking factor as presented in Table 13. It is noted that these values are approximately the same as the PDQ calculated average fission densities.

5. CONCLUSIONS AND RECOMMENDATIONS

- An ELAF fuel core with 73 wt% of the brittle phase (UAl_x) gave excellent performance to burnups of $1.84 \times 10^{21} \text{ f/cm}^3$ with peaking factors of 1.63 (peak burnup of $3.0 \times 10^{21} \text{ f/cm}^3$).
- The ELAF fuel plates operated at surface temperatures of about 395 K (120°C) with the only evidence of failure due to pitting corrosion.
- Blister temperatures from post irradiation tests of 763 K for the UAl_3 composition, and 776 K for the UAl_2 composition, indicated large margins of safety from overheating for short periods of time.
- The 50 vol% UAl_2 composition plates performed as good or better than the 50 vol% UAl_3 composition plates and will provide higher fuel loading. Although pitting corrosion caused the failure of three plates of the UAl_2 composition, a large pit, in the UAl_3 composition, in the side of the plate (that would have produced failure) was found.
- Neither the pitting corrosion rate, or the probability of pitting, seemed any greater in the ELAF plates than fuel elements in other reactors when consideration is taken of the plate surface temperature and the time in the water.
- Evidences of small bubbles in pockets were seen in conjunction with uranium oxide, which was probably formed during fabrication of the powder and plates. The blisters that form during post irradiation testing may be associated with these pockets.
- Reaction of the UAl_2 to produce UAl_3 and the $\text{U}_{1-x}\text{Al}_4$ defect phase causes an increase in core volume of 6 to 12%. The core volume percent thus approaches 60 vol% of the brittle constituent.
- It is recommended that the specification for oxygen in the powder blends be examined with the view of reducing the allowed oxygen.
- It is recommended that management of the fuel element irradiation sequence be considered as a way to reduce the depth of pitting corrosion and extending fuel element life.

REFERENCES

1. L. G. Miller and J. M. Beeston, *Fuel Plate and Fusion Insulator Irradiation Test Program*, EGG-FT-5273, November 1980.
2. L. G. Miller, K. R. Brown, J. M. Beeston, and D. M. McGinty, *Extended Life Aluminide Fuel for University Research Reactors*, EGG-SE-6464, December 1983.
3. G. W. Gibson, M. J. Graber, and W. C. Francis, *Annual Progress Report on Fuel Element Development for FY-1963*, IDO-16934, 1963.
4. M. J. Graber et al., *Performance Evaluation of Core II and III Advanced Test Reactor Fuel Elements*, ANCR-1027, Aerojet Nuclear Company, 1971.
5. M. M. Martin, A. E. Richt, and W. R. Martin, *Irradiation Behavior of Aluminum-Base Fuel Dispersions*, ORNL-4856, 1973.
6. M. J. Graber et al., *Results of ATR Sample Fuel Plate Irradiation Experiment*, IDO-16958, 1964.
7. V. A. Walker, M. J. Graber, and G. W. Gibson, *ATR Fuel Materials Development Irradiation Results—Part II*, IDO-17157, 1966.
8. W. C. Francis, *Metallurgy and Materials Science Branch Annual Report Fiscal Year 1970*, IN-1437, 1970.
9. J. M. Beeston et al., "Development and Irradiation Performance of Uranium Aluminide Fuels In Test Reactors," *Nuclear Technology*, 49, June 1980, pp. 136-149.
10. W. Dienst, S. Nazare, and F. Thummler, "Irradiation Behavior of UAl_x -Al Dispersion Fuels for Thermal High Flux Reactors," *Journal of Nuclear Material*, 64, 1, 1977.
11. D. F. Atkins, *Results and Evaluation of Productibility Studies Using UAl_x for Low Enriched Fuel Plates*, N275TR000001, Rockwell International, 1979.
12. J. M. Beeston, L. G. Miller, K. R. Brown, and D. M. McGinty, *ELAF Failed Fuel Plate Examination*, EGG-SE-6696, October 1984.
13. *ATR Fuel Element Specification*, IN-F-9-ATR, Rev. 5.
14. *Extended Life Aluminide Fuel Plates*, ES-50607A, November 5, 1980.
15. D. F. Atkins, *Development and Fabrication of Extended-Life Aluminide Fuel Plates*, N345 TR 000001, Rockwell International, June 1982.
16. Performed by G. Hoffman, Argonne National Laboratory, Chicago.
17. M. L. Griebenow et al., "ATR Startup Fuel-Plate-Cladding Corrosion Test: Preliminary Data and Conclusions," *Trans. Am. Nucl. Soc.*, 14, 761, 1971. Also in *TRA Oxide Film Control and Surveillance*, RE-77-059, 1972.
18. L. D. Koeppen and J. W. Rogers, *Fission Product Distributions in ELAF Fuel Plates*, ST-CS-002-86, January 1986.
19. W. J. Maeck, et al., *Isotope Correlation Studies Relative to High Enrichment Test Reactor Fuels*, ICP-1156, June 1978.
20. B. S. Borie, Jr., "Crystal Structure of UAl_4 ," *Journal of Metals*, 3, September 1951, pp. 800-802.
21. H. J. Eding and E. M. Carr, *High Purity Uranium Compounds*, ANL-6339, March 1961.
22. M. I. Ivanov, V. A. Tumbakov, and N. S. Podol'skaya, "The Heats of Formation of UAl_2 , UAl_3 , and UAl_4 ," *Atomnaya Energiya*, 5, p. 166 [Sov. S. Atomic Energy, 5, 1958, 1997].

23. P. R. Openshaw and L. L. Shreir, "Oxidation of Uranium-Aluminum Intermetallic Compounds," *Corrosion Science*, 3, 1963, pp. 217-237.
24. P. R. Openshaw and L. L. Shreir, "Oxidation of Uranium-Aluminum Intermetallic Compounds II, Nature and Surface Topography of Oxide Films," *Corrosion Science*, 4, 1964, pp. 335-344.
25. L. L. Shreir, *Corrosion, Volume 1, Metal/Environmental Reactions*, Newnes - Butterworths, Boston, 1976, pp. 1:162 and 4:16.
26. N. G. Fontana and N. D. Greene, *Corrosion Engineering*, McGraw Hill, New York, 1978, pp. 48-58.
27. M. Pourbaix, *Atlas of Electrochemical Equilibrium in Aqueous Solutions*, Pergamon Press, New York, 1966, pp. 168-176.
28. J. E. Draley, *Aqueous Corrosion of 1100 Aluminum and of Aluminum-Nickel Alloys*, TID-7587, 1959.
29. D. R. Dickinson, "Oxide Dissolution In Corrosion of Aluminum Cladding on Nuclear Reactor Fuel Elements," *Corrosion*, 21, January 1965, pp. 19-27.
30. K. Nisancioglu and H. Holtan, "The Protection Potential of Aluminum," *Corrosion Science*, 18, 1978, pp. 1011-1023.
31. A. Broli and H. Holean, "Determination of Characteristic Pitting Potentials for Aluminum by Use of the Potentiostatic Methods," *Corrosion Science*, 17, 1977, pp. 59-69.
32. O. Hunderi, "Diffuse Light Scattering: A Way to Study Pitting Corrosion In Situ," *Corrosion Science*, 19, 9, 1979, pp. 621-630.
33. K. Vinjamuri, *Postirradiation Examination of Advanced Test Reactor Fuel Elements XA377N and XA379N*, EGG-TFBP-5968, September 1982.
34. J. M. Beeston, *ETR Fuel Element Pitting*, RE-M-78-012, April 1978.
35. American Society for Testing and Materials, Philadelphia, PA, ASTM G46, *Standard Recommended Practice for Examination and Evaluation of Pitting Corrosion*.
36. American Society for Testing and Materials, Philadelphia, PA, ASTM G16, *Standard Recommended Practice for Applying Statistics to Analysis of Corrosion Data* (Reapproved 1977).
37. C. B. Barger and R. B. Givens, "Localized Corrosion of Aluminum: Blister Formation as a Precursor of Pitting," *Journal of Electrochemical Society*, 124, 2, 1977, pp. 1845-48.

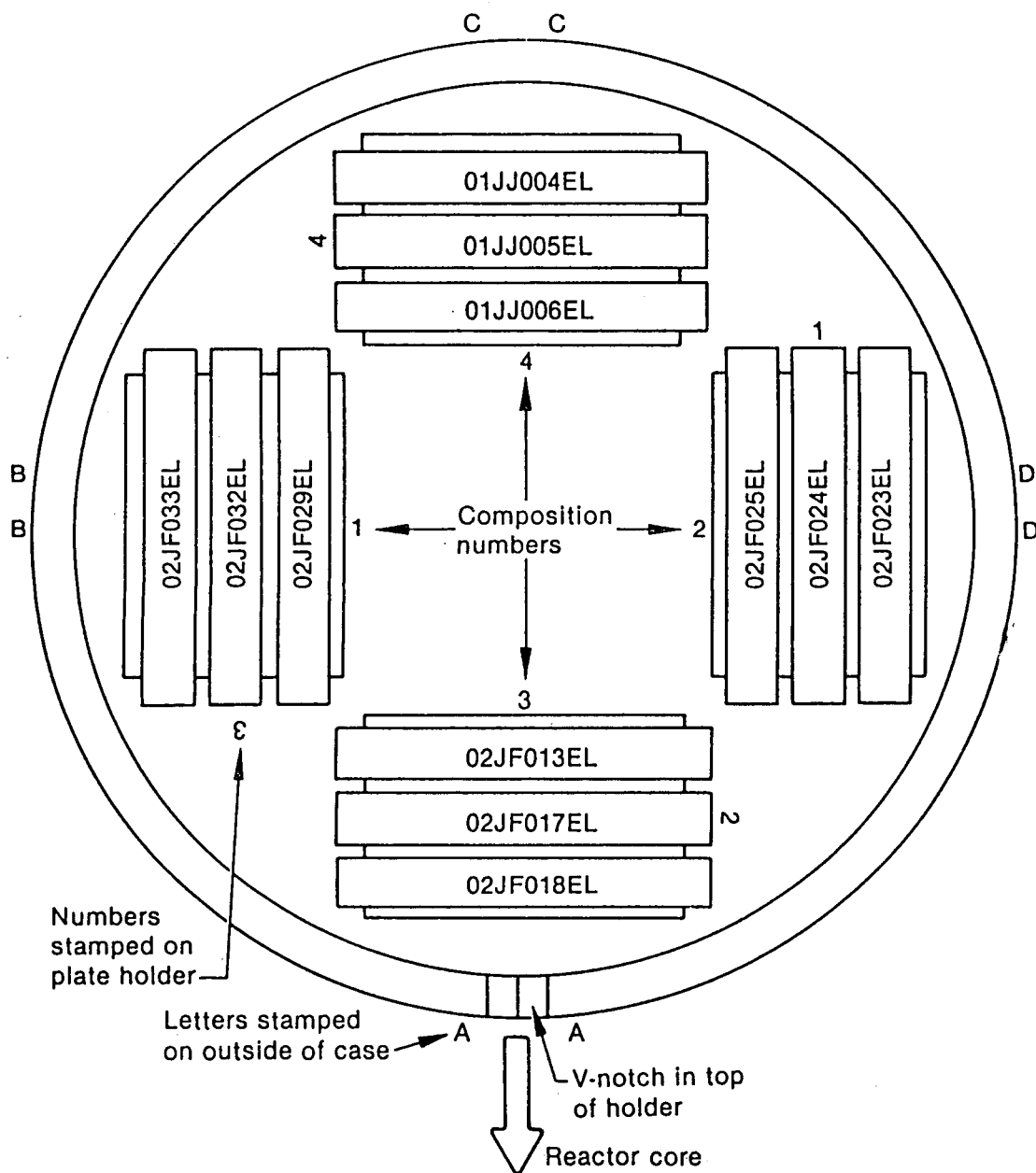
APPENDIX A
IRRADIATION DATA

APPENDIX A

IRRADIATION DATA

Table A-1. Plate irradiation history

Position	Irradiation Times								
	7-19-81 to 5-6-82	10-1-82 to 3-16-83	1-27-84 to 3-7-84	3-7-84 to 4-24-84	4-24-84 to 7-29-84	7-29-84 to 9-9-84	9-9-84 to 10-21-84	10-21-84 to 3-31-85	3-31-85 to 6-23-85
Plate Number									
A	18	33	30	30	30	30	20	20	20
A	17	32	32	32	36	8	19	19	19
A	13	31	31	31	34	34	13	9	6
B	33	16	20	20	20	20	30	30	30
B	32	15	19	19	19	19	8	8	8
B	29	13	13	13	13	13	34	34	34
C	4	5	5	5	1	1	1	1	5
C	5	6	6	6	6	6	6	6	6
C	6	3	7	7	7	7	7	7	7
D	23	28	28	28	28	28	28	28	28
D	24	27	27	27	27	27	27	10	10
D	25	26	26	22	22	22	22	22	22



Position	Composition Material	Number
A	UAl ₂ 50 vol%	3
B	UAl ₂ 40 vol%	1
C	UAl ₃ 50 vol%	4
D	UAl ₂ 45 vol%	2

6 3162

Figure A-1. Fuel plate experimental configuration.

FISSION PRODUCT RADIONUCLIDE DISTRIBUTIONS IN ELAF FUEL PLATES

INTRODUCTION

Twelve ELAF (Extended Life Aluminide Fuel) fuel plates, which were irradiated^a in the ATR (Advanced Test Reactor) I type irradiation positions, were examined by gamma-ray spectroscopy measurements at the TRA (Test Reactor Area) Hot Cell Facility. This work is part of a joint research program to develop fuels for University reactors. The fuel plates were examined at spatial locations along the axis and edges of the fuel containing regions. The purpose of these measurements was to determine the distribution of gamma-ray emitting fission product radionuclides in the fuel. These results will be combined with radiochemical analyses of samples taken from the fuel plates to determine the overall fuel burn-up in each plate.

SCANNING EQUIPMENT AND ANALYSIS METHODS

Scanning is accomplished using the TRA Hot Cell scanner which consists of: (1) the scanner bed with a horizontal and vertical drive system, (2) a collimator which penetrates the hot cell well, (3) a Ge (Li) gamma-ray detector with associated electronics, (4) a two peak precision pulser for automatic spectral gain calibration, and (5) a Fabri-Tek MP-12 microcomputer for local control of the scanner bed and gamma spectral data acquisition. The system is controlled remotely via a Vadic Full Duplex Modem data link between the Fabri-Tek computer and the PDP-11/44 computer, located in the Radiation Measurements Laboratory (RML). The operator can load a sequence of commands on the PDP-11 which will execute a predetermined scan sequence. During remote operations, the scanner bed can be positioned at a predetermined point; a 4096 channel gamma-ray spectrum accumulated for a predetermined period of time, and the spectral data transferred to the PDP-11/44 where it is automatically stored and analyzed. The scanner bed will then be automatically positioned at the next predetermined scan point and the entire process repeated. The operation is terminated when the last scan point entered in the command sequence has been analyzed.

a. See Table A-1 and Figure A-1.

The scanner bed has two Slo-Syn stepping motors which are directly coupled to the X (Horizontal) and Y (Vertical) drive lead screws with end-of-travel limit switches for each drive. The scanner bed travel is limited to 60 in. of horizontal movement and 7 in. of vertical movement, with a spatial resolution of 0.01 in. The stepping pulses for each motor and the limit switch signals to the MP-12 motor drive interface are optically coupled to reduce the effects of noise from the motors and translators. The X drive can be operated at two speeds. The fast speed is 16 in./min and is utilized during initial "set-up" when determining the location of the radioactive objects and the variations of their radioactivity. The slow speed is 2 in./min and is used mostly for the gross activity profile scanning. The Y drive operates at a fixed speed of 2 in./min.

Six different sized collimators are presently available for use. The collimators are a section of round stainless steel stock about 4 ft long and 3 in. in diameter, each with a different size collimation opening (slit) which penetrates through the entire length. Five collimators have openings which are all 0.500 in. in height and have widths of 0.010 in., 0.020 in., 0.040 in., 0.080 in. and 0.250. A collimator with a larger opening is also available; it has a collimation opening of 1.00 in. height and 0.50 in. width. The collimator penetrates the hot cell wall and presents a collimated gamma-ray beam to the detector which is situated outside the hot cell. The selection of collimator size is dependent on the gamma intensity of the item being scanned. The size selected is usually determined by the counting rate the detector is experiencing. Occasionally there exist situations where the item being scanned has such a relatively low count rate that the collimator needs to be completely removed and the gamma scanning done through the resultant 3 in. diameter opening. The collimator can be rotated to position the slit for either axial (horizontal) or transverse (vertical) scans. The 0.040 in. width collimator was used during scanning of the ELAF fuel plates.

The reference locations of the top and bottom of a fuel region, and its centerline, are determined by a gross scan stepping technique. With the collimator oriented horizontally, the rod is moved in small steps in the vertical direction. A 10 s count is done at each location (step) and a visual inspection is made of the resultant spectrum. A total integrated gross count is also tabulated at that time. The two locations at which sharp changes in

total gross gamma count rate occur and "key" isotopes are observed are noted. The axial centerline of the fuel is calculated from the measurement of the fuel axial boundaries. The locations of the fuel top and bottom are determined by orienting the collimator vertically, positioning its midpoint at the axial centerline of the fuel, and noting the point at which the gross gamma count rate changes sharply and "key" isotopes are observed while stepping from a position clearly off the fuel to a position clearly on the fuel. "Key" isotopes are defined at the radionuclides, which are determined to be unique to the fuel being scanned.

After all the initial gross activity data is examined and the isotopic scan locations are determined, the RML PDP-11/44 is programmed for the automatic scan sequence of the fuel plate. The RML PDP-11/44 analysis procedure performs the following functions on each gamma-ray spectrum:

- Energy calibrates the spectrum based on the pulser data.
- Searches the spectrum for all prominent peaks.
- Energies of selected peaks from the summary file will be written to the limit library. This ensures answers will be obtained for all desired peaks.
- Fit all found and selected peaks to a Gaussian distribution.
- Performs decay corrections if necessary.
- Subtracts background values for each peak if they exist in the background spectrum.
- Prints the results from all peaks on a line printer.
- Writes results of the specified energy peaks to a summary file.

DESCRIPTION OF MEASUREMENTS

The spectroscopy data consists of 4096 channel spectra of gamma counts versus energy at preselected locations on each fuel plate. The spatial locations for gamma-ray spectroscopy measurements on each fuel

plate were selected in order to: (1) provide both axial (fuel length) and transverse (fuel width) distributions, (2) obtain spectroscopy measurements at exactly the same spatial locations where the samples for radiochemical analyses will be removed, and (3) provide sufficient high quality data in a cost effective and timely way.

Sketches of radiographs from each plate showed the location and dimensions of the fuel region, and the distance from the end of the fuel to the end of the plate. Each fuel plate was gamma-scanned from the bottom to the top. From these scans, the ends of the fuel regions were accurately determined and the zero reference positions were established relative to the bottom end of each plate. The fuel dimensions determined by the gamma-scans step technique agreed (on the average) with the dimensions from the radiographs to within 0.04 in. on the lengths and within 0.02 in. on the widths. This good agreement demonstrates that very accurate positioning is established relative to the bottom end of the plates.

The collimator used in the measurements has actual opening dimensions of 0.040 in. x 0.500 in. Because of the distance from the collimator to the fuel plates, the actual area of the fuel plate which is viewed by the collimator-detector arrangement is 0.055 in. x 0.688 in.

In order to obtain sufficient counting statistics, count times for the gamma-ray spectroscopy measurements (to determine the fission products radionuclide distributions in these plates) varied from 500 s to 900 s depending on the counting rates.

RESULTS

The results from these measurements are given in relative counts per second for each individual radionuclide. Since no efficiency calibrations exist for these measurements, quantitative activities and gamma-intensities are undetermined. Therefore, *the counts per second of one radionuclide are not related to another radionuclide*. All the data have been decay corrected to 6-23-85 @ 2000 hr, and corrected for any background activities in the hot cell.

The results are presented on sketches of the fuel plates which illustrate the location where each measurement was taken, the orientation of the collimator, and the area viewed by the collimator detector. Each scan-point location is shown with an asterisk. The

associated count rate (counts/second) and uncertainty is shown to the right of each asterisk.

Random uncertainties, including the counting statistics and photopeak fitting components, are reported.

At the centerline locations (1.75 in., 4.54 in., 6.40 in. and 9.40 in.) the uncertainty also includes the scanner system reproducibility component. These positions were each measured twice in order to better establish the uncertainties, including positioning.

APPENDIX B
CORE AND PLATE DATA

APPENDIX B

CORE AND PLATE DATA

Table B-1. Core and plate specifications

Plate Number	Core Compact wt (g)	UAl _x wt (g)	Plate Preirradiation					Actual Core Volume (cm ³)	U Density (g/cm ³)	Void Volume (%)	Plate Thickness (in.)	Core Length (in.)
			Dry wt (g)	Wet wt (g)	B-10 wt (g)	U wt (g)						
<u>50 vol% UAl₃</u>												
01	11.94	8.076	32.25	21.92	0.014	5.73	2.882	2.0	7.23	0.0510	10.31	
03	11.96	8.075	32.17	21.86	0.014	5.73	2.899	—	7.51	0.0510	10.44	
04	11.95	8.076	32.29	21.95	0.014	5.73	2.881	—	7.07	0.0512	10.37	
05	11.94	8.076	31.99	21.73	0.014	5.73	2.908	1.970	8.04	0.0510	10.50	
06	11.95	8.076	32.23	21.91	0.014	5.73	2.883	1.988	7.13	0.0512	10.56	
07	11.95	8.075	32.18	21.85	0.014	5.73	2.912	1.968	8.04	0.0511	10.44	
08	11.94	8.075	32.10	21.82	0.014	5.73	2.888	—	7.39	0.0511	10.50	
09	11.96	8.075	32.31	21.95	0.014	5.73	2.898	—	7.47	0.0514	10.56	
10	11.95	8.075	32.16	21.85	0.014	5.73	2.899	—	7.50	0.0512	10.69	
Average										7.49		
<u>50 vol% UAl₂</u>												
13	13.70	10.057	33.41	23.18	0.020	7.93	2.998	2.645	10.98	0.0510	10.62	
15	13.70	10.057	33.53	23.23	0.020	7.93	3.024	2.622	11.75	0.0512	10.56	
16	13.69	10.057	33.41	23.16	0.020	7.93	3.014	2.631	11.49	0.0510	10.62	
17	13.69	10.057	33.47	23.19	0.020	7.92	3.023	—	11.72	0.0511	10.62	
18	13.70	10.057	33.56	23.30	0.020	7.92	2.973	—	10.23	0.0513	10.62	
19	13.68	10.058	34.02	23.60	0.020	7.93	2.956	2.683	9.87	0.0519	10.69	
20	13.69	10.057	33.96	23.52	0.020	7.92	3.002	2.638	11.02	0.0520	10.75	
Average										11.01		
<u>45 vol% UAl₂</u>												
22	13.01	9.039	33.04	22.83	0.018	7.12	2.860	2.49	7.23	0.0510	10.37	
23	13.02	9.038	32.95	22.77	0.018	—	2.867	—	7.32	0.0509	10.56	
24	13.02	9.038	33.12	22.90	0.018	—	2.845	—	6.59	0.0513	10.56	
25	13.02	9.038	32.96	22.74	0.018	—	2.904	—	8.48	0.0511	10.50	
26	13.01	9.037	33.08	22.84	0.018	—	2.875	—	7.73	0.0512	10.56	
27	13.03	9.037	32.84	22.68	0.018	7.13	2.891	2.466	8.08	0.0509	10.62	
28	13.00	9.039	33.12	22.86	0.018	7.12	2.877	2.475	7.62	0.0510	10.62	
Average										7.58		

Table B-1. (continued)

Plate Number	Core Compact wt (g)	UAl _x wt (g)	Plate Preirradiation					Actual Core Volume (cm ³)	U Density (g/cm ³)	Void Volume (%)	Plate Thickness (in.)	Core Length (in.)
			Dry wt (g)	Wet wt (g)	B-10 wt (g)	U wt (g)						
<u>40 vol% UAl₂</u>												
29	12.51	8.018	32.82	22.50	0.016	6.33	2.867	2.208	5.81	0.0513	10.62	
30	12.51	8.018	32.93	22.56	0.016	6.32	2.877	2.197	6.02	0.0519	10.62	
31	12.51	8.019	32.81	22.46	0.016	6.32	2.901	—	6.80	0.0515	10.62	
32	12.51	8.019	32.99	22.63	0.016	6.32	2.845	2.221	4.96	0.0515	10.69	
33	12.50	8.018	32.49	22.28	0.016	6.32	2.875	2.198	6.08	0.0510	10.62	
34	12.51	8.018	32.98	22.60	0.016	6.32	2.868	—	5.75	0.0519	10.62	
36	12.51	8.018	33.09	22.66	0.016	6.33	2.878	—	5.94	0.0520	10.62	
Average 5.91												

CHEMICAL ANALYSIS REPORT				REQUEST NO.		
<div style="display: flex; justify-content: space-between;"> <div> BLIND JF CAN <u>005-004</u> VOUCHER NO. <u>9272</u> </div> <div> REQUESTED BY <u>E. Peters</u> ACCEPTED BY <u>M. M. Khan</u> DATE <u>1-15-81</u> <u>2:15</u> </div> <div> 19465 ANAL. CHEM LAB NO. 2456, 2457, 2458 </div> </div>						
Element	(X) Factor	EBC	Element	Spec. Wt%	Anal	Lab Notebook and Chemist
Ag	<0.5 ppm	0.008236	U	30.0±1	78.98	<u>N-22617-32</u>
Dy	<0.5 ppm	0.097064	Al			
B	<0.5 ppm	0.999999	O	0.60 max	0.11	<u>N-22603-12</u>
Ba	<10 ppm	0.000122	C	0.18 max	0.02	<u>N-22642-33</u>
Be	<0.5 ppm	0.000015	N	0.045 max	0.004	<u>N-22603-12</u>
Bu	<0.5 ppm	0.433973	H	0.020 max	0.001	<u>N-19474-46</u>
Ca	<25 ppm	0.000158	URANIUM ISOTOPIC COMPOSITION			
Cd	<0.5 ppm	0.325097	Isotope	Spec. Wt%	Anal	Lab Notebook and Chemist
Co	<2 ppm	0.009239	U 235	93.0±1.0	93.162	<u>Teledyne TWX</u> <u>4-002952 C028</u>
Cr	10 ppm	0.000799	U 234	1.2 max.	1.009	
Cu	10 ppm	0.000868	U 236	0.700 Max.	0.462	
Fe	100 ppm	0.000672	U 238	6.0 ± 1.0	5.368	
Gd	<0.5 ppm	4.19458	CRYSTALLINE CONSTITUENTS			
Hg	<5 ppm	0.000040	Phase	Spec. Wt%	Anal	Lab Notebook and Chemist
Mn	4 ppm	0.003443	UAl ₂	70 Min.	67	<u>MK</u> <u>X-ray Data File</u>
Mo	<5 ppm	0.000403	UAl ₃		33	
P	<50 ppm	0.000087	UAl ₄		<1	
Ni	<10 ppm	0.001122	UnAlloy		Not Detected	
Pb	<2 ppm	0.000011	95% CONFIDENCE LEVEL			
Si	100 ppm	0.000066	Total U <u>78.98 ± 0.086</u>			
Sn	8 ppm	0.000072	U 235 <u>93.162 ± 0.004</u>			
V	<100 ppm	0.001496				
V	200 ppm	0.001406				
Zn	<10 ppm	0.000241				
Zr	<250 ppm	0.000029				
Sm	<1 ppm	0.524575				
Chemist and Lab Notebook <u>MK N22632-11</u>			Total EBC <u><4.1409</u> (X) $\frac{100}{78.98} = <5.3$ EBC in U			

LEDGER ACCT. <u>38001</u>		G.O. <u>09399</u>		SUB. <u>71000</u>		RPO <u>0100180</u>	
CHEMICAL LABORATORY APPROVAL				DATE <u>1/28/81</u>			
QUALITY ASSURANCE LAB DISPOSITION							
CA LAB NO. <u>16172</u>		<input type="checkbox"/> ACCEPTED		<input type="checkbox"/> IDR			
SIGNATURE _____				DATE _____			

02
002

FUEL PLATE CORE VOID VOLUME PERCENT

DATE _____

6/18/81

ELLEN

IF

WFO 060300Z

ELAF

[illegible]

WATER TEMP & INSPECTION

24°C.

INSPECTED BY:

TE INSPECTED

LOT SUMMARY			
AVERAGE VOID %	"CRITICAL" VALUE %	SAMPLING ACCEPTANCE	Q.A. ENG. APPROVAL
11.02	Min 4.00 1.7047 PER 3-11 2.7047 PER REEL	YES	[Signature]
		NO	
		—	

003

DATE _____

6/18/81

١٢٠

0602003

230

'TE INSPECTED

art

BLEND JF
MPC 0602009

ELAF

[illegible]

WATER TEMP 3 INSPECTION

24°C.

INSPECTED BY

WE INSPECTED

6/18/81

LOT SUMMARY				
AVERAGE VOID %	"CRITICAL" VALUE %	SAMPLING ACCEPTANCE		Q.A. ENGR APPROVAL
5.94	Min 4.00 4.947 FOR S-33 3.947 FOR REST	YES	NO	apf
		/		

REPORT NO. W6102532
 RUN DATE 05/12/81
 ALLOTMENT NO. JWN321903Y
 FABRICATION DATE 05/06/81

PROGRAM NO. EL01

ATOMIC INTERNATIONAL
 NUCLEAR PLATE FABRICATION PLCCFC
 NPM FABRICATION NO. A1JF-C4
 MFC FABRICATION NO. 02002-EL

PAGE 1

BLENCE XL= 78.98 XL235=53.162
 BCFCA LCT 12512 1810 14.21

PLATE-NO	CAL(X) WT	B(4)C WT	AL WT	SUM CF INPUT-WT	DEBURRED WT	INV WT	U WT	U(235) WT	B(10) WT	** DEBURRED NET-WT	U	APCALY U(235)
2JF0011EL	10.057	.141	3.525	13.72	13.67	10.02	7.91	7.37	.020	.05	.03	.02
2JF0012EL	10.058	.141	3.526	13.73	13.70	10.04	7.93	7.39	.020	.03	.01	.00
2JF0013EL	10.057	.141	3.526	13.72	13.70	10.04	7.93	7.39	.020	.02	.01	.00
2JF0014EL	10.058	.141	3.526	13.73	13.70	10.04	7.93	7.39	.020	.03	.01	.00
2JF0015EL	10.057	.141	3.526	13.72	13.70	10.04	7.93	7.39	.020	.02	.01	.00
2JF0016EL	10.057	.141	3.525	13.72	13.69	10.03	7.92	7.38	.020	.03	.02	.01
2JF0017EL	10.057	.141	3.524	13.72	13.69	10.03	7.92	7.38	.020	.03	.02	.01
2JF0018EL	10.057	.141	3.526	13.72	13.70	10.04	7.93	7.39	.020	.02	.01	.00
2JF0019EL	10.058	.141	3.525	13.72	13.68	10.03	7.92	7.38	.020	.04	.02	.01
2JF0020EL	10.057	.141	3.525	13.72	13.69	10.03	7.92	7.38	.020	.03	.02	.01
TOTALS=	100.573	1.410	35.254	137.22	136.92	100.34	79.24	73.64	.200	.30	.16	.06
										SCHAF NET =	.15	
										DIFFERENCE	.15-	

PLATE NO. 213781
 ELEMENT NO. 02021003Y
 FABRICATION DATE 05/07/81

NUCLEAR FUEL FABRICATION RECORD
 NAME FABRICATION NO. A1JF-06
 NEG FABRICATION NO. 02006-11

COOPER NO. 8101

BLEND %U= 79.98 20235=93.162
 BORON LOT 12512 %B10 #14.21 *revised*

PLATE NO	U(235) WT	B(10) WT	AI WT	SUM OF INPUT-WT	DEBURRED WT	INV WT	U WT	U(235) WT	B(10) WT	** NET-WT	DEBURRED U	AMOUNT U(235)
02021001	8.018	.113	4.399	12.53	12.51	8.01	6.33	5.89	.016	.02	.00	.00
02021002	8.018	.113	4.401	12.53	12.51	8.00	6.32	5.89	.016	.02	.01	.00
02021003	8.019	.113	4.401	12.53	12.51	8.00	6.32	5.89	.016	.02	.01	.00
02021004	8.019	.113	4.400	12.53	12.51	8.00	6.32	5.89	.016	.02	.01	.00
02021005	8.018	.113	4.400	12.53	12.50	8.00	6.32	5.89	.016	.03	.01	.00
02021006	8.018	.113	4.400	12.53	12.51	8.00	6.32	5.89	.016	.02	.01	.00
02021007	8.019	.113	4.399	12.53	12.50	8.00	6.32	5.89	.016	.03	.01	.00
02021008	8.018	.113	4.399	12.53	12.51	8.01	6.33	5.89	.016	.02	.00	.00
TOTALS=	64.167	.906	35.199	100.24	100.06	64.02	50.58	47.12	.128	.18	.06	.00

SCRAP NET = .15
 DIFFERENCE = .03-

REPORT NO. W6102532
 RUN DATE 05/12/81
 ELEMENT NO. JWN021903Y
 FABRICATION DATE 05/07/81

PROGRAM NO. 1101

AICMICS INTERNATIONAL
 NUCLEAR PLATE FABRICATION REC'D
 NPM FABRICATION NO. A1JF-05
 MFG FABRICATION NO. 02003-EL

PAGE 2

BLEND 10= 7E-9E 10235=53.162
 BCFEN LCT 12512 1E10 14.21

PLATE-NO	UAL(X) WT	BI4(C) WT	AL WT	SUM OF INFCT-WT	DEBURRED WT	INV WT	U WT	U(235) WT	E(10) WT	% DEBURRED NET-WT	AMOUNT L	U(235) L
2JF0021LL	9.038	.127	3.883	13.05	13.02	9.02	7.12	6.64	.018	.03	.02	.01
2JF0022LL	9.039	.127	3.881	13.05	13.01	9.01	7.12	6.63	.016	.04	.02	.01
2JF0023EL	9.038	.127	3.883	13.05	13.02	9.02	7.12	6.64	.018	.02	.02	.01
2JF0024EL	9.038	.127	3.882	13.05	13.02	9.02	7.12	6.64	.018	.03	.02	.01
2JF0025EL	9.038	.127	3.882	13.05	13.02	9.02	7.12	6.64	.018	.03	.02	.01
2JF0026EL	9.037	.127	3.881	13.05	13.01	9.01	7.12	6.63	.016	.04	.02	.01
2JF0027LL	9.037	.127	3.882	13.05	13.03	9.03	7.13	6.64	.018	.02	.01	.00
2JF0028LL	9.039	.127	3.882	13.05	13.00	9.01	7.12	6.63	.016	.05	.02	.01
TOTALS=	72.304	1.016	31.056	104.40	104.13	72.14	56.97	53.09	.144	.27	.15	.07
										SCRAP NET =	.26	
										DIFFERENCE	.01-	

JJ			REQUESTED BY <u>F. PETERS</u>		19469	
ONE ONLY			ACCEPTED BY <u>[Signature]</u>		ANAL. CHEM. LAB NO.	
VOUCHER NO. <u>9292</u>			DATE <u>2-13-81</u>		<u>2475, 2476, 2477</u>	

Element	(X) Factor	EBC	Element	Spec. Wt%	Anal	Lab Notebook and Chemist
Ag	<0.5 ppm	0.008236	U	69.0 ± 3	71.13	TN/M N22612-41
Dy	<0.5 ppm	0.097054	Al		28.344	
B	<0.5 ppm	0.999999	O	0.60 max	0.37	N22603-14
Ba	<10 ppm	0.000122	C	0.18 max	0.12	N22642-34
Be	<0.5 ppm	0.000015	H	0.045 max	0.007	N22601-14
Bu	<0.5 ppm	0.433973	H	0.020 max	0.007	N19474-47
Ca	50 ppm	0.000158	URANIUM ISOTOPIC COMPOSITION			
Cd	<0.5 ppm	0.325097	Isotope	Spec. Wt%	Anal	Lab Notebook and Chemist
Co	<2 ppm	0.009239	U 235	93.0 ± 1.0	93.149	Teledyne Tbx H-010032A056
Cr	<10 ppm	0.000799	U 234	1.2 max.	1.003	
Cu	5 ppm	0.000858	U 236	0.45 ± 0.2	0.456	
Fe	100 ppm	0.000672	U 238	16.0 ± 1.0	5.394	
Gd	<0.5 ppm	4.19458	CRYSTALLINE CONSTITUENTS			
Hf	<5 ppm	0.000040	Phase	Spec. Wt%	Anal	Lab Notebook and Chemist
Mo	2 ppm	0.003443	UAl ₃		8	MK X-ray Data File 19469
P	<5 ppm	0.000403	UAl ₃	50.0 min	66	
P	<50 ppm	0.000087	UAl ₄		26	
Ni	<10 ppm	0.001122	UnAlloy		Not Detected	
Pb	<2 ppm	0.000011	95% CONFIDENCE LEVEL			
Si	75 ppm	0.000055	Total U <u>71.13 ± 0.066</u>			
Sn	4 ppm	0.000072	U 235 <u>93.149 ± 0.007</u>			
V	<100 ppm	0.001406				
V	100 ppm	0.001406				
Zn	<10 ppm	0.000241				
Zr	<250 ppm	0.000029				
Sb	<1 ppm	0.524575				

Chemist and Lab Notebook MK N22632-12	Total EBC <3.9910	(X) $\frac{100}{71.13} = <5.7$	EBC in U
--	----------------------	--------------------------------	----------

LEADER ACCT. 38001 I.O. 09399 SUB. 71000 WPO 0100183

CHEMICAL LABORATORY APPROVAL [Signature] DATE 2/27/81

QUANTITATIVE ANALYSIS LAB DISPOSITION

QA LAB NO. 16189 ☐ ACCEPTED ☐ IDR

BLEND JS
MPO 0601001
ELAF


[illegible]

WATER TEMP @ INSPECTION 26.0°C

INSPECTED BY

TE INSPECTED

6-17-81

LOT SUMMARY				
AVERAGE VOID %	"CRITICAL" VALUE %	SAMPLING ACCEPTANCE		Q.A. ENGR. APPROVAL
7.50	Min 4.00 4.75% FOR 3-15 3.75% FOR REST	YES	NO	
		<input checked="" type="checkbox"/>	<input type="checkbox"/>	

PORT NO. 102532
 DATE 05/12/81
 GIPMENT NO. JWA021903Y
 RICATION DATE 05/06/81

ATMICS INTERNATIONAL
 NUCLEAR PLATE FABRICATION RECORD
 NPP FABRICATION NO. A1JJ-21
 MFC FABRICATION NO. 01C01-EL

PAGE 4

GRAM NO. EL01

BLEND %L= 71.13 %L235=53.145
 BGRN LCT 12512 %B1C 14.21

ATE-NO	CAL(X) WT	B(4)C WT	AL WT	SLM OF INPUT-WT	DEBURRED WT	INV WT	U WT	U(235) WT	U(10) WT	** DEBURRED NET-WT	AMOUNT U	U(235)
00001EL	8.076	.098	3.806	11.98	11.94	8.05	5.73	5.33	.014	.04	.01	.00
00002EL	8.075	.098	3.807	11.98	11.94	8.05	5.73	5.33	.014	.04	.01	.00
00003EL	8.075	.098	3.807	11.98	11.96	8.06	5.73	5.34	.014	.02	.01	.00
00004EL	8.076	.098	3.806	11.98	11.95	8.06	5.73	5.34	.014	.03	.01	.00
00005EL	8.076	.098	3.807	11.98	11.94	8.05	5.73	5.33	.014	.04	.01	.00
00006EL	8.076	.098	3.805	11.98	11.95	8.06	5.73	5.34	.014	.03	.01	.00
00007EL	8.075	.098	3.805	11.98	11.95	8.06	5.73	5.34	.014	.03	.01	.00
00008EL	8.075	.098	3.806	11.98	11.94	8.05	5.73	5.33	.014	.04	.01	.00
00009EL	8.075	.098	3.807	11.98	11.96	8.06	5.73	5.34	.014	.02	.01	.00
00010EL	8.075	.098	3.806	11.98	11.95	8.06	5.73	5.34	.014	.03	.01	.00
TOTALS=	80.754	.980	38.062	119.80	119.48	80.56	57.30	53.36	.140	.32	.10	.00

SCRAP NET = .04
 DIFFERENCE .26-

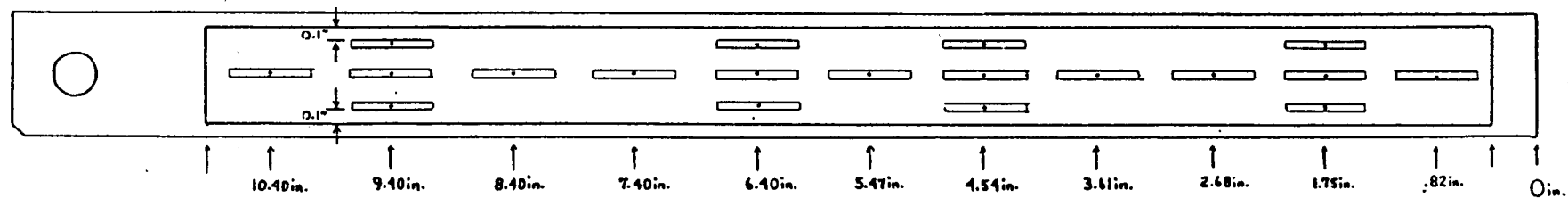
B-14

ELAF FUEL PLATE

Gamma Scan

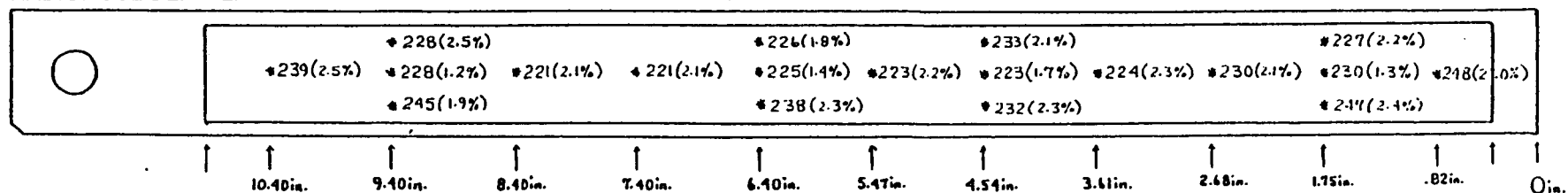
(.040 in. x .500 in. collimator)

ACTUAL AREA VIEWED = .055 in. x .688 in.



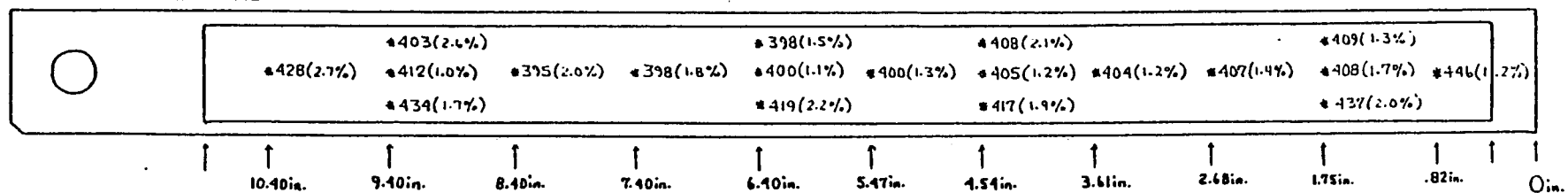
No. 5

RADIONUCLIDE: ^{95}Zr



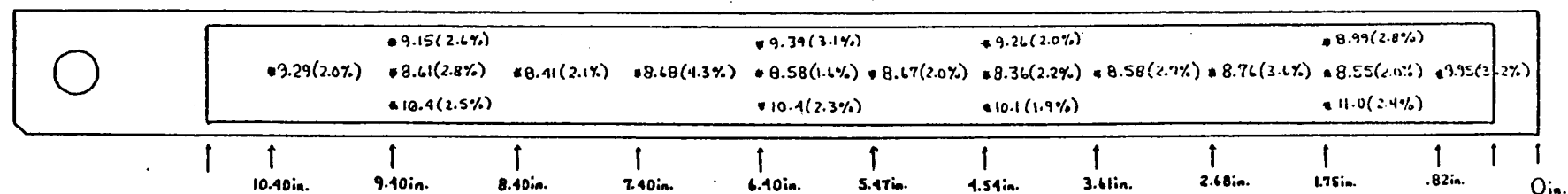
No. 5

RADIONUCLIDE: ^{103}Ru



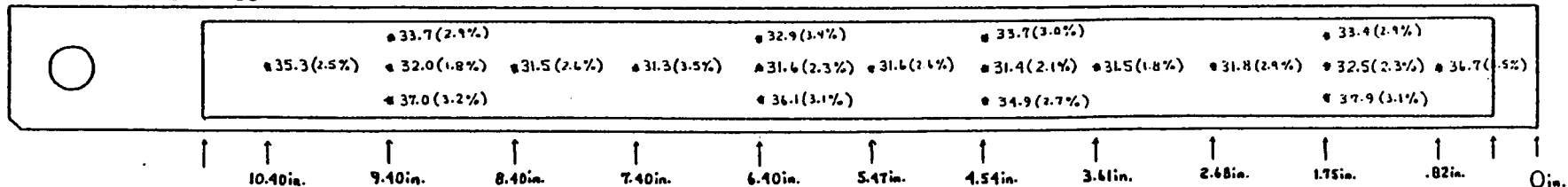
No. 5

RADIONUCLIDE: ^{134}Cs



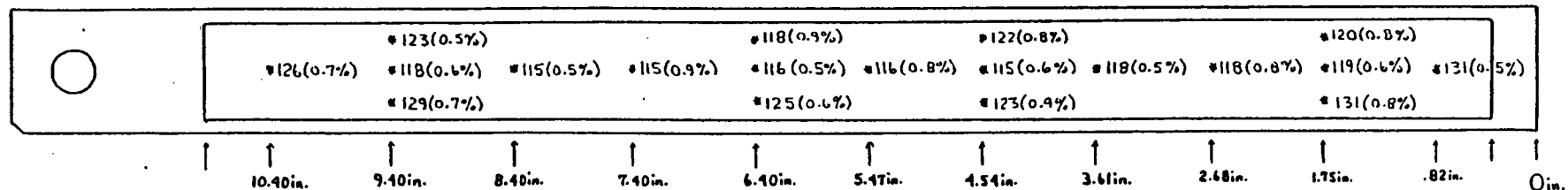
No. 5

RADIONUCLIDE: ^{137}Cs



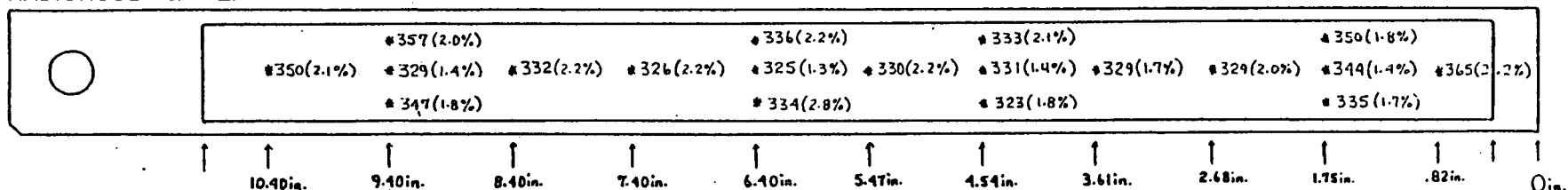
No. 5

RADIONUCLIDE: ^{144}Ce



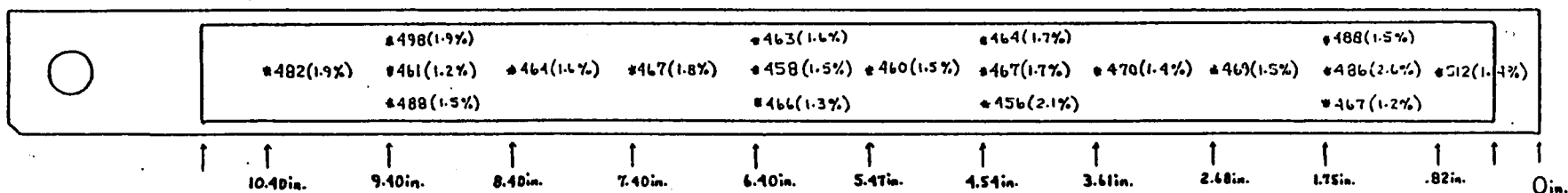
No. 6

RADIONUCLIDE: ^{95}Zr



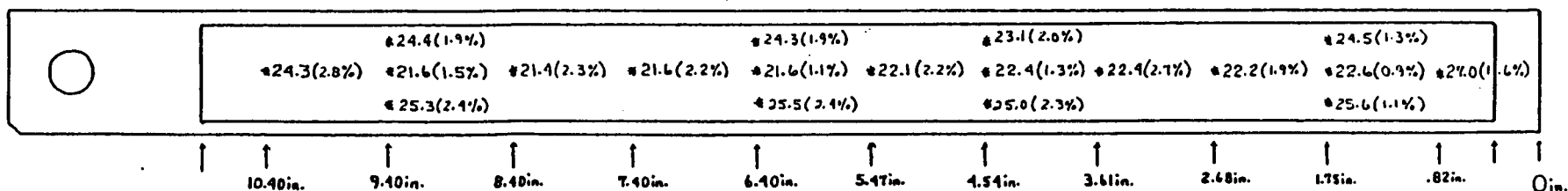
No. 6

RADIONUCLIDE: ^{103}Ru



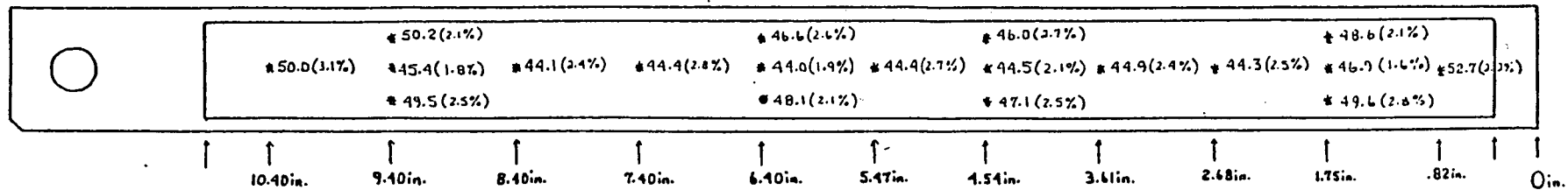
No. 6

RADIONUCLIDE: ^{134}Cs



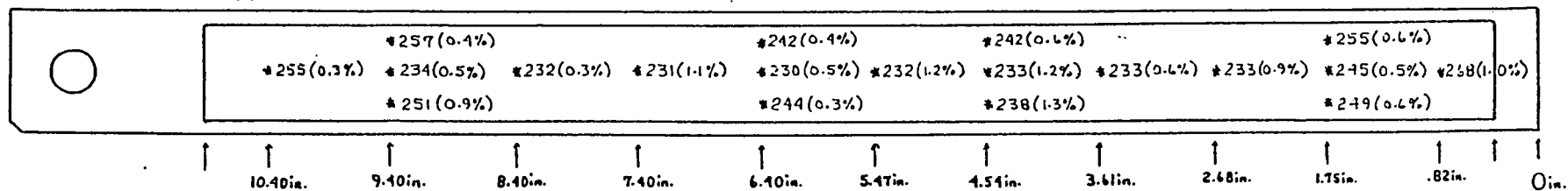
No. 6

RADIONUCLIDE: ^{137}Cs



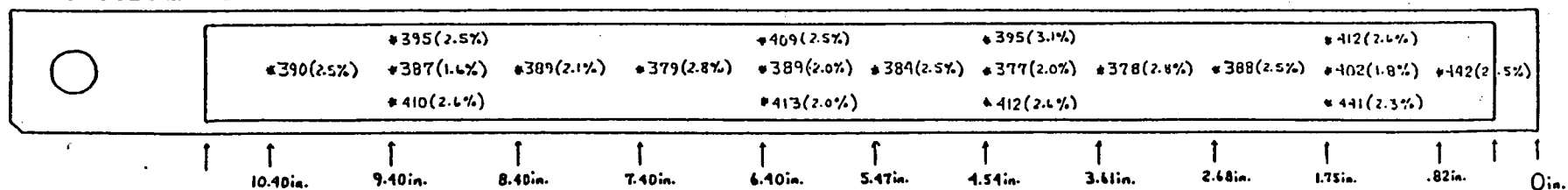
No. 6

RADIONUCLIDE: ^{144}Ce



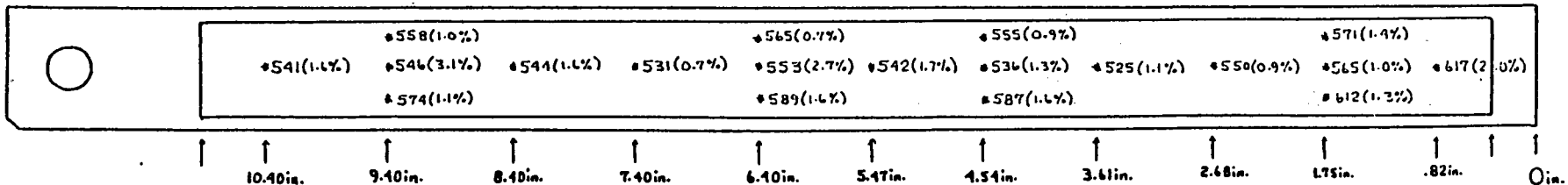
No. 7

RADIONUCLIDE: ^{95}Zr



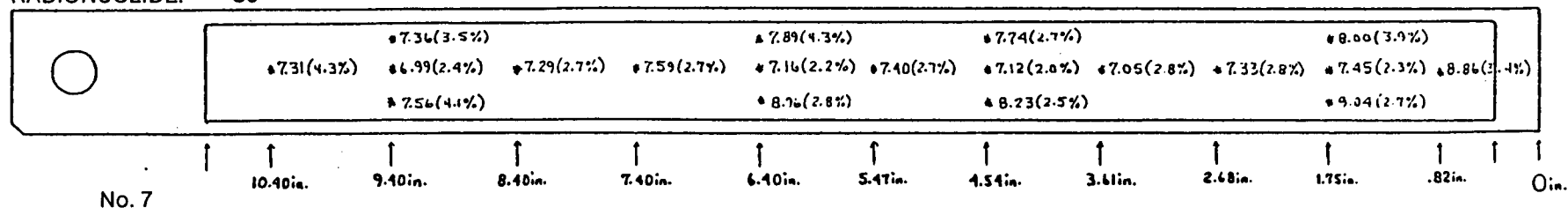
No. 7

RADIONUCLIDE: ^{103}Ru

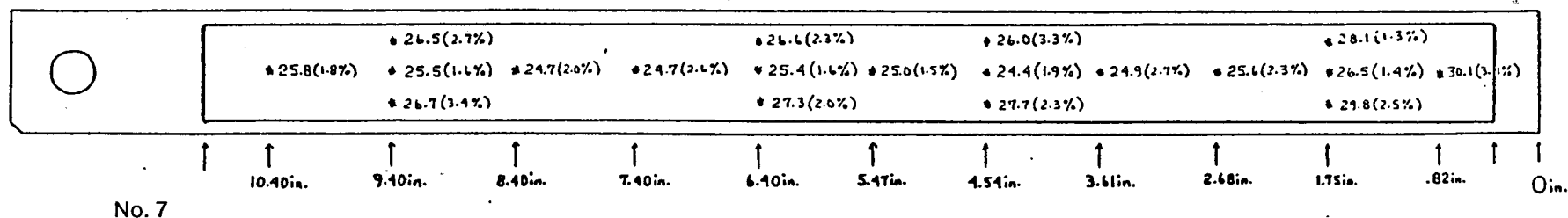


No. 7

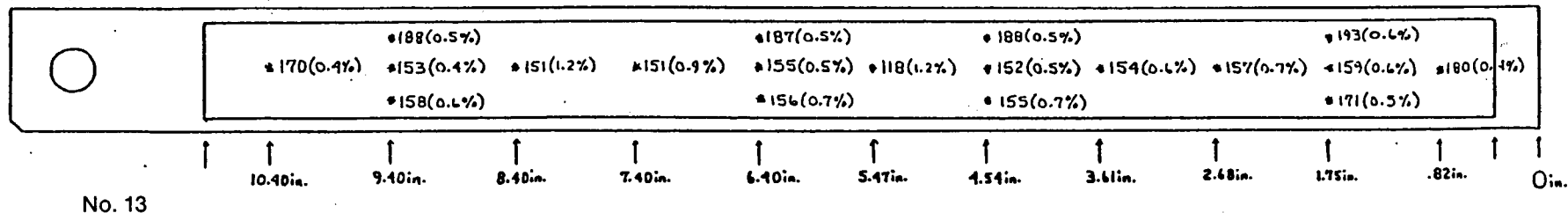
RADIONUCLIDE: ^{134}Cs



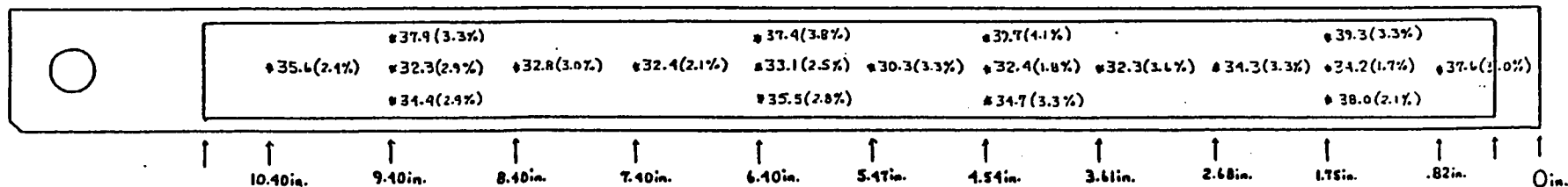
RADIONUCLIDE: ^{137}Cs



RADIONUCLIDE: ^{144}Ce

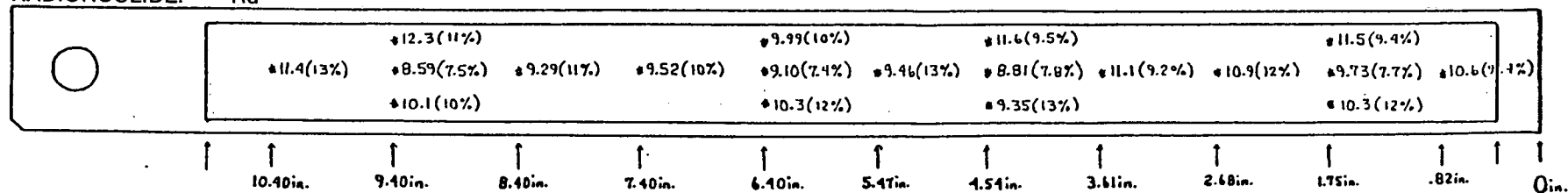


RADIONUCLIDE: ^{95}Zr



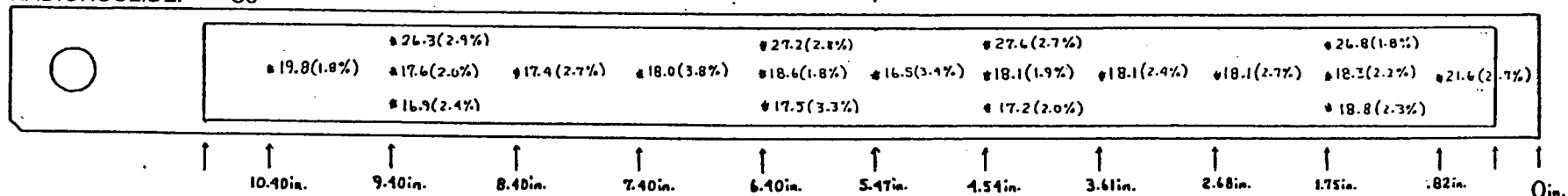
No. 13

RADIONUCLIDE: ^{103}Ru



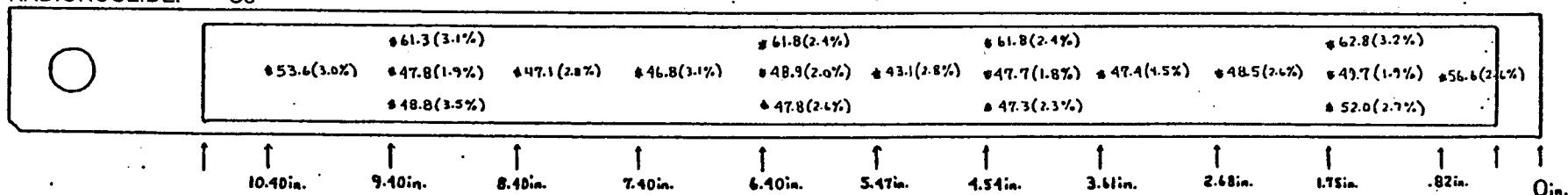
No. 13

RADIONUCLIDE: ^{134}Cs



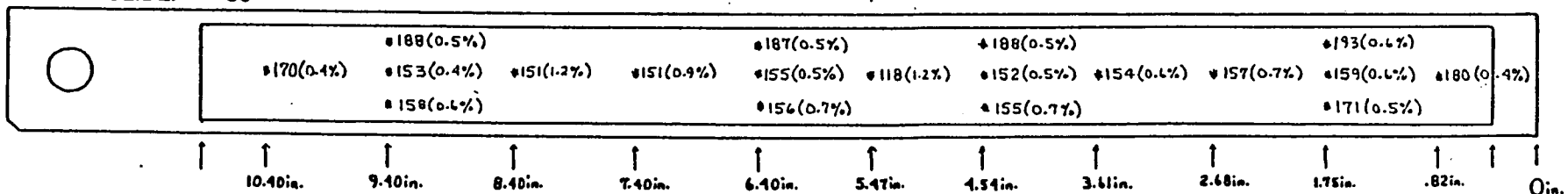
No. 13

RADIONUCLIDE: ^{137}Cs



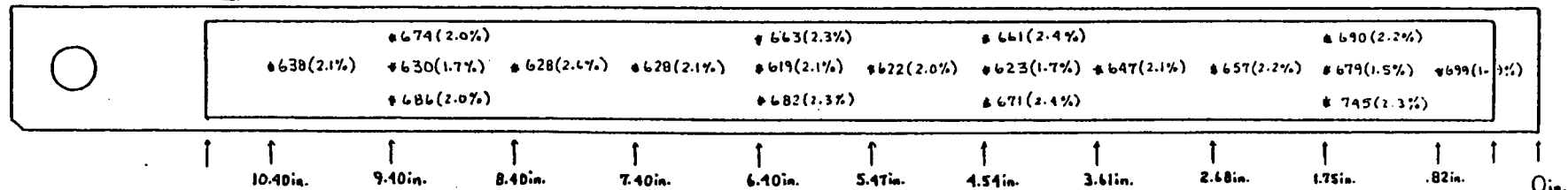
No. 13

RADIONUCLIDE: ^{144}Ce



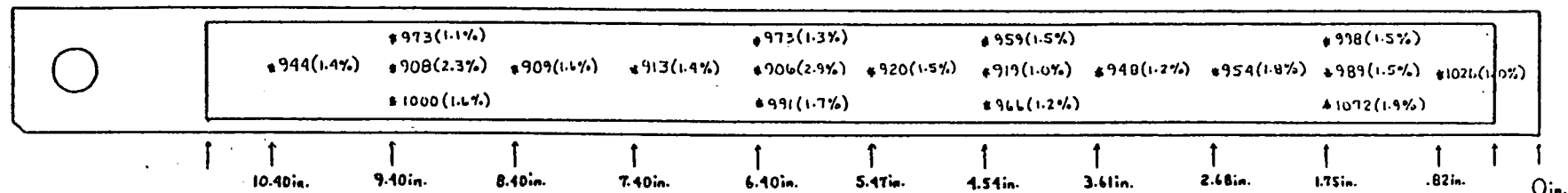
No. 19

RADIONUCLIDE: ^{95}Zr



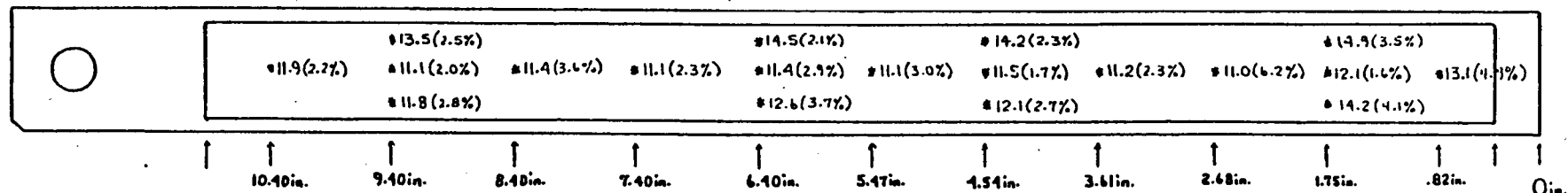
No. 19

RADIONUCLIDE: ^{103}Ru



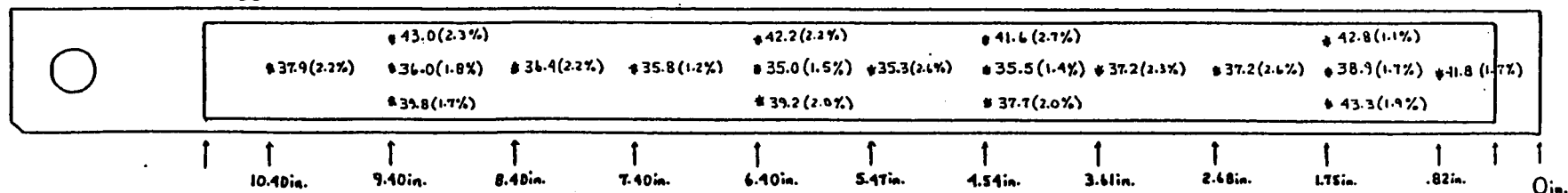
No. 19

RADIONUCLIDE: ^{134}Cs



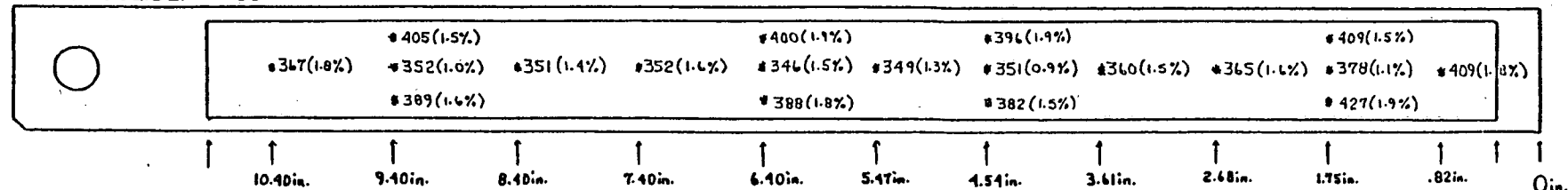
No. 19

RADIONUCLIDE: ^{137}Cs



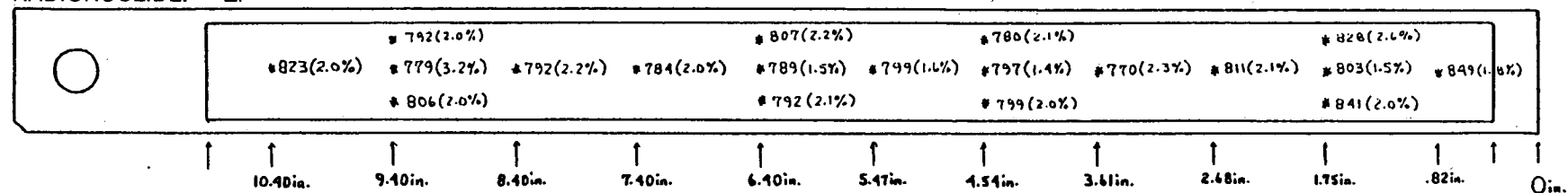
No. 19

RADIONUCLIDE: ^{144}Ce



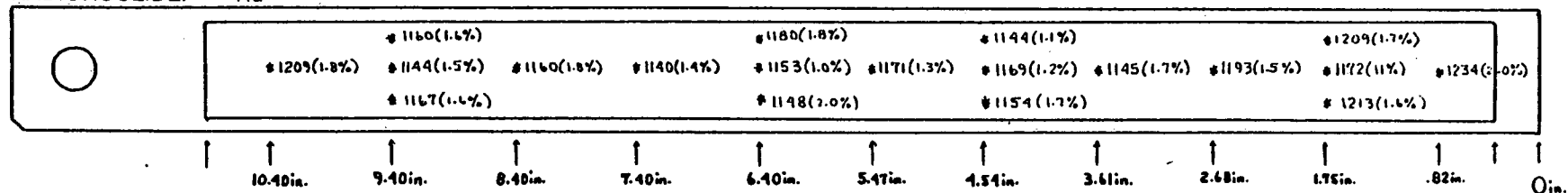
No. 20

RADIONUCLIDE: ^{95}Zr



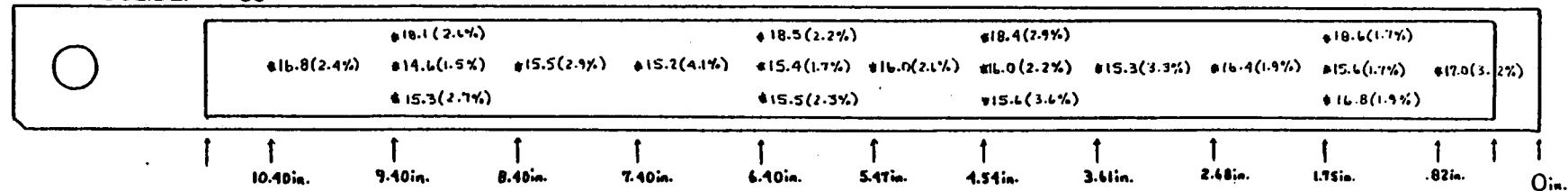
No. 20

RADIONUCLIDE: ^{103}Ru



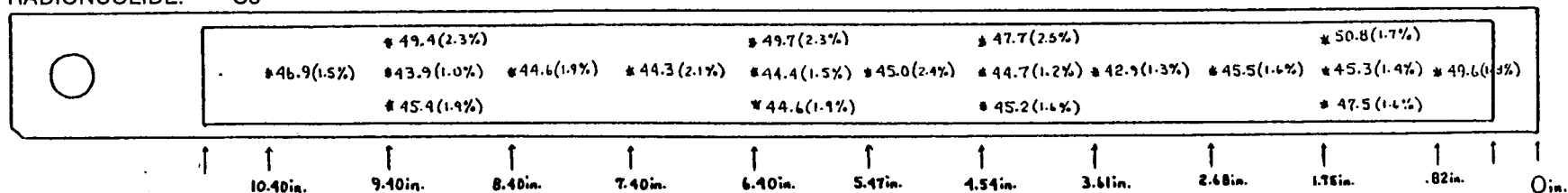
No. 20

RADIONUCLIDE: ^{134}Cs



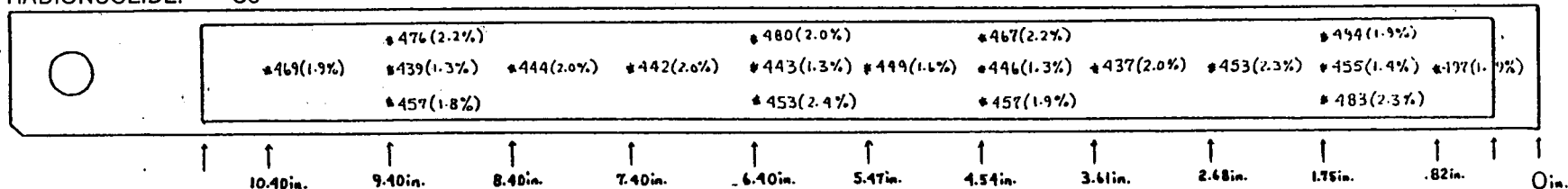
No. 20

RADIONUCLIDE: ^{137}Cs



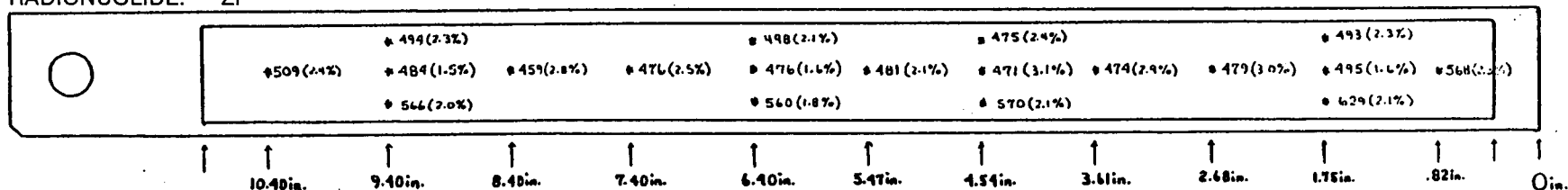
No. 20

RADIONUCLIDE: ^{144}Ce



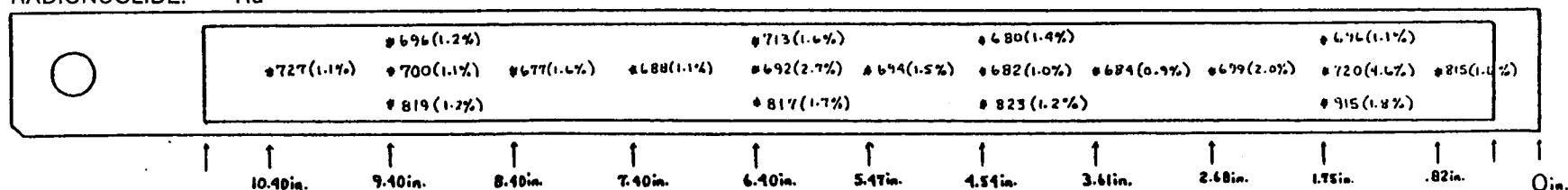
No. 22

RADIONUCLIDE: ^{95}Zr



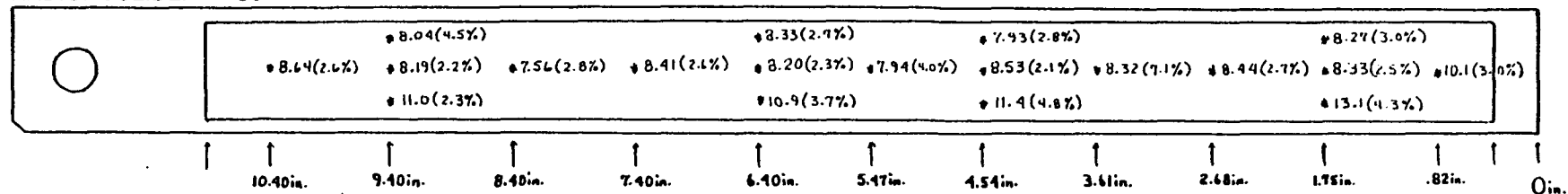
No. 22

RADIONUCLIDE: ^{103}Ru



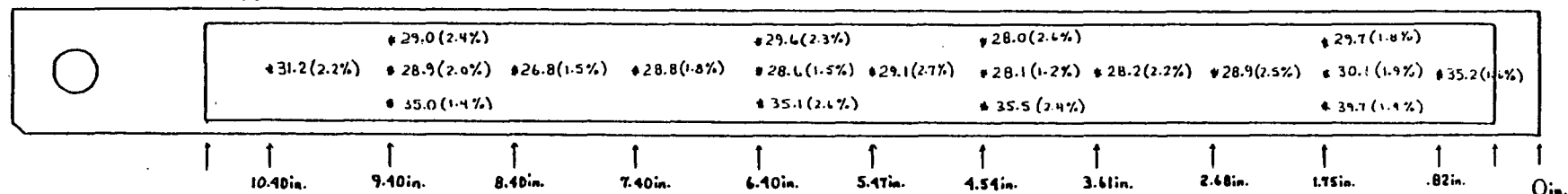
No. 22

RADIONUCLIDE: ^{134}Cs



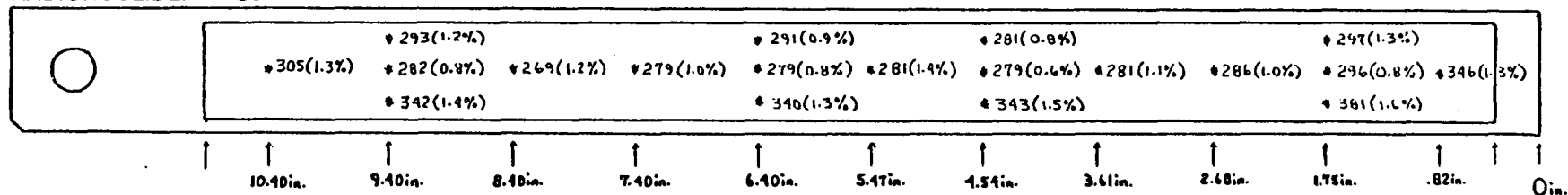
No. 22

RADIONUCLIDE: ^{137}Cs



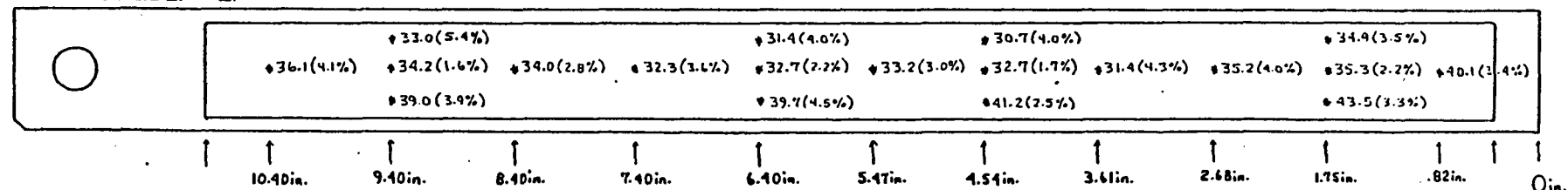
No. 22

RADIONUCLIDE: ^{144}Ce



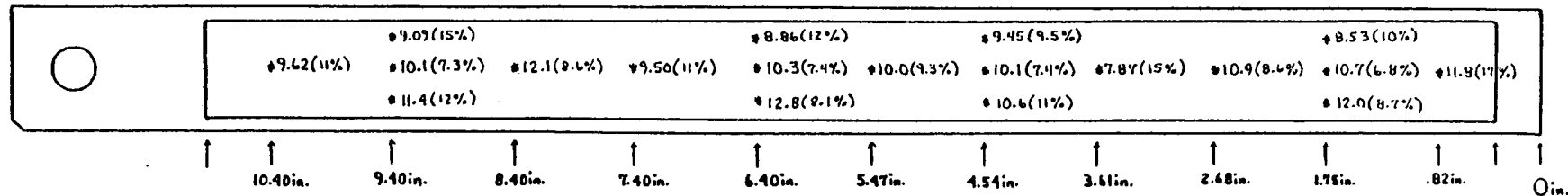
No. 27

RADIONUCLIDE: ^{95}Zr



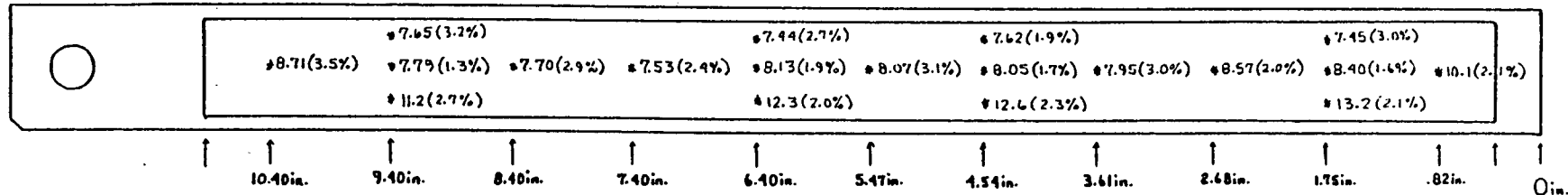
No. 27

RADIONUCLIDE: ^{103}Ru



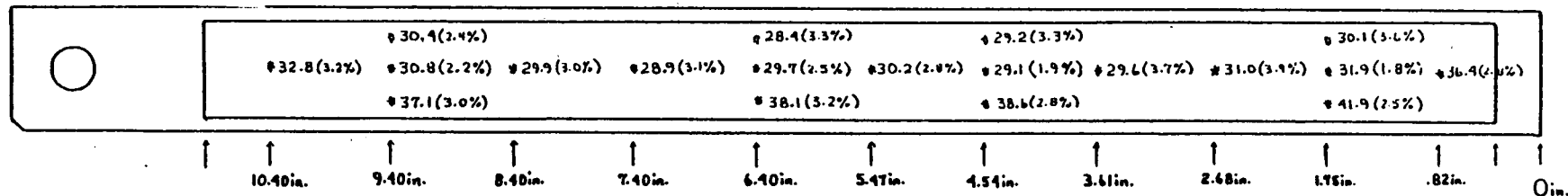
No. 27

RADIONUCLIDE: ^{134}Cs



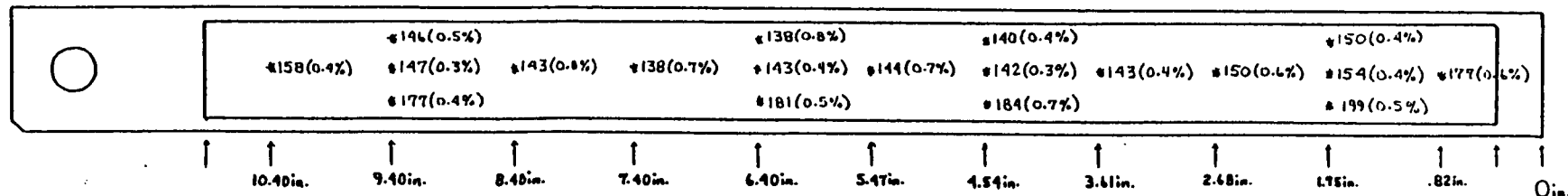
No. 27

RADIONUCLIDE: ^{137}Cs



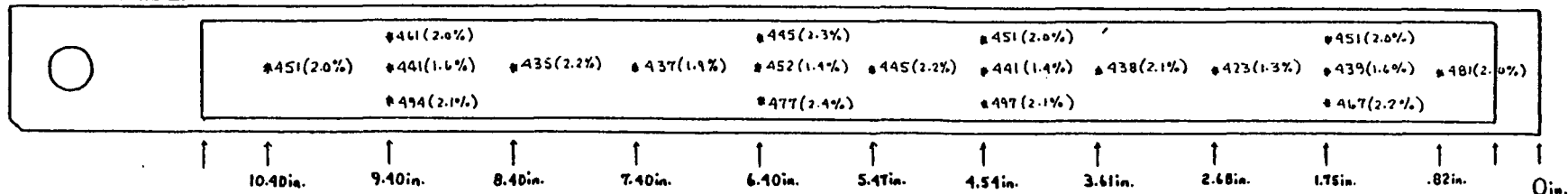
No. 27

RADIONUCLIDE: ^{144}Ce



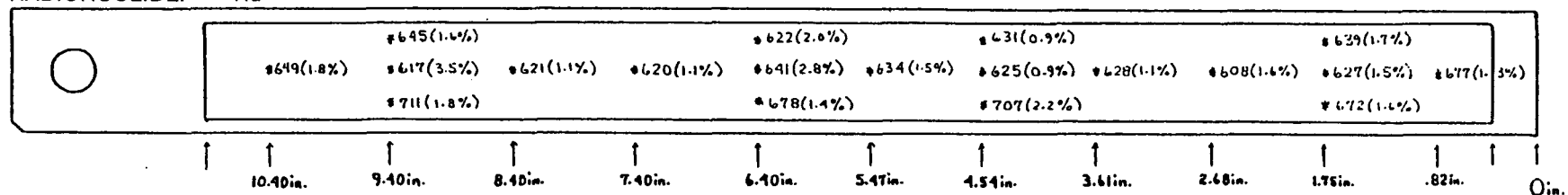
No. 28

RADIONUCLIDE: ^{95}Zr



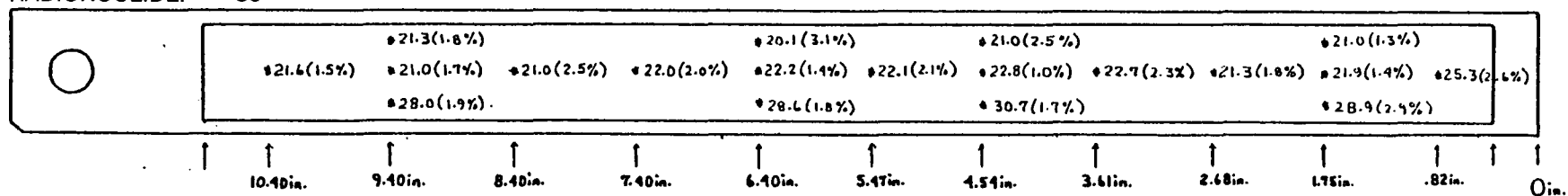
No. 28

RADIONUCLIDE: ^{103}Ru



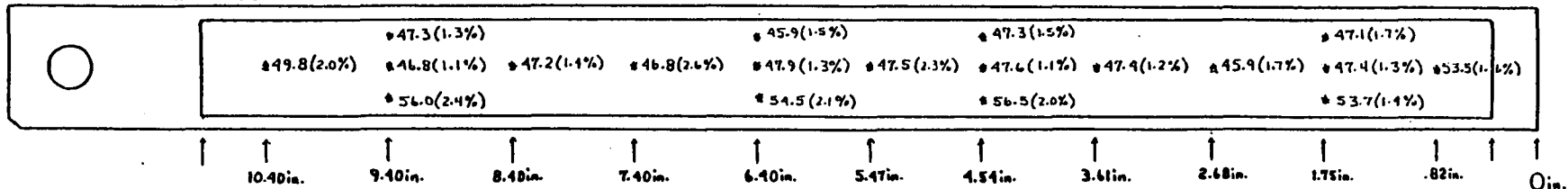
No. 28

RADIONUCLIDE: ^{134}Cs



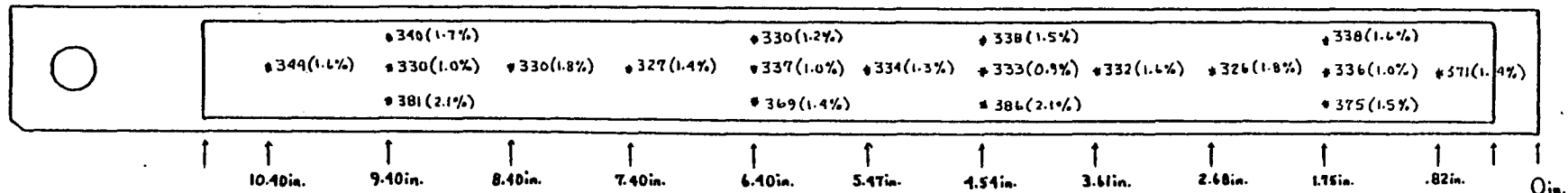
No. 28

RADIONUCLIDE: ^{137}Cs



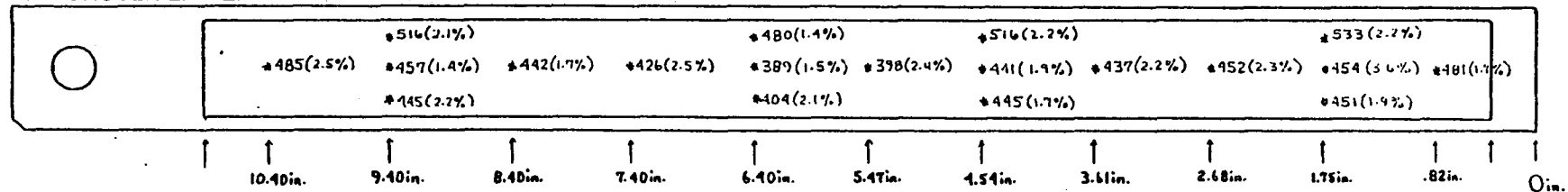
No. 28

RADIONUCLIDE: ^{144}Ce



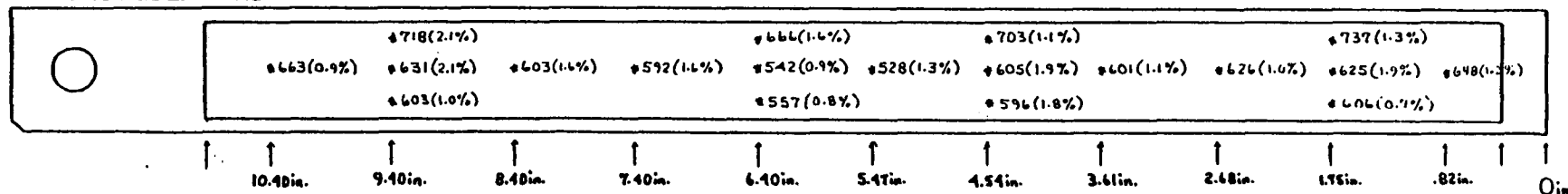
No. 30

RADIONUCLIDE: ^{95}Zr



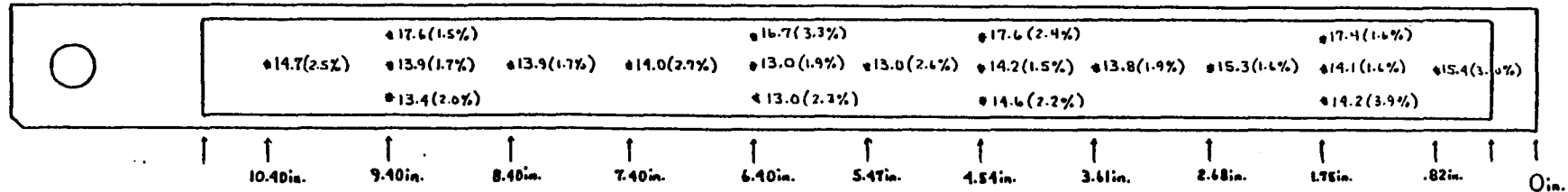
No. 30

RADIONUCLIDE: ^{103}Ru



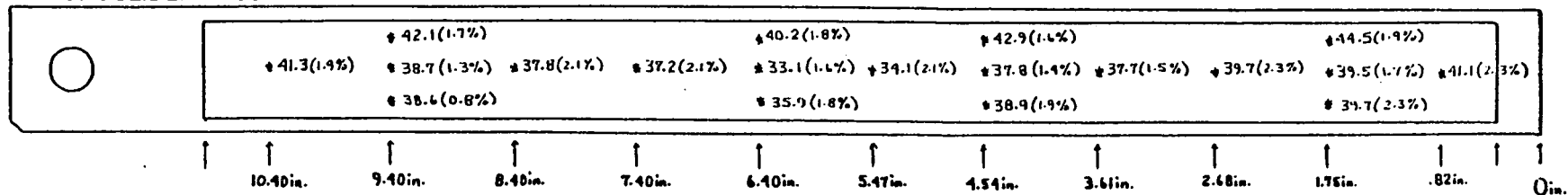
No. 30

RADIONUCLIDE: ^{134}Cs



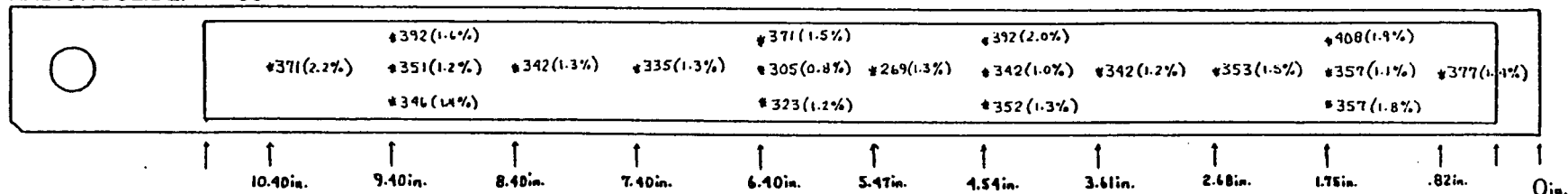
No. 30

RADIONUCLIDE: ^{137}Cs



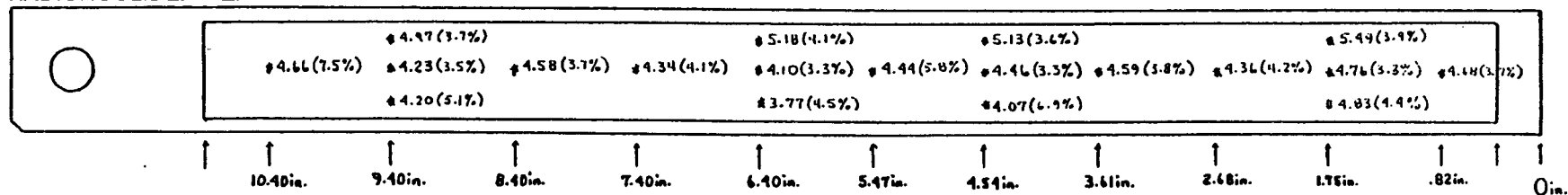
No. 30

RADIONUCLIDE: ^{144}Ce



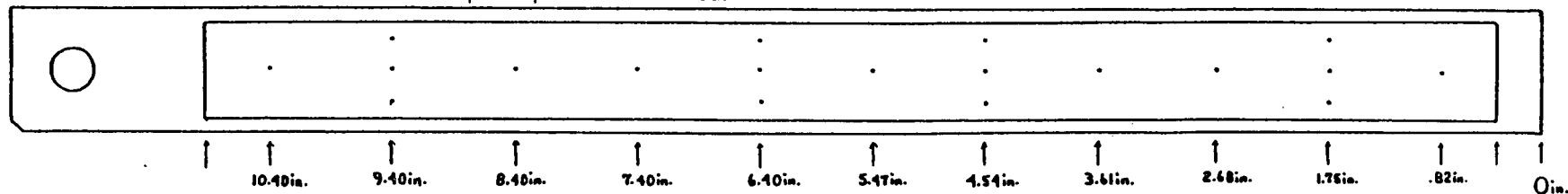
No. 32

RADIONUCLIDE: ^{95}Zr



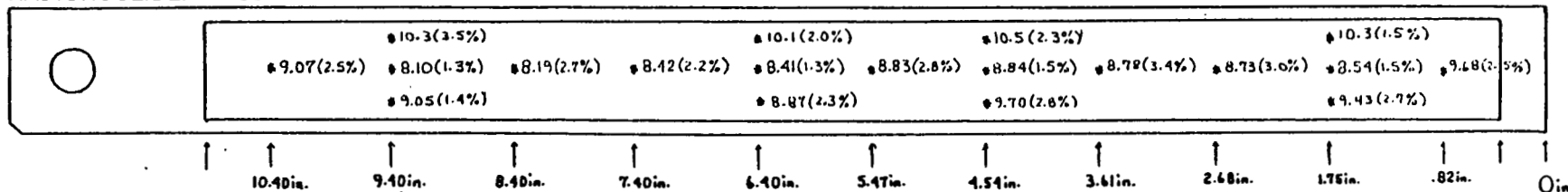
No. 32

RADIONUCLIDE: ^{103}Ru —none detected—photo peak not observed.



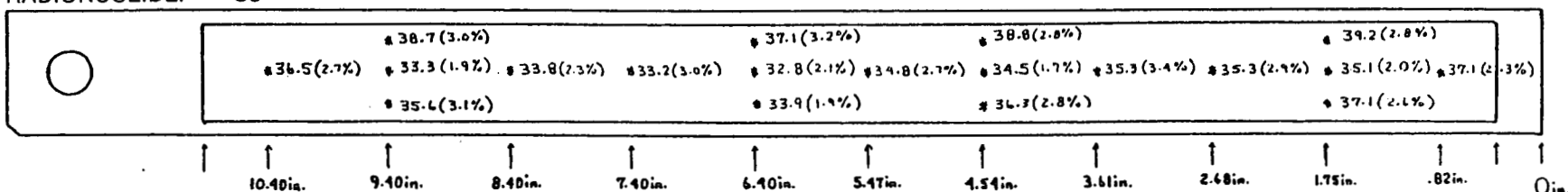
No. 32

RADIONUCLIDE: ^{134}Cs



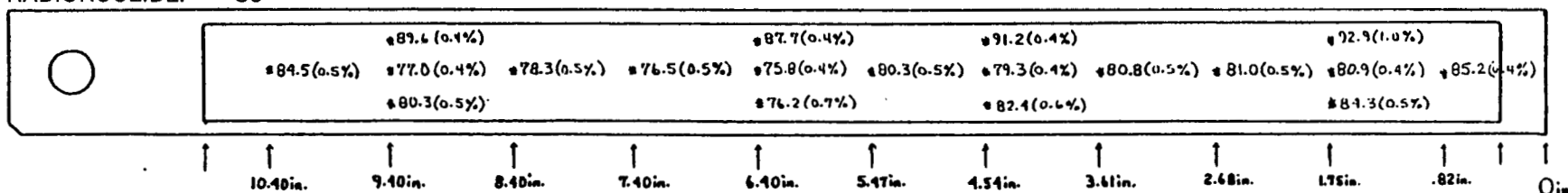
No. 32

RADIONUCLIDE: ^{137}Cs



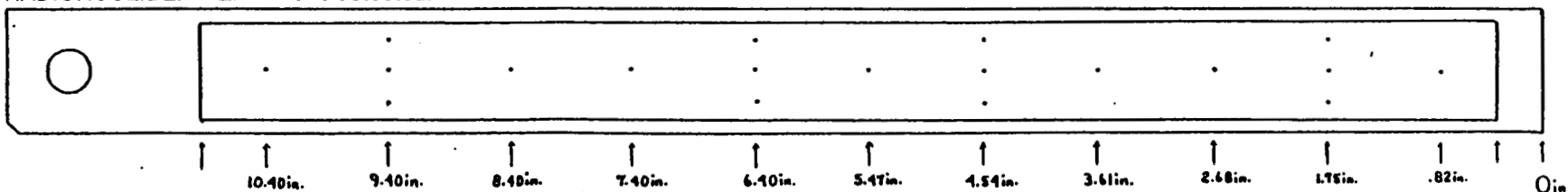
No. 32

RADIONUCLIDE: ^{144}Ce



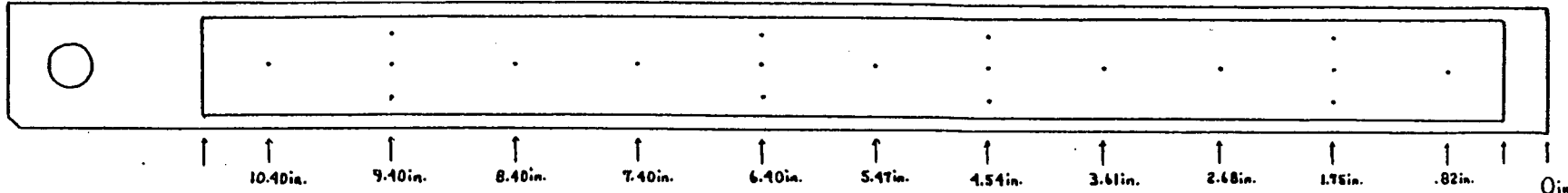
No. 33

RADIONUCLIDE: ^{95}Zr —none detected.



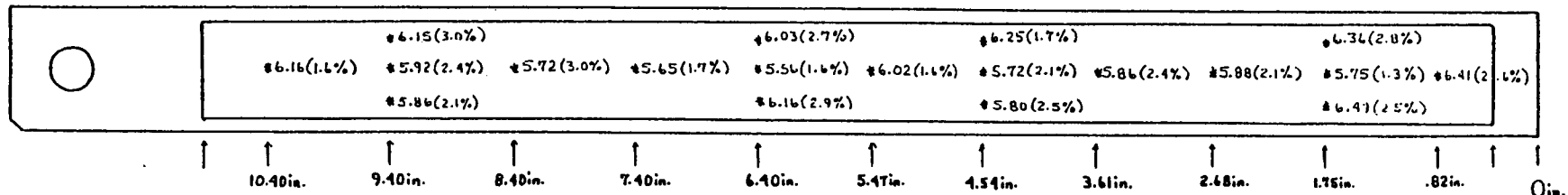
No. 33

RADIONUCLIDE: ^{103}Ru —none detected.



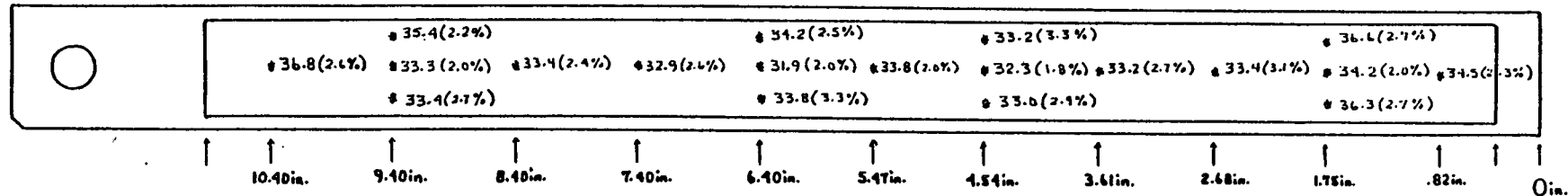
No. 33

RADIONUCLIDE: ^{134}Cs



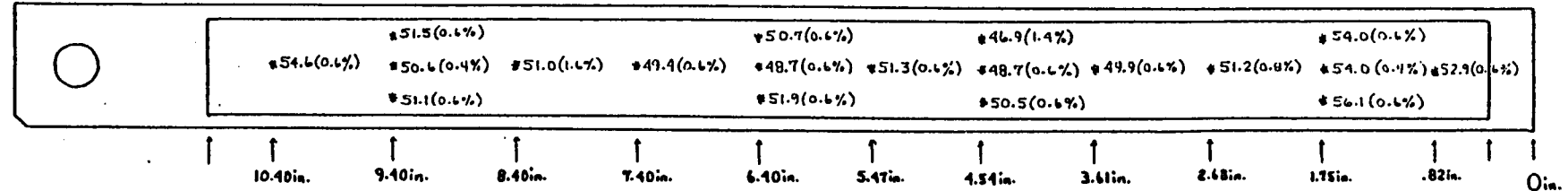
No. 33

RADIONUCLIDE: ^{137}Cs



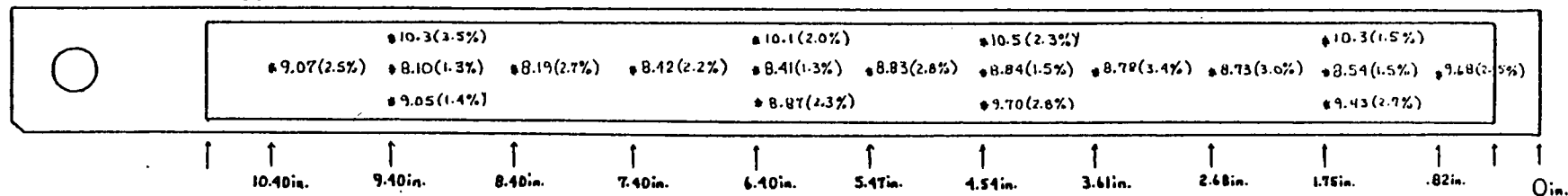
No. 33

RADIONUCLIDE: ^{144}Ce



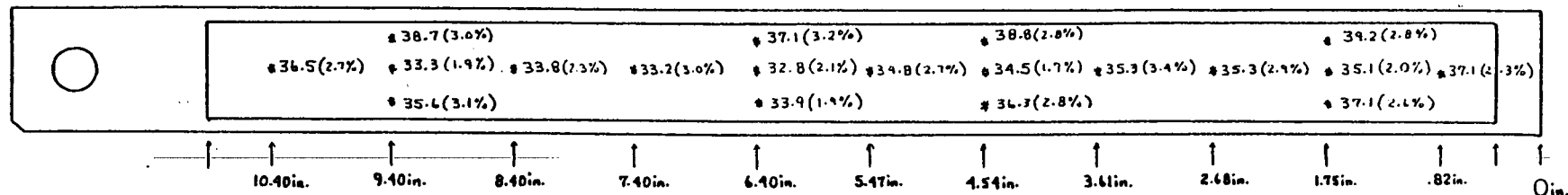
No. 32

RADIONUCLIDE: ^{134}Cs



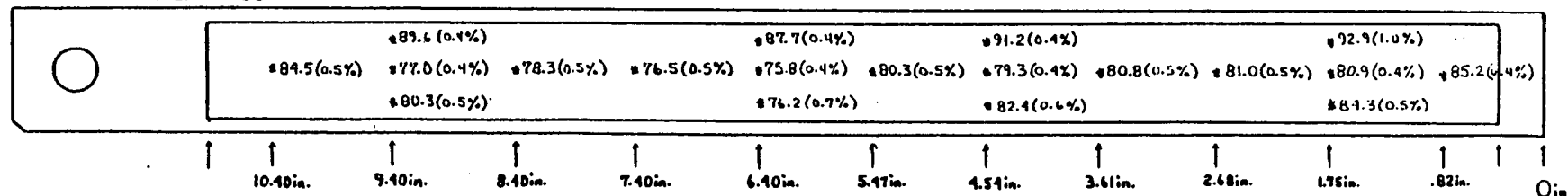
No. 32

RADIONUCLIDE: ^{137}Cs



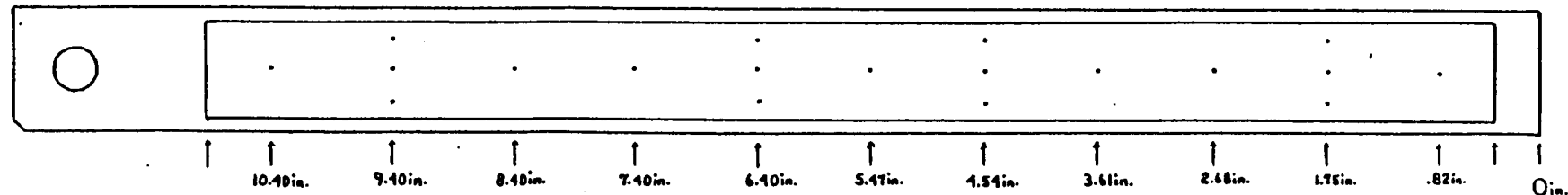
No. 32

RADIONUCLIDE: ^{144}Ce



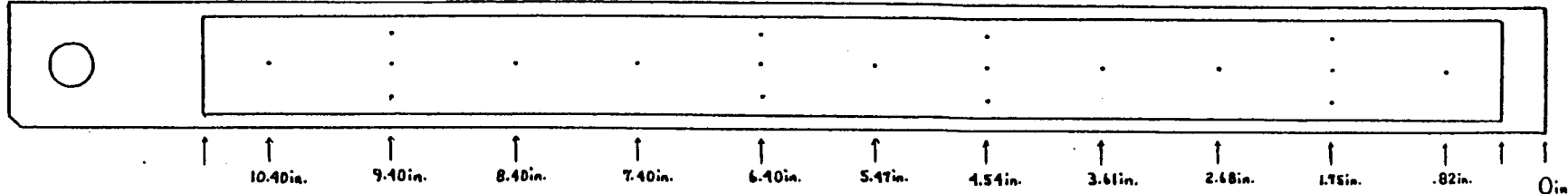
No. 33

RADIONUCLIDE: ^{95}Zr —none detected.



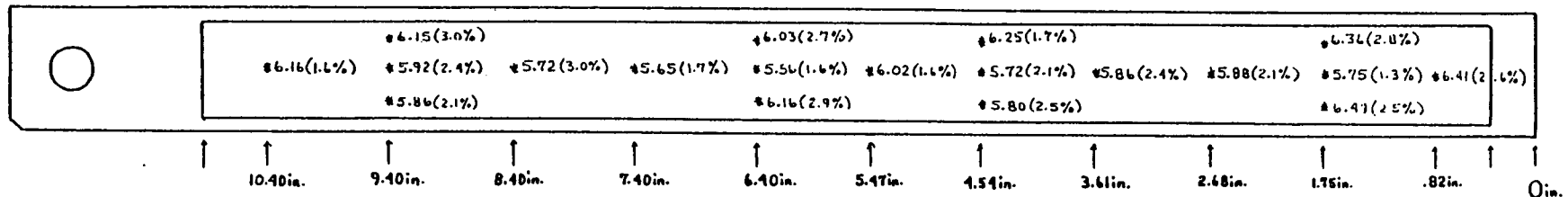
No. 33

RADIONUCLIDE: ^{103}Ru —none detected.



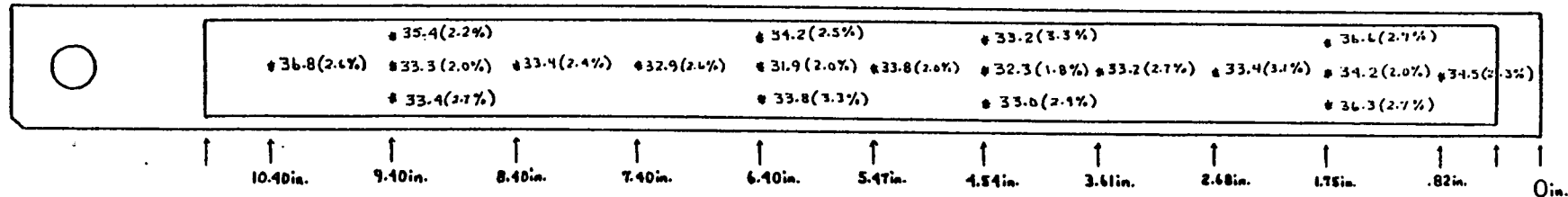
No. 33

RADIONUCLIDE: ^{134}Cs



No. 33

RADIONUCLIDE: ^{137}Cs



No. 33

RADIONUCLIDE: ^{144}Ce

